AD-A254 514

Technical Report 1484
March 1992

Li/SOCl$_2$ Battery Technology: Problems and Solutions

DTIC
ELECTE
S AUG 2 0 1992
A D

P. A. Mosier-Boss
S. J. Szpak

92-23125

92 8 19 60

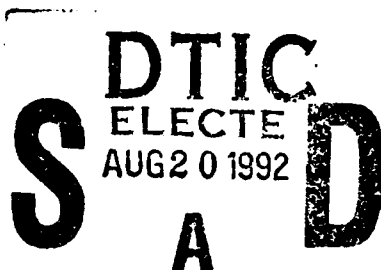4245 21   95

Technical Report 1484
March 1992

Li/SOCl$_2$ Battery Technology: Problems and Solutions

P. A. Mosier-Boss
S. J. Szpak

Accesion For		
NTIS CRA&I	☑	
DTIC TAB	☐	
Unannounced	☐	
Justification		
By		
Distribution /		
Availability Codes		
Dist	Avail and / or Special	
A-1		

NAVAL COMMAND, CONTROL AND OCEAN SURVEILLANCE CENTER
RDT&E DIVISION
San Diego, California 92152-5000

J. D. FONTANA, CAPT, USN
Commanding Officer

R. T. SHEARER
Executive Director

ADMINISTRATIVE INFORMATION

MA

SUMMARY

OBJECTIVE

The objective is to illustrate the advantages arising from a rational transition process when developing an electrochemical power source designed to operate at its limit. Here, we summarize our approach and results based on such a transition philosophy. Although we selected the $Li/SOCl_2$ couple for this purpose, such an approach is applicable to other systems as well and is an example of current trends in the development of electrochemical cells.

RESULTS AND CONCLUSIONS

In the early 1980s, the $Li/SOCl_2$ system was a candidate power source for propulsion. A major effort was undertaken to develop this power source. To maximize the power density of this power source, two design approaches were suggested: the construction of a module containing in-series connected thin cells, as one choice, and the employment of a flowing electrolyte, as the other. To improve the performance in each of the proposed designs, modifications of both electrolyte composition and cathode structure and composition were undertaken, with mixed results. Optimization of this system was not achieved and the programs developing this source were terminated.

The $Li/SOCl_2$ system is an example of technology prematurely transitioned from directed research to battery development. In this communication we outline a rational approach to battery development. The $Li/SOCl_2$ technology has come a long way since the initial recognition of its value as a battery chemistry. Much of this progress has resulted from a focused effort to pursue a logical progression of transitions through the R&D cycle. These efforts have elucidated the chemistry and electrochemistry of the system, the optimal design features of cells and modules, the assembly of these cells or modules into batteries, and the resultant characteristics of these assemblies. Although the $Li/SOCl_2$ system is used as an example, other battery technology developments would benefit from such an approach.

CONTENTS

FIGURES

TABLES

1. LITHIUM BATTERY TECHNOLOGY

1.1. INTRODUCTORY NOTES

Today, electrical energy is indispensable. In the broad concept of energy management, batteries occupy a prominent role due to their very high efficiencies of conversion and their ability to act as portable energy storers. A battery is probably the most versatile electrical energy source both in its performance and construction. It covers a wide range of power outputs: from 10^{-5} W needed to power a wrist watch to ca 10^7 W required for propulsion applications. It can be constructed in various sizes: from a button size for hearing aids, to large installations for load leveling. Furthermore, it can deliver this power in millisecond pulses or continuously for several years.

1.2. EMERGENCE OF LITHIUM BATTERY TECHNOLOGY

The past few decades have seen a rapid growth in battery technology. In addition to time-honored and proven lead acid storage battery, new types of electrochemical power sources have appeared. Among them, perhaps faster than expected, are lithium (Li) batteries, which have emerged as a new class of energy-dense cells. The emergence of Li as an anode material can be traced to early research at the University of California, Berkeley, where Harris (1958) showed that Li could be electrodeposited from solutions of lithium salts dissolved in propylene carbonate. The energy-dense $Li/SOCl_2$ system, first disclosed in 1973 (Auborn et al., 1973), was borne unexpectedly as a "spin-off" from fundamental research on new concepts in liquid lasers, a program sponsored by the Office of the Chief of Naval Research. Following this disclosure, considerable research, including applied research and exploratory development led to an early transition to engineering development about 1980. Somewhat later, a full-scale effort to construct a multimodule, high-discharge-rate battery was underway.

The $Li/SOCl_2$ system is an example of rapidly expanding electrochemical power source technology. Since its discovery, the battery has been developed for use in a number of diverse specialty applications. Its main feature is that it has the highest energy density of any, as yet, available. Recent advances in the lithium battery tech-

1

nology, including $Li/SOCl_2$, have been treated in a number of monographs discussing various aspects of this technology (Salkind, 1987; Dey, 1987; Venkatasetty, 1984; Gabano, 1983). While much progress has been made, a number of issues remain and must be addressed before the system is ready for full-scale applications. In our opinion, the activities associated with the development process itself, i.e., the transition from research concepts to the construction of engineering models, have not been sufficiently emphasized. Consequently, we focus on those aspects that were, and are, of interest to us, viz., application of engineering principles when evaluating and/or constructing an electrochemical converter. In fact, in an earlier communication, Szpak and Smith (1990) discussed the $Li/SOCl_2$ battery development program, identified several problems and issues associated with it, and proposed a systematic approach to meet design objectives.

In preparing this report, we share our experience gained during the development process of a specific, highly specialized $Li/SOCl_2$ battery, one designed for high-discharge rates (Szpak & Driscoll, 1987). The need for a systematic approach is evident considering the energy density of advanced lithium systems is on the order of 30–50 percent of common explosives. This high-energy density simultaneously offers great flexibility to the designer and presents potential danger to the user. The issues addressed here range from research topics dealing with electrocatalysis, kinetics of electroreduction of $SOCl_2$, physico-chemical properties of electrolytes, growth habits of $LiCl$ crystallizing within the confines of the porous structure of the positive plate to engineering aspects such as thermal management, scale-up problems, inter-cell currents, dimensional tolerances, and quality control measures. All these topics are developed in the context that a battery is an electrochemical reactor operating in response to imposed demands wherein reactants are converted to products in a controlled manner with the release of electrical energy and heat. When applying this concept to the $Li/SOCl_2$ battery, not only are the overall chemical reactions of interest, but also the partial reactions taking place within well-defined sections of the reaction space. An understanding of these partial reactions provide data needed to design a safe and efficient power source.

1.3.   THERMODYNAMIC CONSIDERATIONS

A detailed discussion of the thermodynamic structure of electrochemical systems was given by van Rysselberghe (1966) and that of the $Li/SOCl_2$ by Godshall and Driscoll (1984). In its simplest case, an electrochemical cell is a constrained system

2

that reacts spontaneously as the constraints are removed. The thermodynamic properties of the reactants and products give a measure of the energy available from the system. The enthalpy of the reaction, ΔH, is the total energy released while Gibbs free energy of reaction, ΔG, is the maximum amount of energy that can be converted to electrical energy. These quantities are related by

$$\Delta G = \Delta H - T\Delta S. \tag{1}$$

Two additional thermodynamic quantities are of interest: first, the thermodynamic potential, $U_0 = -\Delta G/zF$, and second, the thermoneutral potential, $U_t = -\Delta H/zF$. The open circuit potential, $U_c(0)$, is the potential measured between the positive and negative electrodes under the condition of no current flow, i.e., $U_c(0) = (U_+ - U_-)|_{i=0}$. This quantity is always positive and depends only on the system chemistry and not on the physical size of a cell. The measured $U_c(0)$ cannot exceed U_0 if the stoichiometry of the reaction is properly written. The thermoneutral potential, U_t, is of practical importance because it provides the basis for calculating the efficiencies of discharging cells, and is the basis for the thermal management of battery systems. The total heat released, when the cell operates at a potential very close to $U_c(0)$, is the thermodynamically unavailable energy for conversion, which is given by $q_{ent} = -T\Delta S$. This quantity is also expressed by $q_{ent} = zF(U_t - U_0)$. In normal battery operation, the cell potential U_c is less than U_0 and the cell produces additional heat equal to $q_d = zF(U_0 - U_c)$. Therefore, the total heat released is given by

$$q_{cell} = zF(U_t - U_c). \tag{2}$$

Conclusions based on applying eq. (1) are valid only when the thermodynamic functions are accurately known. To illustrate, early in the development period of the $Li/SOCl_2$ cell, it was reported that $\Delta S > 0$ for the cell reaction. Consequently, it was thought that thermal management would be no problem and that the system would cool during the discharge (Schlaikjer, Goebel & Marincic, 1979). This was shown not to be the case, however, and heat is generated in the course of battery operation (Godshall & Driscoll, 1984).

1.4.   WHY ELECTRICAL ENERGY CONVERSION?

Often the performance of galvanic cells is compared with the performance of other systems. For such comparisons to be meaningful, it must start from the same form

of energy and terminate with the same usable form (Bronsted, 1955). To illustrate, we consider the generation of electrical energy by the combustion of fossil fuels and contrast it with the production by galvanic cells (Bockris & Srinivasan, 1969). In both cases, the initial form is the chemical energy, $-\Delta H$. In thermal combustion, the stored energy is converted into electrical energy, $U_c(i)e^-$, by the following set of consecutive transformations:

$$-\Delta H \rightarrow Q_t \rightarrow W(pV) \rightarrow U_c(i)e^-. \tag{3}$$

The intermediate step, $W(pV)$, is necessary because the direct conversion of heat to another form of energy is impossible. The inefficient step is the $Q_t \rightarrow W(pV)$ conversion because thermal energy can only be utilized through its transfer to an auxiliary system which, in turn, can deliver work, e.g., mechanical compression of stored gas from which heat is rejected at lower temperature. The thermodynamic efficiency of an ideal heat engine is $\epsilon_h = 1 - T_2/T_1$, where T_1 is the fluid intake temperature and T_2 its rejection temperature. This restriction, the Carnot limitation, makes electrochemical conversion a very attractive method. The corresponding set of events for a direct electrochemical conversion is as follows: the negative electrode is an electron source while the positive electrode functions as an electron sink, thereby causing a flow of electrons in an external circuit without any additional ordering process, and

$$-\Delta H \rightarrow U_c(i)e^-. \tag{4}$$

The bypass of the $Q_t \rightarrow W(pV)$ step enormously increases the conversion efficiency. Physically, the Q_t term in eq. (3) represents the chaotic motion of molecules while the term, $U_c(i)e^-$, is the work done by an orderly flow of electrons in an external circuit. In electrochemical systems, apart from parasitic chemical reactions taking place in the cell interior, the chaos of the chemical reaction occurs at well-defined positions within the reaction space, i.e., at the electrode surface (Bagotzky & Skundin, 1980; Bockris & Reddy, 1972).

The thermodynamic efficiency of galvanic cells is defined as the ratio of electrical energy extracted to the heat of reaction. In electrochemical systems operating close to the $U_c(0)$, the term $q_{ent} = -T\Delta S$ is negligible. Therefore, the thermodynamic efficiency is nearly one and is dependent upon temperature through the Gibbs-Helmholtz relation, eq. (5)

$$U_0 = U_t + TdU_0/dT. \tag{5}$$

4

Using this relationship, the thermodynamic efficiency may be written in a form resembling the efficiency of a thermal engine, viz. $\epsilon_{cell} = 1 + T\frac{dU_0 dT}{U_t}$. The temperature-dependent efficiencies are compared in figure 1. It is seen that the thermodynamic efficiency of a $Li/SOCl_2$ cell operating near the rest potential and at the melting point of Li is ca 0.97. To obtain the same efficiency in an ideal heat engine, the temperature of the working fluid rejected into a 300-K sink, would have to be about 10^4 K. At high-discharge rates, e.g., for cells operating at 80 mA cm^{-2}, efficiencies on the order of 0.7 were recorded experimentally. Such a comparison might be misleading inasmuch as the actual cell efficiency is a product of thermal, voltaic, and faradaic efficiencies, of which the voltaic and faradaic efficiencies are temperature-dependent. For practical reasons, however, an additional efficiency can be introduced, namely an engineering efficiency that includes efficiencies associated with construction materials, reliability requirements, cell design, parasitic reactions, etc. The parasitic reactions are those that do not contribute to the production of electrical power and, at times, may cause the device to fail. The most common examples of parasitic reactions are corrosion, reactant and/or solute decomposition, and film and dendrite formation. These parasitic reactions must be included in the process of battery optimization as well as for safety considerations. In Li batteries, they arise because of the highly reactive nature of the cell components – a prerequisite associated with the construction of high-energy and power-dense systems.

Evaluation of battery efficiency can be made using an expression consisting of two terms: the electrochemical efficiency and the engineering efficiency. Specifically, the first is a dimensionless number related to the efficiency of all energy-conversion processes, whereas the second is defined as the weight ratio of active material to the whole system, accessories included (Gabano, 1983). It should be noted, however, there is no general agreement as to the procedures and test methods used for system evaluation. For this reason it is difficult, and often impossible, to compare results reported by various laboratories.

1.5.   ORGANIZATION OF DEVELOPMENT PROGRAM

To illustrate the challenges encountered during the development phase, we consider the following set of requirements: a battery voltage of 300 V and power output of ca 9 kW for a period of ca 10 minutes with an activation time no greater than 30 seconds. Moreover, because of space limitations and weight restrictions, an energy density of 560 Wh dm^{-3} and 200 Wh kg^{-1} would have to be realized. The module
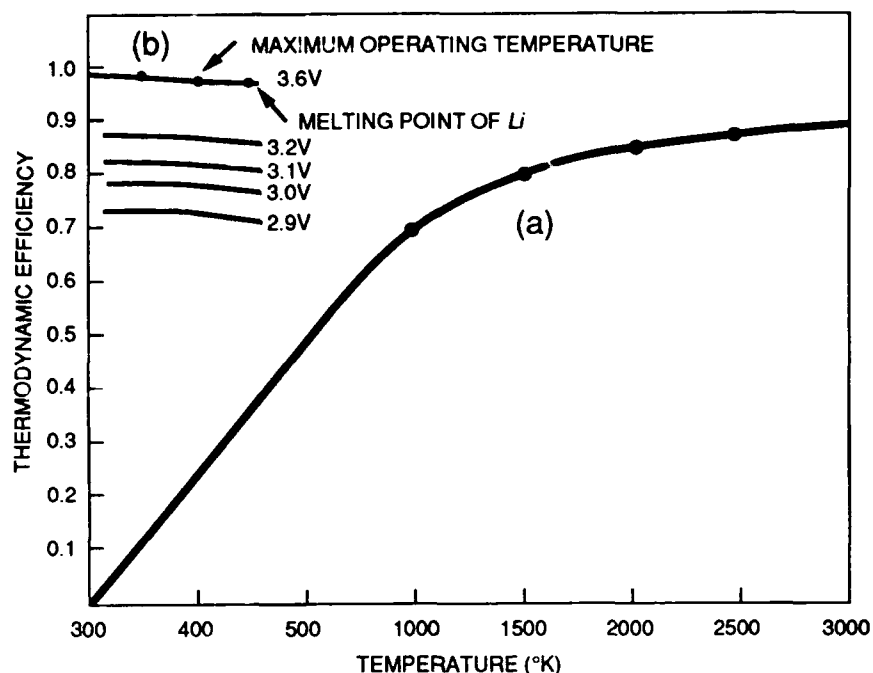
Figure 1. Thermodynamic efficiency as a function of temperature. (a) Efficiency of an ideal heat engine with a 300-K sink temperature, (b) efficiency of a $Li/SOCl_2$ cell at indicated cell potentials, V.

necessary to meet these requirements in a static electrolyte system must consists of 90 to 100 thin cells, of bipolar design, connected in series, each containing approximately 10 to 15 cm^3 of electrolyte. The short activation time necessitates the installation of more than one filling port. The module designed to satisfy these requirements is shown in figure 2.

During the development period, a number of failures were reported. These can be divided into three categories, viz., failures detected during module assembly; those that occurred in the course of module discharge, inclusive of the post-discharge period; and those which led to an unacceptable performance, e.g., inadequate battery lifetime. Intercell short circuits were the major problem during the manufacturing cycle. These undoubtedly were due to the contradictory nature of the system requirements. The thin cell design meant a separator thickness on the order of 5×10^{-5} m in the compressed cell. The separator must be highly porous to minimize the ohmic drop across the cell and permit rapid filling during the activation process. In addition, the separator must be mechanically strong to prevent distortion and tearing during assembly and activation and must act as a barrier to eliminate any migration of carbon particles. This balance between porosity and strength leaves little margin

6
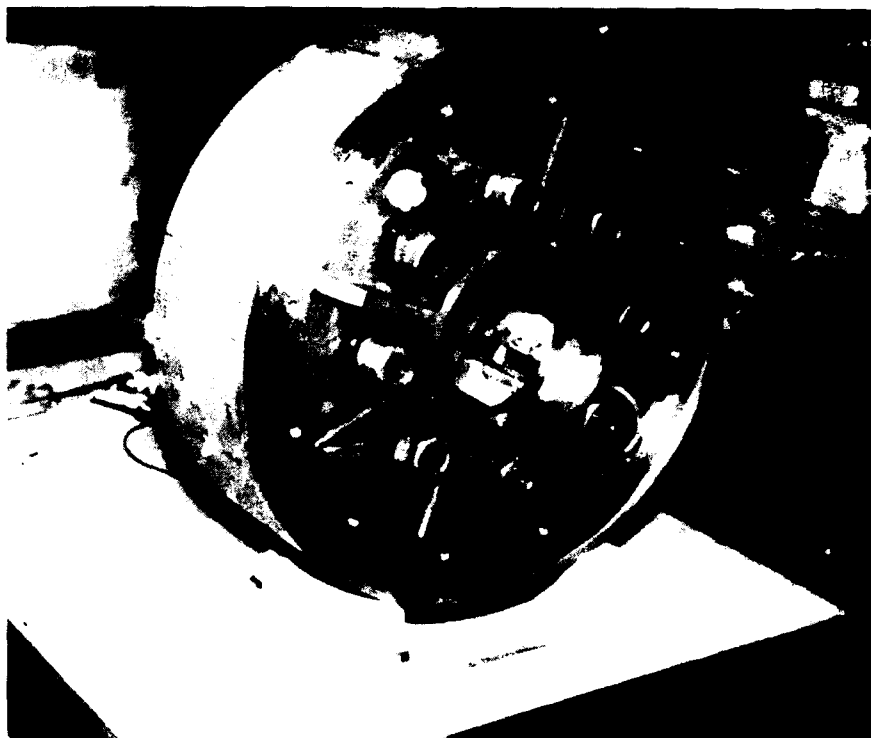
Figure 2. An experimental 9-kW module of thin cell design, reserve type, built by Altus Corp., San Jose, CA.

for error in construction. Figure 3 presents the chronology of failures and corrective measures in the test program. Most of these failures were attributed to short circuits. Even though the repeated failures were the consequence of inadequate quality control procedures, the initial remedy was to increase cell thickness, followed by a change in the activation procedure. The final remedy was to revise the quality control measures and to improve manufacturing techniques.

Examination of the third category, i.e., failure to meet the performance criteria, can be traced to the lack of a clear understanding of technology issues and transition activities. Transition is defined as a passage from one stage to another. In the context of battery development, the identifiable stages are: research, directed research, development process, etc. We define research as an activity that seeks an extension of knowledge for its own sake; directed research is one that examines observations for the purpose of isolating technology issues; and the development process is concerned with reduction to practice. With these definitions in mind, we present an idealized model for transition activities in figure 4a and contrast it with one applied during
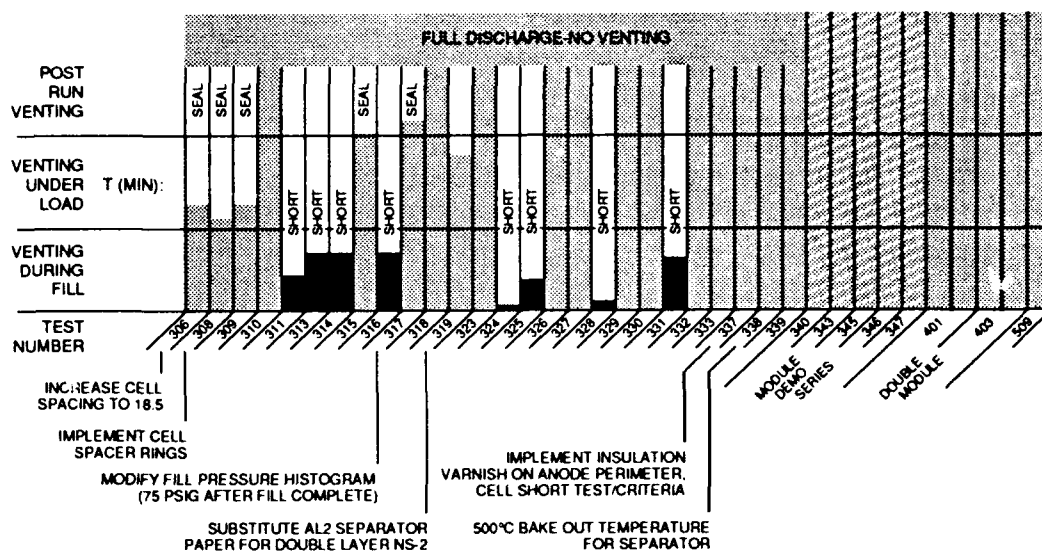
Figure 3. Histogram of testing. Times and modes of failure indicated.
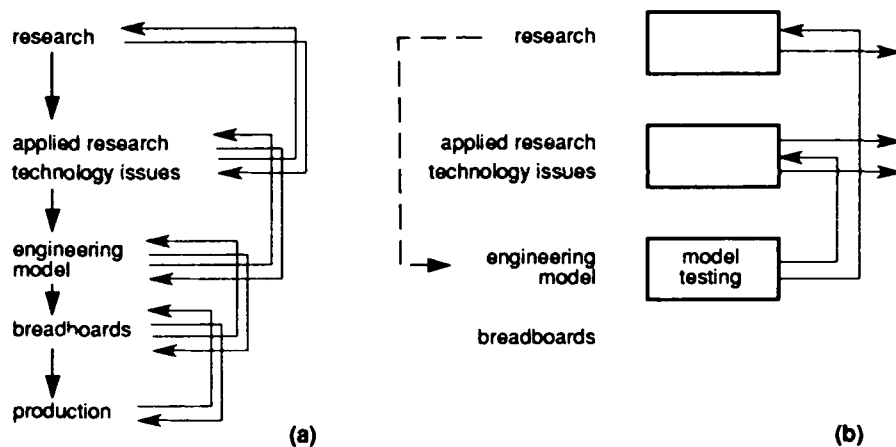
Figure 4. Model for transition activities. (a) Idealized model for R&D transition steps. (b) model for accelerated R&D transition steps.

the construction of a module rated at ca 8 kW and energy density of 200 Wh kg^{-1}, figure 4b. Evidently, in the course of the early developmental activities it was forgotten that, for the transition to occur, ideas or results generated within the context of activities of one stage must satisfy the constraints imposed by the next stage. The nature of these constraints may vary, but, in general, they can be reduced to human factors, including management philosophy and technical considerations (Szpak & Smith, 1990). The course of this development program provides clear evidence that the application of solid engineering principles is less expensive and less time

consuming than intuitive solutions and rapid fixes.

2. CHEMISTRY AND ELECTROCHEMISTRY OF THE LITHIUM/THIONYL CHLORIDE SYSTEM

2.1. INTRODUCTORY COMMENTS

While the energy density of a system, i.e., the total useful energy content is determined by the thermodynamics of the galvanic couple, its rate capabilities are determined by electrochemical kinetics and transport phenomena. This, in turn, involves an understanding of the partial reactions and processes that occur at the individual electrodes and the behavior of the electrolyte during discharge. The thermodynamic and kinetic data are then used in modeling exercises to follow the overall system behavior.

2.2. LITHIUM/THIONYL CHLORIDE OVERALL CELL REACTIONS

In determining the correct reaction stoichiometry, a battery containing known amounts of Li and $SOCl_2$ is assembled and discharged at a constant rate. The amount of charge passed is monitored and when discharge is complete, the battery is disassembled and examined for evidence of corrosion or dendrite formation. Finally, the electrodes and electrolyte are subjected to chemical analysis to determine the products of electroreduction.

Table 1 lists a number of proposed overall cell reactions (Szpak & Driscoll, 1987). The fact that as many as 12 reaction schemes have been proposed indicates the complexity of the chemistry, as well as the experimental difficulties encountered in analyzing this system. A brief review of the early literature indicates disagreement among investigators. For example, Auborn et al. (1973) suggested that eq. (II), table 1, adequately represents the cell reaction, while Dey (1976) postulated that eq. (I), was the correct reaction. In 1976, Driscoll, Holleck, and Toland reported analytical data in favor of eq. (I), giving Li^+, Cl^- and S in the expected stoichiometries.

Table 1. Summary of postulated overall cell reactions for the Li/SOCl$_2$ system.

Reaction Scheme No.	Overall Reaction	F/mole SOCl$_2$	V$_o$ (volts)	-ΔG$_r$ (kJ)	(Wh/kg)[a]
I	4Li + 2SOCl$_2$ → 4LiCl + S + SO$_2$	2.00	3.72	1436	1502
II	8Li + 3SOCl$_2$ → 6LiCl + 2S + Li$_2$SO$_3$	2.67	3.60	2779	1875
III	8Li + 4SOCl$_2$ → 6LiCl + S$_2$Cl$_2$ + Li$_2$S$_2$O$_4$	2.00	3.50	2702	1413
IV	14Li + 6SOCl$_2$ → 12LiCl + 4S + Li$_2$S$_2$O$_6$	2.33	3.70	4998	1710
V	10Li + 4SOCl$_2$ → 8LiCl + 2S + Li$_2$S$_2$O$_4$	2.50	3.57	3445	1756
VI	10Li + 4SOCl$_2$ → 8LiCl + 3S + Li$_2$SO$_4$	2.50	3.73	3599	1834
VII	8Li + 3SOCl$_2$ → 6LiCl + S + Li$_2$S$_2$O$_3$	2.67	3.56	2748	1854
VIII	6Li + 4SOCl$_2$ → 6LiCl + S$_2$ Cl$_2$ + 2SO$_2$	1.50	3.68	2130	1144
IX	10Li + 6SOCl$_2$ → 8LiCl + 2S$_2$Cl$_2$ + Li$_2$S$_2$O$_6$	1.67	3.64	3512	1249
X	7Li + 4SOCl$_2$ → 5LiCl + 3/2S$_2$Cl$_2$ + Li$_2$SO$_4$	1.75	3.68	2486	1317
XI	6Li + 3SOCl$_2$ → 4LiCl + S$_2$Cl$_2$ + Li$_2$SO$_3$	2.00	3.52	2038	1421
XII	7Li + 3SOCl$_2$ → 5LiCl + 1/2S + Li$_2$S$_2$O$_3$	2.33	3.52	2377	1627

a — Energy density calculated from total energy (-ΔG$_r$) according to the equation

$$= \frac{-\Delta G_r}{3.6(6.94 n_{Li} + 118.9 n_{SOCl_2})} \; ; \text{ where } -\Delta G_r \text{ is in Joules}$$

and n_{Li}, n_{SOCl_2} are the stoichiometric coefficients from column 2.

They also identified SO_2 as a reaction product; however, the amount of SO_2 found was not consistent with eq. (I). It was later shown that a side reaction in the analytical procedure resulted in this discrepency. In 1979, Schlaikjer et al. reported that the reaction pathway is dependent upon the operating temperature of the cell, viz., at temperatures above 253 K, eq. (I), table 1, dominates, while below 253 K eq. (II) represents the correct reaction. Therefore, on the basis of the best presently available evidence, eq. (I), table 1, is considered to represent the overall cell reaction and is used as the basis for the modeling of the $Li/SOCl_2$ system.

2.3.   PROPOSED MECHANISMS OF THIONYL CHLORIDE ELECTROREDUCTION – AN EARLY PERIOD

The interest in determining the mechanism of $SOCl_2$ electroreduction dates back to the mid 1970s and extends through the 1980s. The methods employed include cyclic voltammetry, spectroscopic examination of spent electrolytes, gas chromatography, and electron spin resonance (esr) spectrometry. In all reported mechanisms, the key role was assigned to the formation of $SOCl^.$ radical:

$$SOCl_2 + e^- \rightarrow SOCl^. + Cl^- ,$$ (I)
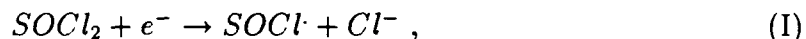
which then reacts, via a series of steps, to form the products of electroreduction. The proposed reaction schemes are summarized in table 2. Bowden and Dey (1980) examined the reduction of cell electrolytes using cyclic voltammetry. To avoid difficulties associated with electrode passivation by the precipitation of $LiCl$, they examined voltammograms of elemental sulfur, $SOCl_2$,SO_2, and S_2Cl_2 dissolved in organic solvents, e.g., $N(CH_3)_2CHO$; CH_3CN; $(CH_3)_2SO$. From the shape of voltammograms, augmented by ultraviolet-visible (UV-VIS) spectra of cell electrolytes sampled during discharge, they concluded that, after the formation of the $SOCl^.$ radical, the reduction proceeds via the production of a hazardous intermediate $(SO)_x$. Investigations by Istone and Brodd (1984) further supported the Bowden and Dey mechanism.

Table 2. Postulated reaction mechanisms for the reduction of thionyl chloride

Overall reaction: $2SOCl_2 + 4e^- \longrightarrow S + SO_2 + 4Cl^-$

I. Bowden and Dey, 1980	II. Blomgren et al, 1979	III. Carter et al, 1985
$SOCl_2 + e^- \longrightarrow SOCl + Cl^-$	$SOCl_2 + e^- \longrightarrow SOCl + Cl^-$	$SOCl_2 + e^- \longrightarrow OSCl + Cl^-$
$SOCl_2 + e^- \longrightarrow SO + 2Cl^-$	$2\ SOCl \longrightarrow SO_2 + SCl_2$	$OSCl \longrightarrow OClS$
$SO + SOCl_2 \rightleftharpoons SO \cdot SOCl_2$	$SCl_2 + e^- \longrightarrow SCl + Cl^-$	$2\ OClS \longrightarrow (OClS)_2$
$SO \longrightarrow (SO)_x$	$2\ SCl \longrightarrow S_2Cl_2$	$(OClS)_2 \longrightarrow SO_2 + SCl_2$
$(SO)_x \longrightarrow x\ S + xSO_2$	$S_2Cl_2 + 2e^- \longrightarrow 2\ S + 2Cl^-$	$2\ SCl_2 \rightleftharpoons S_2Cl_2 + Cl_2$
• $(SO)_x$ a hardardous intermediate	• No apparent hazardous intermediate	$SO_2 + Cl_2 \rightleftharpoons SO_2Cl_2$
		$SCl_2 + 2e^- \longrightarrow S + Cl_2$
		$S_2Cl_2 + 2e^- \longrightarrow 2\ S + 2\ Cl^-$
		$Cl_2 + 2\ e^- \longrightarrow 2\ Cl^-$
		$SO_2Cl_2 + 2\ e^- \longrightarrow SO_2 + 2Cl^-$
		• $OClS$ a hazardous intermediate

Blomgren et al. (1979) also took, as the starting point, the formation of $SOCl$
radical, followed by a number of steps yielding SCl_2 and S_2Cl_2 without the formation
of a hazardous intermediate. In 1985, Carter et al. (1985) using modern tools, includ-
ing esr spectrometry, monitored the electroreduction of $LiAlCl_4/SOCl_2$ electrolytes.
Their gas chromatographs showed an increase in Cl_2, SO_2, and SO_2Cl_2 in the dis-
charged samples. Similarly, the infrared (IR) spectra indicated formation of SO_2 in
the discharged solutions as well as formation of SO_2Cl_2. An esr signal was observed
for these solutions, implying the existence of a radical, presumably $SOCl$. They pro-
posed a rather complex mechanism with the formation of a hazardous intermediate,
$OClS$, cf. table 2.

It is noteworthy that the objective of this research was to find an intermediate
responsible for the catastrophic events during discharge. For example, Salmon et al.
(1982) reported formation of Cl_2O and ClO_2; however, later work (Carter, Frank
& Szpak, 1984) failed to confirm these findings. At present, it is believed that the
forced explosive venting, which sometimes occurs during the discharge of $Li/SOCl_2$
battery is due to the development of hot spots resulting from either internal shorts
or localized exothermic reactions between the metallic lithium and $SOCl_2$.

2.4.   CHEMISTRY OF THE $LiCl - AlCl_3 - SOCl_2$ SYSTEM

The proposed mechanisms summarized in table 2, ignore the fact that $SOCl_2$
forms adducts with $AlCl_3$ (Long & Bailey, 1963; Hecht, 1947; and Spandau & Brun-
neck, 1952) and is able to enter the solvation sheet of ionic species either initially
present or generated in the course of the charge transfer process. If the composition
of the electrode/electrolyte interphase is related to the bulk, eq. (I) as written does
not identify which $SOCl_2$ molecules reside in the reaction space and participate in the
charge transfer process. Furthermore, Madou and Szpak (1984) and Madou, Szpak,
and Smith (1987) have shown, that more than one $SOCl_2$-bearing species undergo
electroreduction. Consequently, it is essential to know what species are present in
solution, their structures, and equilibria. Experimental details are given in appendix
A.

2.4.1.   The Structure of Neat $SOCl_2$

Thionyl chloride is a weakly associated liquid. It has a rather low latent heat of vaporization and there is a slight change in the $S - O$ stretching frequency due to condensation (the $S-O$ stretching vibration occurs at 1251 cm^{-1} in the gas phase and 1231 cm^{-1} in the liquid phase). Further evidence of weak association is the numerical value of the slope of the fluidity as a function of specific volume, which indicates the presence of small, interacting molecular clusters (Szpak & Venkatasetty, 1984). Examination of the $S - O$ stretching vibration of neat $SOCl_2$ at 1231 cm^{-1}, shown in figure 5, indicates that it is actually a composite band composed of two Voigt profiles. When cooled to, e.g., 250 K the band due to the $S - O$ stretching vibration is composed of three Voigt profiles, (Mosier-Boss et al., 1989a). These Voigt profiles have been assigned to dimers and oligomers of $SOCl_2$, which according to molecular orbital (MO) calculations have an open-chain spatial structure, shown in figure 6.

2.4.2.   Structure of the $Al_2Cl_6/SOCl_2$ System

With the addition of Al_2Cl_6, a new set of bands appear in the Raman spectra, as shown in figure 7, indicating the formation of adduct(s). At low concentrations of Al_2Cl_6, a new band at 1108 cm^{-1} appears. This band has been assigned to the $S - O$ stretching vibration of the 1:1 adduct (Long & Bailey, 1963). Since the observed shift of the $S - O$ stretching vibration occurs at lower frequency and the symmetric and asymmetric $S - Cl$ stretching vibrations shift to higher frequency, complexation occurs through the oxygen atom, $Cl_SO \rightarrow AlCl_3$. As the Al_2Cl_6 concentration increases, a new $S - O$ stretching vibrational band at ca 1055 cm^{-1} appears, as shown in figure 7. This new band is very broad and is due to a $S - O$ stretching vibration of a second $AlCl_3 - SOCl_2$ species. The broadness of this band as well as the shift of the $S - O$ stretching vibration to lower frequency indicates further electron withdrawal from the oxygen atom perhaps from the formation of a 1:2 complex, $Cl_2SO(AlCl_3)_2$, as suggested by others (Long & Bailey, 1963; Hecht, 1947). Such a conclusion would be consistent with the existence of a 1:2 complex in the solid state (Long & Bailey, 1963); however, the appearance of this band coincides with an increase in the solution conductivity (Szpak & Venkatasetty, 1984). Molecular adducts are neutral and, as such, are nonconductive. Therefore, this new band occurring at 1055 cm^{-1} is due to an ionic species and not to $Cl_2SO(AlCl_3)_2$. Formation of an ionic species from the
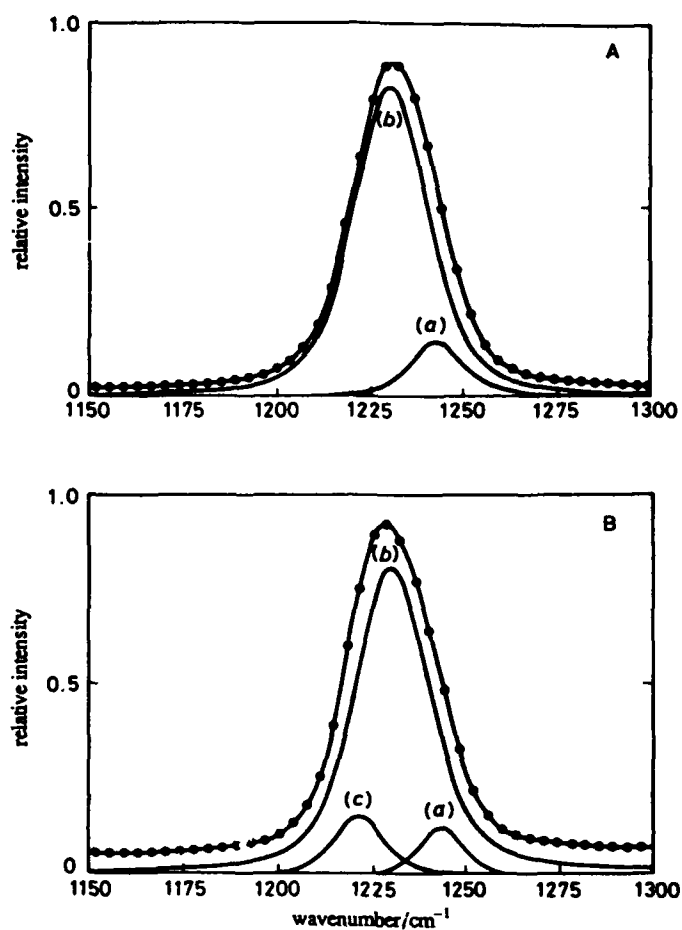
Figure 5. Decomposition of $S - O$ stretching band of neat $SOCl_2$ into Voigt profiles. (a) 273.5 K, (b) 250.0 K (Mosier-Boss et al., 1989*a*).

$Cl_2SO \rightarrow AlCl_3$ adduct can occur either by a halide ion transfer

$$Cl_2SO \rightarrow AlCl_3 \rightleftharpoons SOCl^+ + AlCl_4^- \ , \tag{II}$$
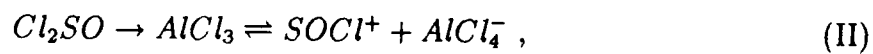
or by an internal exchange reaction

$$2Cl_2SO \rightarrow AlCl_3 \rightleftharpoons Cl_2Al(\leftarrow OSCl_2)_2^+ + AlCl_4^- \ . \tag{III}$$

15
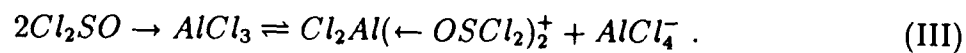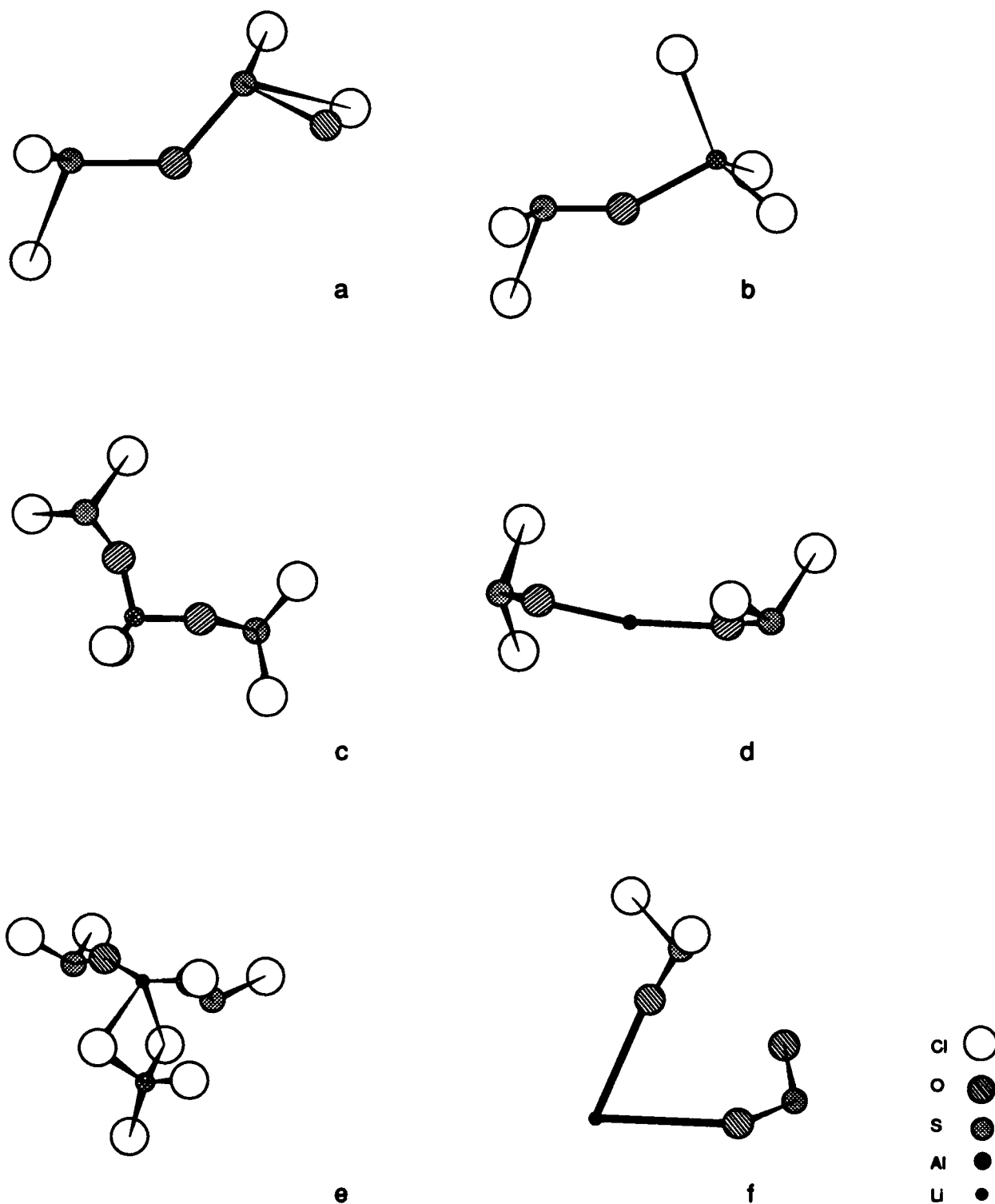
Figure 6. Molecular orbital generated structures for: (a) $(SOCl_2)_2$ open chain dimer, (b) $Cl_3Al \leftarrow OSCl_2$ 1:1 adduct, (c) $[Cl_2Al(\leftarrow OSCl_2)_2]^+$, (d) $[Li(\leftarrow OSCl_2)_2]^+$ solvated Li^+ ion, (e) $[Li(\leftarrow OSCl_2)_2]^+[AlCl_4^-]$ ion pair, and (f) $Li(OSCl_2, SO_2)^+$ ion (Mosier-Boss et al., 1991).

16
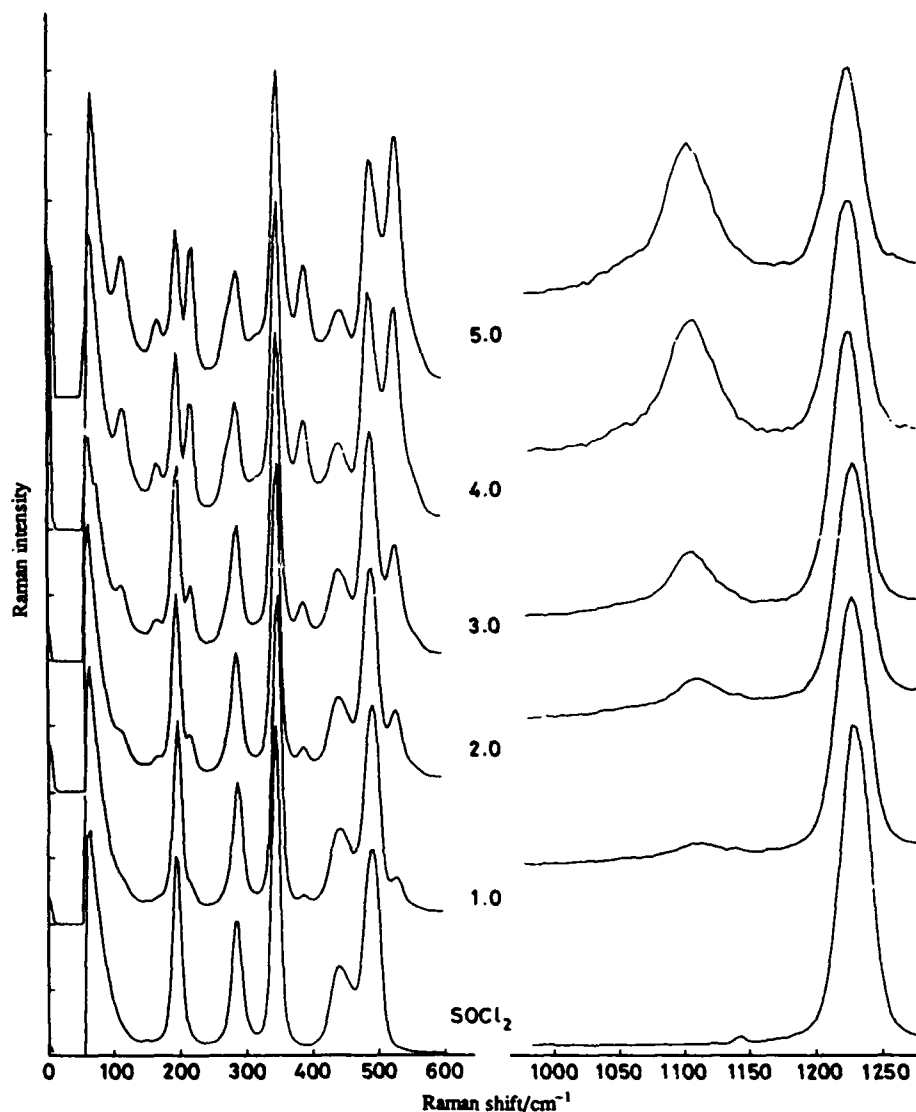
Figure 7. Evolution of Raman spectra of the $AlCl_3 - SOCl_2$ system as a function of $AlCl_3$ concentration as indicated. The $S - O$ stretching region occurs between 1000–1250 cm^{-1}. The symmetric and asymmetric $S - Cl$ stretching region occurs between 400–600 cm^{-1} (Mosier-Boss et al., 1989a).

Both the spectroscopic data and MO calculations favor formation of an onium ion, $Cl_2Al(\leftarrow OSCl_2)_2^+$, via eq. (III) (Mosier-Boss et al., 1989a). The onium ion has a negative $\Delta H_f = -11$ kcal mole^{-1} compared to $SOCl^+$, which has a positive $\Delta H_f = +228.27$ kcal mole^{-1}. Since the $S - O$ bond of $SOCl^+$ has a higher bond order than that for $SOCl_2$, the $S - O$ stretching vibration of $SOCl^+$ would occur at a higher frequency. However, no high-frequency bands were observed in the $S - O$

17

stretching region of the Raman spectra. In contrast, the $S - O$ stretching vibration of $Cl_2Al(\leftarrow OSCl_2)_2^+$ is expected to occur at a lower frequency than for either $SOCl_2$ or the 1:1 adduct. The MO-generated structure for the 1:1 adduct and onium ion are shown in figure 6.

2.4.3.   Structure of the $LiCl/Al_2Cl_6/SOCl_2$ System

The effect of $LiCl$ addition on the structural features of the $AlCl_3 - SOCl_2$ system is illustrated in figure 8. With the addition of $LiCl$ the bands due to the 1:1 adduct, $Cl_3Al \leftarrow OSCl_2$, and onium ion, $Cl_2Al(\leftarrow OSCl_2)_2^+$, disappear. In the $S - O$ stretching region a new band at 1215 cm^{-1} appears which has been assigned to solvated Li^+ ion. Again, the lowering of the $S - O$ stretching vibration of solvated Li^+ indicates coordination is through the oxygen atom, $Li(\leftarrow OSCl_2)_2^+$. At least two $SOCl_2$ molecules are required to solvate Li^+ as a 1:1:2 molar ratio solution of $LiCl : AlCl_3 : SOCl_2$ can be prepared. The Raman spectrum of this solution shows no free $SOCl_2$ to be present (Mosier-Boss et al., 1989b).

Typically, Li^+ has a coordination number of four. In the presence of excess $SOCl_2$, these sites are likely filled with $SOCl_2$ molecules. However, in the 1:1:2 $LiCl : AlCl_3 : SOCl_2$ mole ratio solution, two sites are occupied by $SOCl_2$ and the remaining two coordination sites can be filled by ion pairing with $AlCl_4^-$. While $SOCl_2$ is a polar solvent, as shown by its large dipole moment, it has a low dielectric constant implying that substantial ion pairing should occur in these electrolytes. Indeed, from conductance measurements of $LiAlCl_4$ electrolytes in $SOCl_2$, Venkatasetty and Saathoff (1981) obtained a value of 1.605×10^{-3} for the dissociation constant of the ion pair. MO calculations of solvated Li^+, $Li(\leftarrow OSCl_2)_2^+$, and the ion pair, $[Li(\leftarrow OSCl_2)_2^+][AlCl_4^-]$, favor formation of the ion pair. Not only is the heat of formation, ΔH_f, more negative for the ion pair (-291 kcal mole^{-1} for the ion pair and -56 kcal mole^{-1} for the solvated Li^+ ion), but the $Li - O$ bond length for the $Li^+ \leftarrow OSCl_2$ interaction decreases and the positive charge gets distributed into the $SOCl_2$ moieties of the ion pair. The MO-generated structures for $Li(\leftarrow OSCl_2)_2^+$ and ion pair are shown in figure 6.

2.4.4.   A Brief Summary of the $SOCl_2$ Chemistry

The structures and structural changes of these electrolytes can be summarized
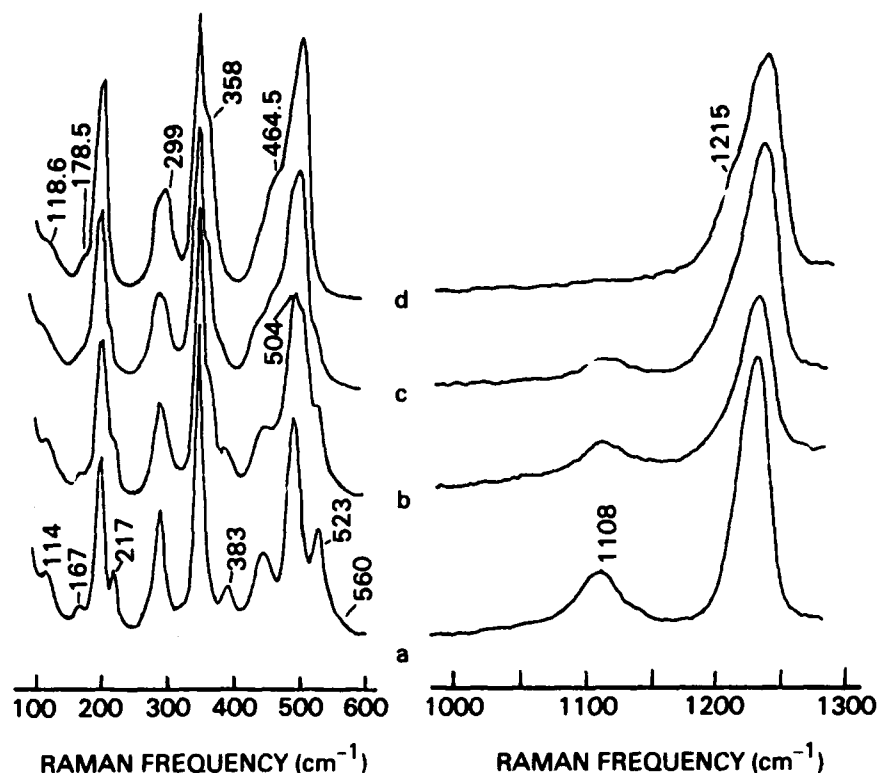
Figure 8. Raman spectra of the $LiCl - AlCl_3 - SOCl_2$ system. 3.0 M $AlCl_3$ in $SOCl_2$. (a) 0 M $LiCl$, (b) 1.0 M $LiCl$, (c) 2.0 M $LiCl$, and (d) 3.0 M $LiCl$ (Mosier-Boss et al., 1989b).

as follows. In the liquid state, $SOCl_2$ forms open-chain dimers and oligomers. The dissolution of Al_2Cl_6 occurs dissociatively with the formation of adducts which, at higher Al_2Cl_6 concentrations, yield onium ions and $AlCl_4^-$. The addition of $LiCl$ causes the destruction of $Cl_3Al \leftarrow OSCl_2$ and the onium ion with the formation of solvated Li^+. At higher $LiAlCl_4$ concentrations, ion pairing between the solvated Li^+ ion and $AlCl_4^-$ occurs. The spectral data, results of the MO calculations, and the viscosity and conductivity measurements are in agreement. These results indicate that the $S - O$ bond strength of the free and complexed $SOCl_2$ diminishes as follows:

$$Cl_2SO > (Cl_2SO)_n > Li(\leftarrow OSCl_2)_2^+ >$$

$$Cl_3Al \leftarrow OSCl_2 > Cl_2Al(\leftarrow OSCl_2)_2^+; n \geq 2.$$

19
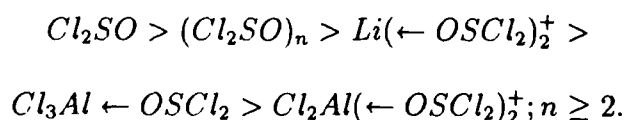
2.5. ELECTROCHEMICAL ASPECTS OF $SOCl_2$ REDUCTION

The reaction path of electroreduction of $SOCl_2$ electrolytes is examined by three techniques: in situ reflectance infrared spectroscopy, cyclic voltammetry, and both galvanostatic and potentiostatic pulsing. Experimental details are given in appendix A. What follows is a brief discussion of the techniques chosen to probe these electrochemical reactions.

2.5.1. In Situ Reflectance Infrared Spectroscopy

In situ reflectance infrared spectroscopy is a useful technique to identify the species present in the electrode–electrolyte interphase region (Ashley & Pons, 1988). This technique provides information regarding surface coverage, the orientation of adsorbates, as well as structural information on the intermediate and product species formed upon electroreduction. By varying the electrode potential, it is possible to determine, from changes in the spectra, the species undergoing electroreduction as well as their orientation on the electrode surface.

2.5.2. Cyclic Voltammetry

Cyclic voltammetry is the experimental technique of choice to assess the complexity of an electrochemical reaction and elucidate, at least qualitatively, its mechanism. The shape of the current/voltage, alternatively, current/time curves, reflects the specific set of events associated with the charge transfer reaction taking place under selected experimental conditions. The current/time relationship, $j(0,t)$, for a linear potential scan, $U(t) = U_i^o + |v|t$, for the N electroactive species and M adsorption processes, is given by

$$j(0,t) = F \left[\sum_{n=1}^{N} z_n D_n \frac{\partial^2 c_n}{\partial x^2} + \sum_{m=1}^{M} \Gamma_m \frac{d\theta_m}{dt} \right], \qquad (6)$$

where Γ_m denotes the maximum surface concentration of the $m - th$ species and θ is the surface coverage. The right-hand side of eq. (6) contains contributions due to the diffusional flux via the sum of concentration gradients of electroactive species and the kinetics of adsorption expressed in terms of the time rate of change in the surface

coverage summed over the number of adsorption processes. Which set of processes dominates the charge transfer reaction depends, among other factors, on the rate of linear scan. In general, slow scan rates relate to the diffusional processes while fast scan rates expose the adsorption characteristics. The concentration(s) gradient of the electroactive species is obtained from the mass balance equation, eq. (7)

$$\frac{\partial c}{\partial t} = D_n \frac{\partial^2 c_n}{\partial x^2} - f_n(\xi, \lambda), \tag{7}$$

which is solved subject to boundary conditions reflecting the experimental constraints. The function, $f_n(\xi, \lambda)$, is formulated for a specific set of events occurring within the interphase in the course of charge transfer. In particular, ξ refers to thermodynamic aspects, e.g., equilibria between species populating the interphase, while λ contains information on the rate of relevant processes, including forcing perturbation, e.g., potential scan rate.

2.5.3. Pulsing Techniques

Additional information can be extracted by changing the nature of the forcing function, $f_n(\xi, \lambda)$. For a class of electrode processes where adsorbed species dominate, the electrode potential can be written in a general form,

$$U = U(\theta_1, \theta_2, ...; j) \tag{8}$$

and its time dependence can be obtained by formal differentiation which, for the galvanostatic case yields

$$\frac{dU}{dt} = \sum_n \frac{\partial U}{\partial \theta_l}\big|_{j,n=\div l}\frac{d\theta_l}{dt}. \tag{9}$$

Galvanostatic and potentiostatic pulsing techniques are often used to probe the kinetics of mass transport, charge transfer, coupled chemical reaction rates and adsorption (Murray, 1986; Bard & Faulkner, 1980). In the galvanostatic pulsing experiment, the constant current applied to the electrode causes the electroactive species, ox, to be reduced to product, red. This process is essentially a titration of the ox species near the electrode by the constant flux of electrons. The potential of the electrode moves to values characteristic of the couple and varies with time as the c_{ox}/c_{red} ratio changes at the electrode surface resulting in a titration curve. In the potentiostatic pulsing experiment, a potential step is applied to the working electrode

21

and the resulting current/time response is measured. The magnitude of the current at any given time and the shape of the current/time response are also dependent upon the mass balance equation through the forcing function, $f_n(\xi, \lambda)$. eq. (7).

2.6. ELECTROREDUCTION OF $SOCl_2$ ELECTROLYTES – REACTION PATH

As expected, a given electrolyte composition may be ideal for one battery application but not another. Electrolyte composition strongly influences the reaction path of $SOCl_2$ electroreduction. In practice, the high-energy dense, reserve batteries usually employ acidic electrolytes whereas the low-rate cells use neutral electrolytes. It was, therefore, of interest to us to determine the similarities and differences in the electroreduction pathways of acidic and neutral electrolytes.

2.6.1. Concept of an Electrode–Electrolyte Interphase

An interphase region is formed whenever an electrode is in contact with an electrolyte. In the simplest case, the interphase region takes the form of the electrical double layer. In the more complex cases and, in particular, during the charge transfer reaction, it consists of layers, each associated with a participating elementary process. In this representation, the interphase region is an open system in which a number of consecutive processes takes place, of which the slowest one determines the rate. These processes include transport of the reactants from the bulk to the electrode surface by diffusion, adsorption on the electrode surface, charge transfer, desorption of the reaction products, followed by transport of the reaction products away from the electrode surface. In a discharging battery, these same processes occur; however, in a battery the electrons ultimately flow into an external circuit where the electrical work is delivered.

2.6.2. Interphase at Rest

Figure 9 shows the $S - O$ stretching region of the $AlCl_3 - SOCl_2$ system reflected off gold at the $U_c(0)$. Varying the path length between the Au electrode and the infrared transparent window clearly indicates an enrichment of both the 1:1 adduct and onium ion near the electrode. Deconvolution of the composite band in the

950–1150 cm^{-1} infrared spectral region into Voigt profiles, shown in figure 10, provides additional information on the structure of the interphase at the rest potential. The band in the transmittance spectrum consists of two Voigt profiles at 1116.9 and 1065.5 cm^{-1}, which are assigned to the adduct and onium ion, respectively. However, the reflectance spectra of Au and Pt show two additional Voigt profiles at 1132 and 1102 cm^{-1}. These two peaks, which disappear upon cathodic polarization, were tentatively assigned earlier as either (i) the symmetric and asymmetric $S - O$ stretching vibrations of adsorbed onium ion or (ii) the $S - O$ stretching vibrations of adsorbed onium ion and 1:1 adduct, respectively (Mosier-Boss et al., 1989b). The disappearance of the 1132 and 1102 cm^{-1} peaks upon cathodic polarization appears to be coupled, suggesting they are derived from the same species. Therefore, the most probable assignment of these two peaks is to adsorbed onium ion. Regardless, since these peaks
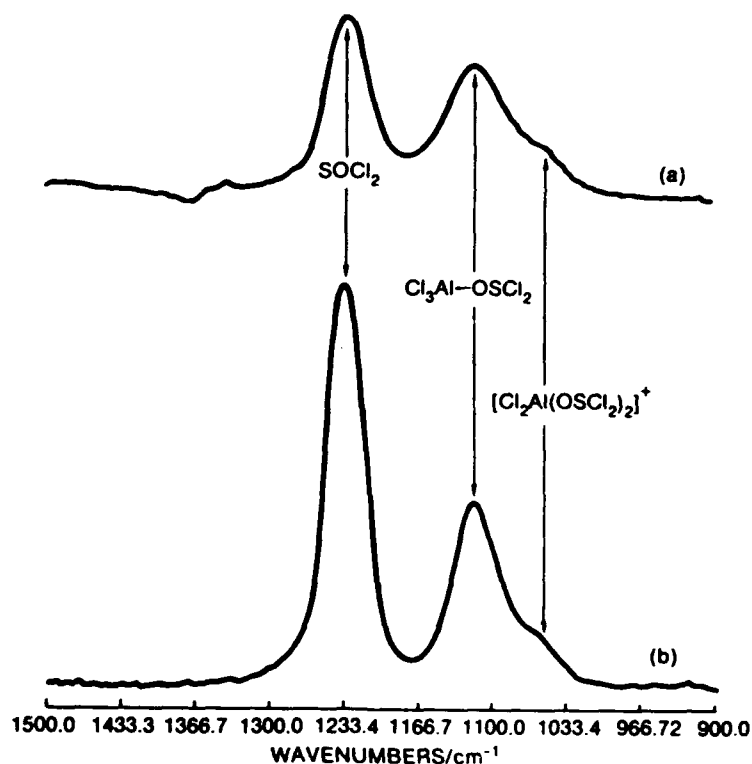
Figure 9. IR reflectance spectra at rest potential at path lengths of 5 and 10 μm, respectively. Electrolyte 4.0 M $AlCl_3$ in $SOCl_2$, electrode material Au (Mosier-Boss et al., 1989c).

are shifted to higher frequencies, it follows that adsorption occurs through the sulfur atom. This conclusion is supported by MO calculations, which indicate that the positive charge rests on the sulfur atom (Mosier-Boss et al., 1989a). Therefore, at rest potential the interphase of the $Me/AlCl_3 - SOCl_2$ system, as illustrated in figure 11, consists of an electrode in contact with an adsorption layer, which is in contact with an enrichment layer of 1:1 adduct, A_1, and onium ion A_2^+, which is in contact with the bulk electrolyte.
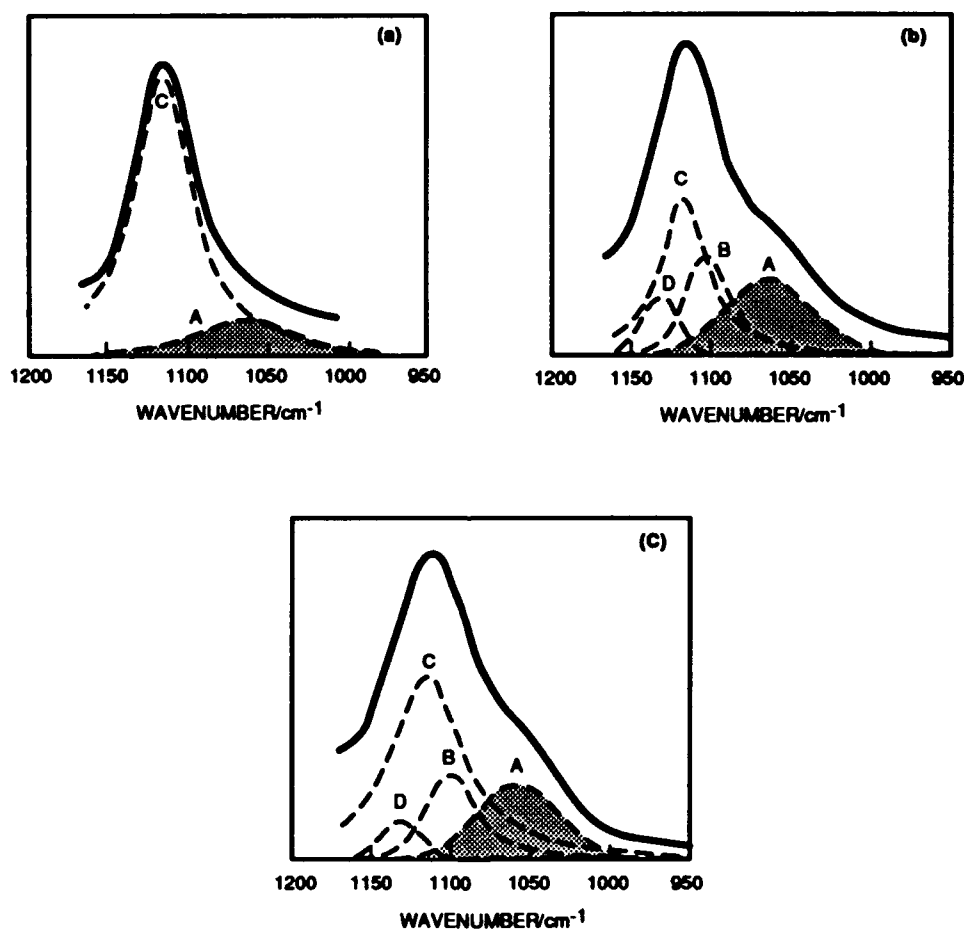
Figure 10. The 950–1150 cm^{-1} IR spectral region decomposed into Voigt profiles. (a) Transmittance spectrum, (b) reflectance spectrum from Au, (c) reflectance spectrum from Pt. Both reflectance spectra are at the rest potential. A,C, $S - O$ vibrations due to onium ion and complex in the bulk electrolyte; B,D, asymmetric and symmetric $S - O$ stretching vibrations of adsorbed onium ion, respectively, or $S - O$ stretching vibrations of adsorbed onium ion and 1:1 adduct, respectively. Electrolyte 4.0 M $AlCl_3$ in $SOCl_2$ (Mosier-Boss et al., 1989c).

24
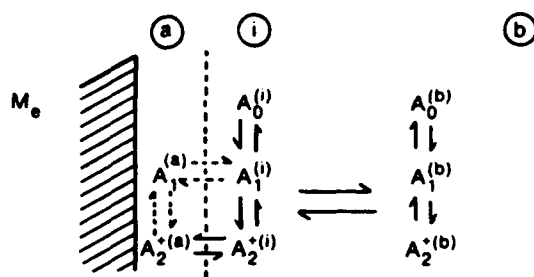
Figure 11. Structure of the electrode/electrolyte interphase at the rest potential: (b) - bulk, (i) - interphase, (a) - adsorption layer (Mosier-Boss et al., 1989c).

2.6.3.   Cathodically Polarized Interphase

The effect of applied overpotential on the $S - O$ stretching region of $Au/4.0$ M $AlCl_3$ in $SOCl_2$ is shown in figure 12. With the passage of current, new peaks appear, viz, at 1331 and ca 1150 cm^{-1} due to the formation of SO_2 and at 1170 cm^{-1} and 1190 cm^{-1} assigned to intermediate species P_1 and P_2 with the peak at 1170 cm^{-1} appearing first. Concurrently, there is a loss of the peaks due to the A_1 and A_2^+ species. These results indicate that the electroactive species is not neat $SOCl_2$, A_0. Instead the species undergoing electroreduction is either the 1:1 adduct, A_1, or the onium ion, A_2^+, or both. It is not clear whether the $SOCl_2$ moieties of the 1:1 adduct and onium ion are simultaneously reduced or if only one species participates in the reduction process. This ambiguity exists because the species are coupled to one another via the chemical equilibrium, eq. (III), and products of the electroreduction of one species may shift the equilibrium to regenerate the electroreducible species. In these potential-dependent spectra, there is no evidence of SO, $(SO)_x$, $SOCl$ or SO_2Cl_2 intermediate species as proposed by others, *vide supra*.

2.6.4.   Relaxation Techniques

A useful technique to explore complex electrochemical processes is cyclic voltammetry, since the shape of the current/voltage curves depends upon the thermodynamics of the system and the kinetics of the charge transfer and associated transport processes, eqs. (6) and (7). Cyclic voltammograms obtained for the $Pt/AlCl_3 - SOCl_2$ systems are shown in figure 13. For 3.0 M $AlCl_3$ in $SOCl_2$, two electron transfers
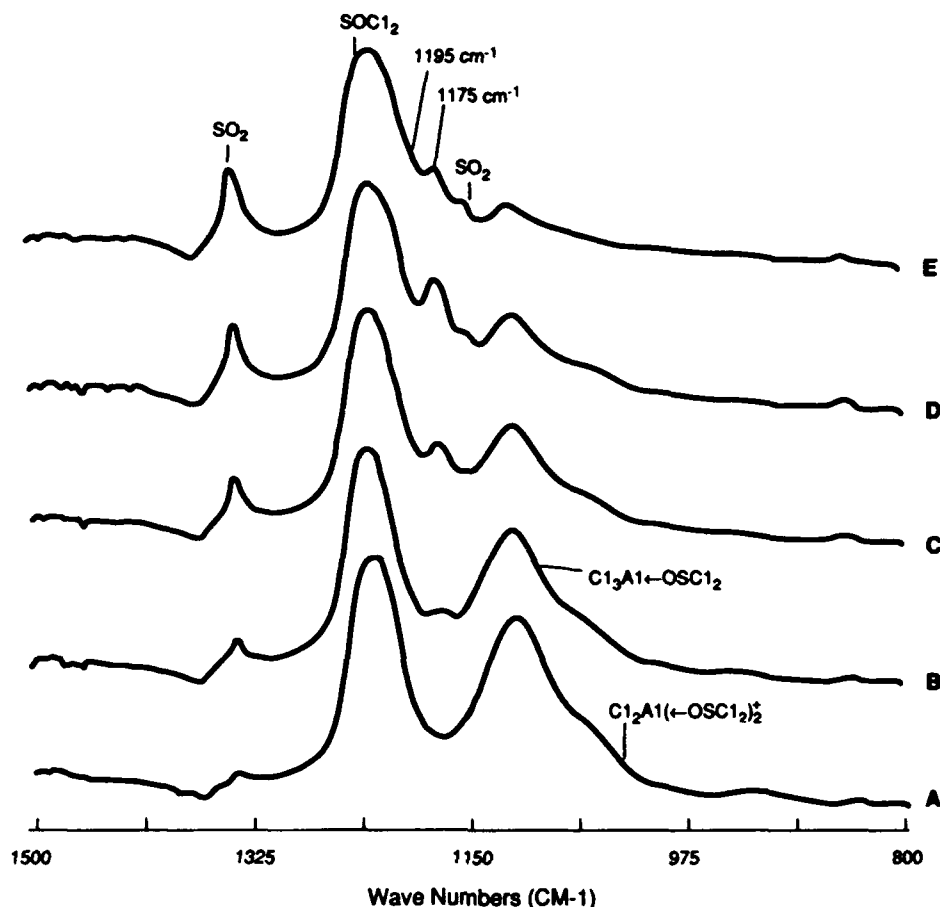
Figure 12. The 900–1500 cm^{-1} IR spectral region of cathodically polarized Au/4.0 M $AlCl_3$ in $SOCl_2$. Overpotentials vs $Ag/AgCl$: (a) 0.0 V, (b) -0.5 V, (c) -1.0 V, (d) -1.5 V, (e) -2.2 V (Mosier-Boss et al., 1991).

are observed of which the first, to form intermediate species P_1, is irreversible and the second electron transfer, to form P_2, is quasi-reversible. A current plateau is associated with the first electron transfer suggesting a coupled chemical reaction either preceding or parallel with the charge transfer (Nicholson & Shain, 1964). Indeed, an equilibrium does exist between onium ion and 1:1 adduct and, from the in situ infrared spectroscopy, a loss of both these species is observed with increasing overpotential. As the scan rate is decreased (figure 13a) or the concentration of $AlCl_3$ is increased (figure 13b), an autocatalytic effect, manifested by a cross-over behavior in the cyclic voltammograms (Nicholson & Shain, 1964), is observed. Increasing the $AlCl_3$ concentration increases the concentration of onium ions. Moreover, since the cross-over point occurs at the juncture between the current plateau and the cathodic
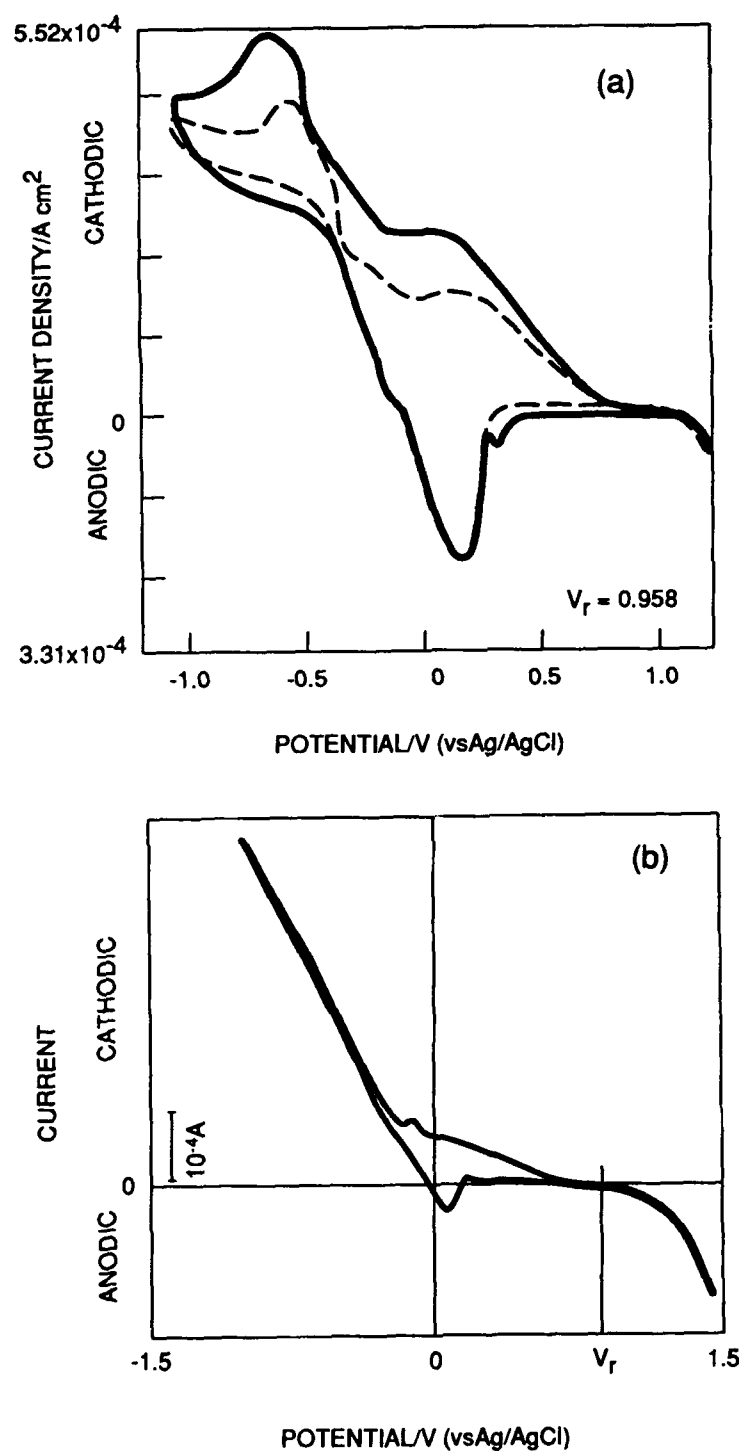
Figure 13. Effect of scan rate and concentration on voltammogram shape for the $Pt/AlCl_3 - SOCl_2$ system. (a) 3.0 M $AlCl_3$, solid line – 10 mV s^{-1}, dashed line – 5 mV s^{-1}, (b) 4.0 M $AlCl_3$, scan rate 10 mV s^{-1} (Mosier-Boss et al., 1991).

peak due to the second electron transfer, the species being regenerated on the electrode surface, via eq. (IV), is P_1.

$$P_2 + A_2^+ \rightarrow 2P_1 .$$ (IV)

These results indicate that the electroactive species is the onium ion and that intermediate species P_1 and P_2 are actually onium ion that has accepted one and two electrons, respectively. The MO calculations show that neutral onium ion and negatively charged onium ion are more stable than positively charged onium ion (Mosier-Boss et al, 1989b).

$$A_2^+ + e^- \rightarrow A_2, \Delta H_f = -310 \text{ kcal mole}^{-1}$$ (V)

$$A_2 + e^- \rightarrow A_2^-, \Delta H_f = -347 \text{ kcal mole}^{-1}.$$ (VI)
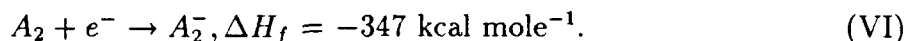
Moreover, since ΔH_f for A_2^+ is only -11 kcal mole^{-1}, one would expect the first electron transfer to be irreversible while the second would be reversible.

Galvanostatic and potentiostatic pulsing experiments provide additional information on the number and charge of adsorbed species. Figure 14a shows the potential/time behavior across a charging and relaxing interphase for the $Pt/AlCl_3-SOCl_2$ system. Three exponential decays are observed in the relaxation curve. In general, the number of exponential decays present in the potential relaxation curve reflects the number of adsorbed species (Conway & Dzieciuch, 1963). Therefore, there are three adsorbed species present on the Pt electrode. The current/time behavior during and after a potentiostatic pulse is applied is shown in figure 14b. Only two exponential decays are observed in the relaxation curve. Since only charged species are conductive, two of the absorbed species, in particular A_2^+ and P_2, are charged. Again, this supports the notion that P_1 and P_2 are actually the neutral and negatively charged onium ion, respectively.

2.6.5. Summary of Events; Acidic Electrolyte

The sequence of events occurring during $SOCl_2$ electroreduction in acidic electrolytes is summarized in figure 15. In figure 15, ζ reflects the thermodynamics and λ the kinetics of the system. The rate constants for adsorption, autocatalysis and

28

Figure 14. (a) Potential/time behavior and (b) current/time behavior across a charging and relaxing interphase. System: $Pt/SOCl_2-$ 2.0 M $AlCl_3$ (Mosier-Boss et al., 1991).

desorption are denoted by k_a, $k^{(c)}$ and k_d, respectively, whereas the rate constants for the first and second electron transfers are given by $k^{(1)}$ and $k^{(2)}$. Surface coverages of A_2^+, P_1 and P_2 are defined by θ_1, θ_2 and θ_3, respectively. According to this scheme, the intermediate species, P_1 and P_2, desorb from the electrode surface into the reaction layer where they react with other species to form the products of electroreduction – Cl^-, SO_2, and S. This reaction layer is sandwiched between the enrichment and diffusion layers. It is interesting to note that in the charging potential/time curve shown in figure 14a, the potential does not rapidly fall off to more negative potentials indicating that the electroactive species is continuously being regenerated in the reaction layer.

In situ infrared spectroscopy of acidic electrolytes from Au, Pt, $n - Si$ and glassy C surfaces at rest potential and cathodically polarized are similar. From this it can be concluded that the reduction path of acidic electrolytes, shown in figure 15, is the same for each surface (Mosier-Boss et al., 1990). However, the shapes of the cyclic voltammograms and the potential/time and current/time curves upon charging and relaxation are greatly dependent upon the electrode material (Mosier-Boss et al., 1990). This is not surprising since the shapes of these curves ultimately depend upon the mass balance equation, eq. (7), through the forcing function $f_n(\xi, \lambda)$. Therefore, the values of the rate constants for the processes summarized in figure 15 should be strongly dependent upon the electrode material.

29
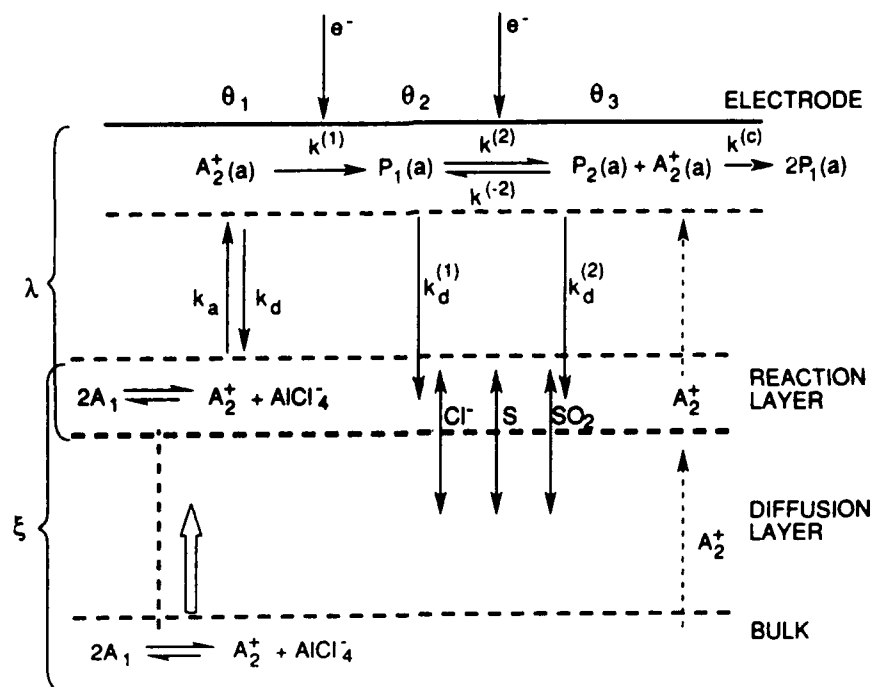
Figure 15. Structure of the electrode/electrolyte interphase and summary of participating processes (Mosier-Boss et al., 1991).

2.6.6. Reaction Path in the Presence of $LiCl$

2.6.6.1. Interphase at Rest and Cathodically Polarized.

Figure 16 shows the in situ reflectance infrared spectra of the $Au/SOCl_2 - AlCl_3 - LiCl$ interphase at the rest potential and cathodically polarized. At rest potential, a new band due to $Li(\leftarrow OSCl_2)_2^+$ is observed. At cathodic potentials less than 0.9 V, this band increases in size, indicating the accumulation of $Li(\leftarrow OSCl_2)_2^+$ in the interphase region. Formation of SO_2 is observed as evidenced by the bands at 1331 and 1150 cm^{-1}. the asymmetric and symmetric $S - O$ stretches of SO_2 respectively. As the amount of SO_2 in the interphase region increases, a new band at 1157 cm^{-1} appears, which has been assigned to the symmetric $S - O$ stretch of SO_2 in the solvation shell of Li^+, i.e. $Li(OSCl_2, SO_2)^+$ (Lanson & Descroix, 1984). The MO-generated structure for this species ($\Delta H_f = -36.4$ kcal mole^{-1}) is shown in figure 6. Concurrently, there is a loss of the bands due to the 1:1 $AlCl_3 - SOCl_2$ adduct and onium ion. Therefore, at cathodic overpotentials less than 0.9 V, the formation of SO_2 in electrolytes containing both $LiAlCl_4$ and $AlCl_3$ occurs through the electroreduction of onium ion. Unfortunately, the band due to the $S - O$ stretch of $Li(\leftarrow OSCl_2)_2^+$

obscures the bands at 1170 and 1190 cm^{-1} assigned to intermediate species P_1 and P_2 (figure 12). Consequently, it is not possible to assess the degree of interaction, if any, between P_1 and/or P_2 and $Li(\leftarrow OSCl_2)_2^+$ and $Li(OSCl_2, SO_2)^+$ present in the interphase region. At cathodic overpotentials greater than 0.9 V, a loss of the band due to $Li(\leftarrow OSCl_2)_2^+$ is observed with further formation of SO_2. No bands due to $Li(SO_2)_3^+$ (Lanson & Descroix, 1984) were observed in the spectra. Therefore, in practical electrolytes, onium ion undergoes electroreduction first followed by the solvated lithium ion. It can be concluded that the order of the charge transfer is inversely related to the strength of the $S - O$ bond. Similar changes in the in situ IR reflectance spectroscopy for the $Pt/AlCl_3 - LiCl - SOCl_2$ system are observed implying that the reaction paths are the same for Au and Pt electrodes.
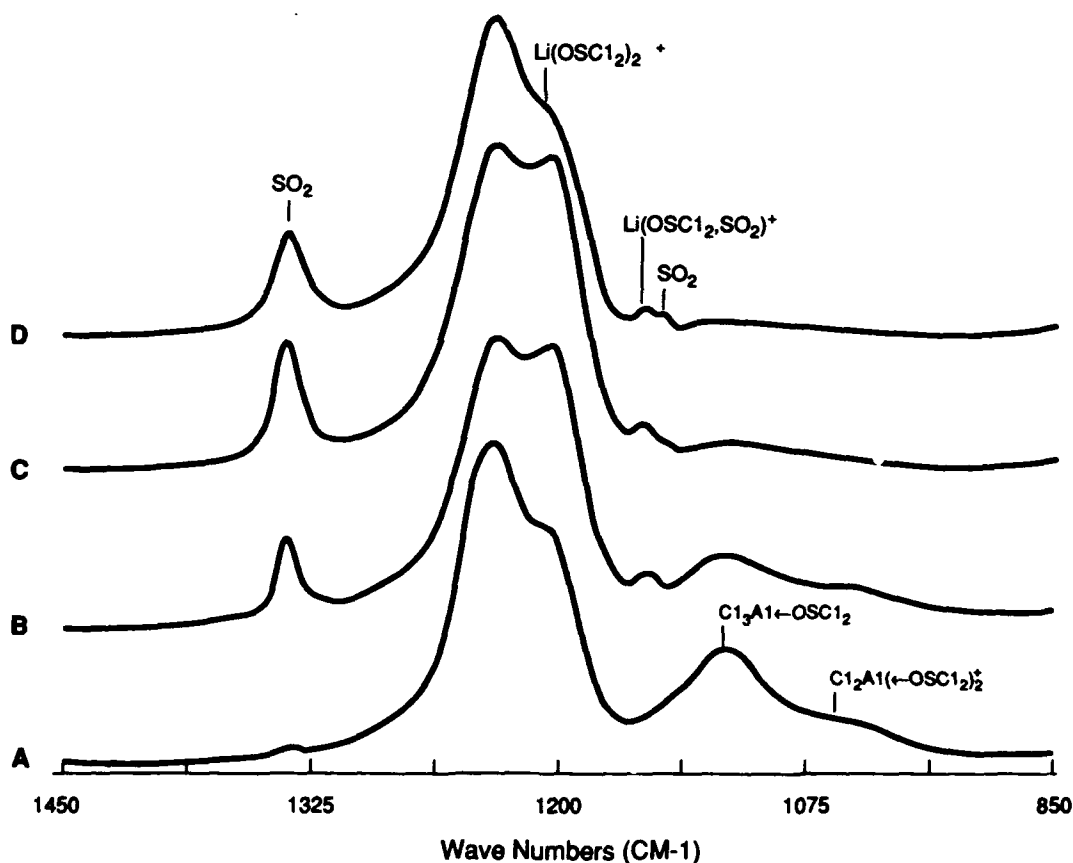
Figure 16.   The 900–1500 cm^{-1} IR spectral region of cathodically polarized $Au/$ 4.0 M $AlCl_3$ and 0.5 M $LiCl$ in $SOCl_2$. Overpotentials vs $Ag/AgCl$: (a) 0.0 V, (b) -0.6 V, (c) -0.9 V, (d) -1.5 V (Mosier-Boss et al., 1991).

31

2.6.6.2. Relaxation Techniques. The addition of a small amount of $LiCl$ to the $Pt/AlCl_3 - SOCl_2$ system was found to greatly modify the reaction path of $AlCl_3 - SOCl_2$ electroreduction as shown in figure 17. With the addition of 0.1 M $LiCl$ to the $Pt/$ 3.0 M $AlCl_3$ in $SOCl_2$ system, a new cathodic peak due to $Li(\leftarrow OSCl_2)_2^+$ electroreduction is observed in the cyclic voltammogram shown in figure 17a. By comparing the cyclic voltammograms for that of the $Pt/AlCl_3 - SOCl_2$ system, figure 13a, with that for the $Pt/AlCl_3 - LiCl - SOCl_2$ system, figure 16a, it can be seen that the reoxidation of P_2 is suppressed in the presence of $LiCl$ as is the autocatalytic reaction, eq. (IV). The presence of $LiCl$ also dramatically suppresses the catalytic reactions occurring in the reaction layer as shown by the charging and relaxation curves obtained from the galvanostatic and potentiostatic pulsing experiments, figures 18a and 18b, respectively. In the charging potential/time curve shown in figure 18a, the potential is observed to rapidly fall off to more negative values, indicating the flux of the electroactive species cannot keep up with the electrons being forced across the electrode/electrolyte interface. This contrasts the potential/time response observed in the $Pt/AlCl_3 - SOCl_2$ system, figure 14a. Furthermore, it takes significantly longer for the interphase of the $Pt/AlCl_3 - LiCl - SOCl_2$ system to return to rest conditions after charging as shown in figure 18a. These results imply that the products of $Li(\leftarrow OSCl_2)_2^+$ electroreduction, i.e., $LiCl$ and $Li(OSCl_2, SO_2)^+$, act as a barrier to the diffusion of onium ion and $Li(\leftarrow OSCl_2)_2^+$ from the bulk electrolyte. It is well known that $LiCl$ is not soluble in $SOCl_2$ and will precipitate on the electrode surface forming a passivating layer. However, in the presence of $Cl_3Al \leftarrow OSCl_2$ and onium ion, the $LiCl$ will be scrubbed off the electrode surface to form $AlCl_4^-$ and $Li(\leftarrow OSCl_2)_2^+$. This may, in part, explain why it takes longer for the interphase to return to rest conditions after charging.

2.6.6.3. Summary of Events; Practical Electrolytes. Figure 17b shows a cyclic voltammogram obtained for a neutral electrolyte off *glassy C*. Similar cyclic voltammograms have been obtained for Pt, Au and $n - Si$ electrodes. These results indicate that the electroreduction of $Li(\leftarrow OSCl_2)_2^+$ is irreversible. This is supported by MO calculations. The ΔH_f of $Li(\leftarrow OSCl_2)_2^+$ is -56 kcal mole^{-1} whereas for the neutral species ΔH_f is -211 kcal mole^{-1}. Therefore, one would expect the first

32
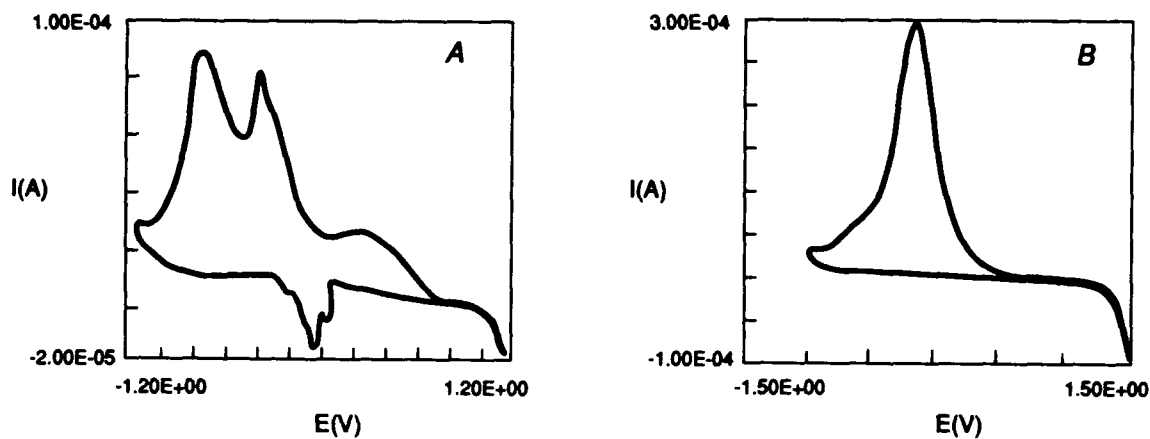
Figure 17. Cyclic voltammograms of the $AlCl_3 - LiCl - SOCl_2$ system. (a)
System: $Pt/$ 3.0 M $AlCl_3$ and 0.1 M $LiCl$ in $SOCl_2$; $v = 10$ mV s^{-1},
(b) $Glassy\ C/$ 3.0 M $AlCl_3$ and 3.0 M $LiCl$ in $SOCl_2$; $v = 10$ mV s^{-1} (Mosier-
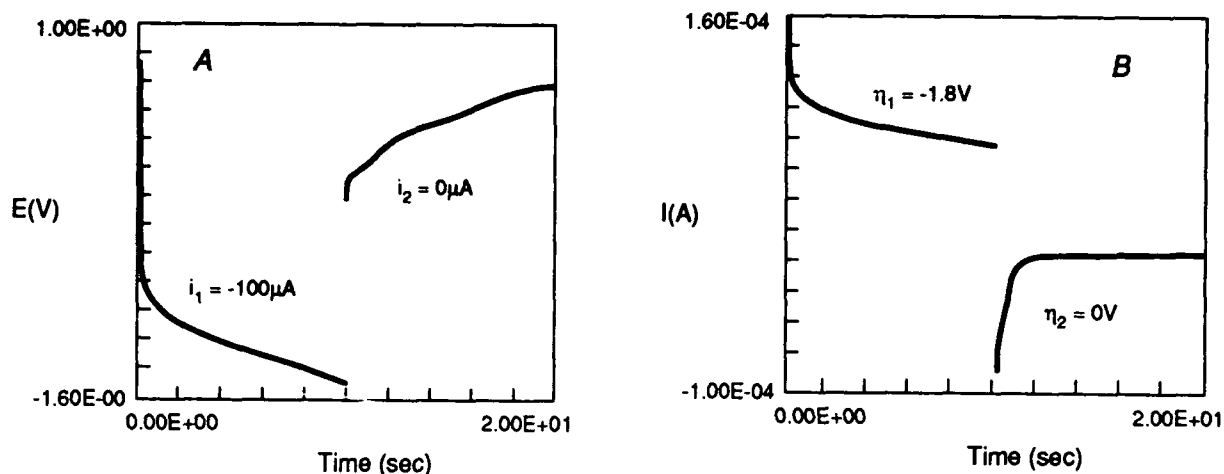Boss et al., 1991).
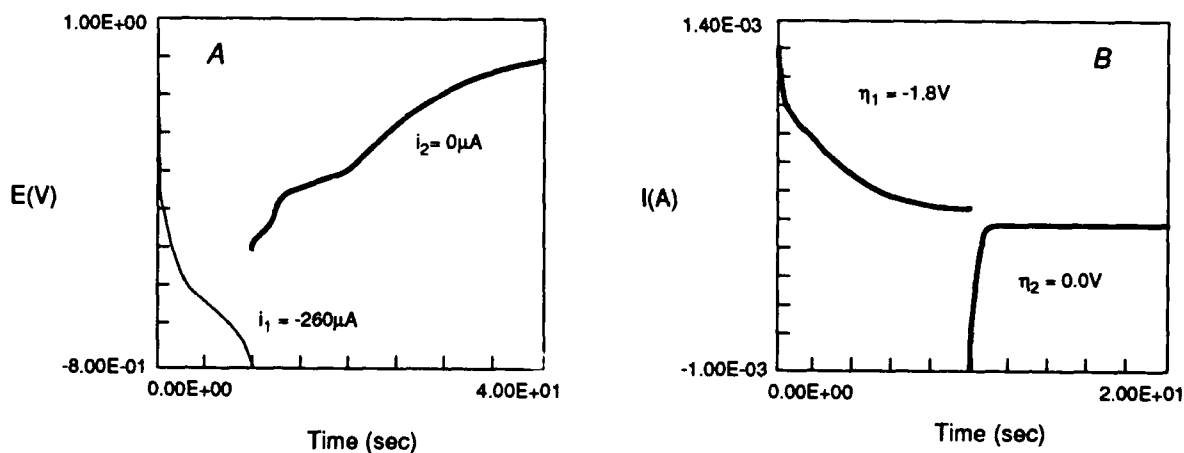
Figure 18. (a) Potential/time behavior and (b) current/time behavior across a charging
and relaxing interphase. System: $Pt/SOCl_2$–3.0 M $AlCl_3$–0.1 M $LiCl$ (Mosier-
Boss et al., 1991).

33

electron transfer, shown in eq. (VII), to be irreversible.

$$Li(\leftarrow OSCl_2)_2^+ + e^- \rightarrow 2Li(\leftarrow OSCl_2)_2 \, . \tag{VII}$$
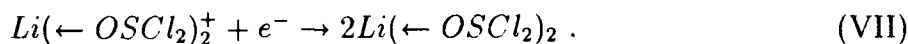
The MO calculations for the second electron transfer would not converge indicating this species is extremely unstable. Apparently, as soon as the electron is transferred to the neutral the species falls apart into the products of electroreduction on the electrode. This may contribute to the passivation observed in $Li/SOCl_2$ cells. Furthermore, there is no indication in the cyclic voltammograms of autocatalytic activities on or near the electrode surface as was observed for the $Me/AlCl_3 - SOCl_2$ system.

3. MODELING EXERCISES

3.1. INTRODUCTORY COMMENTS

The operation of a battery, module, cell, or even a selected functional element is a dynamic event in which the participating processes occur within a well-defined reaction space. This, in turn, implies the existence of constraints on the individual processes. These processes are interactive and can be described by a set of precise mathematical statements. In practice, the difficulty lies in formulating an acceptable model that reflects physical reality and, yet, at least in the preliminary stage, yields solutions in a closed form. This requirement is met only in a few isolated cases, primarily because of the nonlinearity of the function relating current to overpotential.

Modeling can describe a large number of operational situations. For the purpose of illustration, we have selected several examples comparing computed results with experimental data. Those presented here were selected because of their concerns with the cell performance and safety of operation that were pertinent to the $Li/SOCl_2$ battery development effort of the 1980s. They are also limited to the battery designed for high-discharge rates and operating under conditions that tend to maximize the extractable energy content at high-power output. The conditions addressed are electrochemical processes; thermal management, including catastrophic thermal runaway; and intercell currents and their respective effects on the performance and safety of a module and assembly of modules.

34

3.2. $Li/SOCl_2$ CELL – SCHEMATIC

Realistic modeling requires information on the specification of the mode of operation and the description of the physical constraints under which the battery operates. To illustrate, a section of a $Li/SOCl_2$ battery of bipolar construction is shown in figure 19. Each cell contains four functional elements: the negative electrode, the positive electrode, the electrolyte, and a porous separator. The separator serves as a reservoir for the electrolyte and provides an ionically conductive path. A thin metal foil functions simultaneously as a chemical barrier and an electronic conductor between cells. Processes that occur in an operating cell are diffusion of the participating species toward the electrode surface, adsorption on the electrode surface, charge transfer, desorption of reaction products and diffusion of the products away from the electrode surface. The flow of electrons in an external circuit completes the process.

3.3. CELL/BATTERY MODELING – ELECTROCHEMICAL PROCESSES

The first comprehensive modeling of the dynamics of the discharging $Li/SOCl_2$ has been presented by Tsaur and Pollard (1984a and 1984b). In their model, the mathematical statements describing the material balances, flux relations in the electrolyte phase, as well as the Faraday's and Ohm's laws, are unambiguous. However, the formulation of the governing equations involving electrode polarization and the active specific surface in the positive electrode require more care. The exponential form of the kinetic relation usually employed is the Butler-Volmer equation

$$sj = sj_0 \left[\exp(\alpha_a F\eta / RT) - \exp(-\alpha_c F\eta / RT) \right] \tag{10}$$

where s is the specific surface area and j_0 is the exchange current density. This form of the kinetic relation applies only within a rather narrow range of overpotentials and selected group of electrochemical systems. Other forms of kinetic expressions better represent the current/potential relation of the reduction of $SOCl_2$. Nonetheless, eq. (10) has been used because its exact form does not substantially alter the predicted trends; however, the numerical values of the parameters s and $\alpha's$ are essential to evaluate the cell lifetime.

Because of the profound effect that the specific surface area exerts on the cell
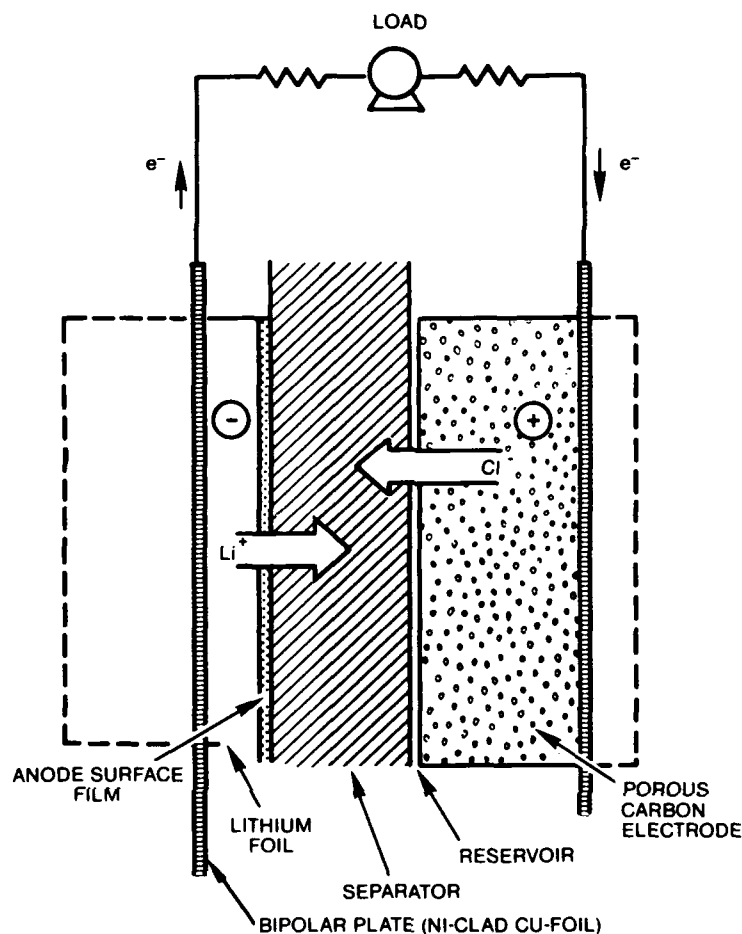
Figure 19. Cross section of a $Li/SOCl_2$ cell.

lifetime and because it can, to a certain degree, be manipulated experimentally, it is necessary to assign a functional form relating it to the amount of charge transferred locally. Initially, an empirical expression, which assumes instant precipitation of $LiCl$ crystallites resulting in a permanent passivation of the electrode surface, was used

$$s(l,t) = s^0 \left[1 - \left(\frac{v}{\epsilon^0_{p(l,t)}} \right)^{p(l,t)} \right] \qquad (11)$$

where ϵ is the void fraction, v is the volume fraction of the precipitate and the exponent $p(l,t)$ is related, in general terms, to the morphology of the $LiCl$ cystallites. The assumption of an instantaneous precipitation of $LiCl$ is, however, doubtful although good agreement has been observed, in particular concerning the optimum electrolyte

36

composition and the thickness of the positive electrode. Later, Tsaur and Pollard (1986) employed a more realistic assumption, that of the solution-precipitation path. To sustain the charge transfer, reactants must be brought to the reaction layer and the products removed. As the charge transferred locally increases and the solubility limits are exceeded, the nucleation process commences and proceeds with the rate given by

$$r_n = k_n[(c_1 c_2) - K_s] \qquad (12)$$

where k_n is the rate constant for the nucleation process, $(c_1 c_2)$ represents the local supersaturation, and K_s is the solubility product. With further passage of current, the growth of crystallites and formation of new nuclei occur simultaneously. The rate of crystallite growth obeys

$$r_g = k_g v^m[(c_1 c_2) - K_s] \qquad (13)$$

so that the precipitation rate constant, k, for the formation of a solid phase and, *ipso facto*, for the removal of Cl^- from the reaction space, is given by

$$k = k_n + k_g v^m. \qquad (14)$$

Solving eq. (14) for v and substituting into eq. (11), yields

$$s(l,t) = s^0 \left\{ 1 - \left[\frac{\left(\frac{k - k_n}{k_g} \right)^{m^{-1}}}{\epsilon^0_{p(l,t)}} \right]^{p(l,t)} \right\}. \qquad (15)$$

The term v^m, in eqs. (13) and (14), describes in general terms the crystal surface available for growth, as does the parameter $p(l,t)$ in eq. (11), the exponent m also reflects the morphology of the growing crystallites: large values of m characterize crystallites with a small surface-to-volume ratio and vice versa. Thus, spherical particles would have a large m while needle- and plate-like growths would be characterized by small m. Equation (15) indicates that the rate of nucleation and crystallite growth, together with the morphology of the precipitate, strongly affect the cell lifetime. Calculations carried out for the $Li/SOCl_2$ cells imply that the cell lifetime can be extended by fast precipitation of $LiCl$. Conceivably, in the limit, the $Li/SOCl_2$ cell lifetime could be doubled (Tsaur & Pollard, 1986).

The importance of the m exponent cannot be overstated. For a specific positive electrode structure, an increase in j_0 tends to decrease cell lifetime. However, an opposite effect was found upon the addition of transition metal phthalocyanines and other additives. While the catalyst certainly affects the exchange current density, its role is much more complex since cell modeling and experimental evidence suggest that the extension of the cell lifetime is connected with a change in the morphology of the emerging new solid phase (Nowak et al., 1988).

3.3.1. Model Predictions vs. Experiment

Experimental and computed galvanostatic discharge curves of a $Li/SOCl_2$ cell employing an acid electrolyte are shown in figure 20. The hump, at the beginning of the discharge, is attributed to $SOCl_2$ reduction in an acid electrolyte, i.e., the width of this hump is proportional to the amount of excess $AlCl_3$ initially present in the discharging cell (for a detailed discussion of the mechanism refer to section 2.6). The slope of the central region of the $U_c(i, t)$ curve depends primarily on the properties of the $LiCl$ film at the negative electrode surface. Toward the end of the discharge, after approximately 65 percent of the available material has been used, the shape of the $U_c(i, t)$ curve is governed by the events occurring within the porous structure of the positive electrode. In agreement with observation, neither the slope nor the cell voltage are sensitive to the sj_0 product; however, this does not apply to the cell lifetime, viz., the larger the sj_0 product, the shorter the lifetime. The effect of the sj_0 product on the cell lifetime can be examined with the aid of an electric circuit analog (Szpak, 1991).

3.3.1.1. Transfer Current Density. In the presence of excess $AlCl_3$, the calculated charge transfer current density profile is dictated by a balance between the effect of the electrode matrix to solution conductivities ratio and the sj_0 product. For the reduction of $SOCl_2$, with $j_0 = 6 \times 10^{-7}$ A cm^{-2} (Madou & Szpak, 1984) the sj_0 product is low enough to force the reaction zone deeper into the electrode porous structure (Tsaur & Pollard, 1986; Szpak, 1991). The evolution of the current density (cd) distribution with time is illustrated in figure 21. Initially, the distribution is normal and characteristic of low matrix resistance (Szpak & Driscoll, 1983). With the passage of time, a change in the reaction path occurs due to the depletion of $AlCl_3$ near the front face while in the back of the electrode the solution remains acidic. The result is the appearance of a minimum in the cd curves, curves 2, 3,
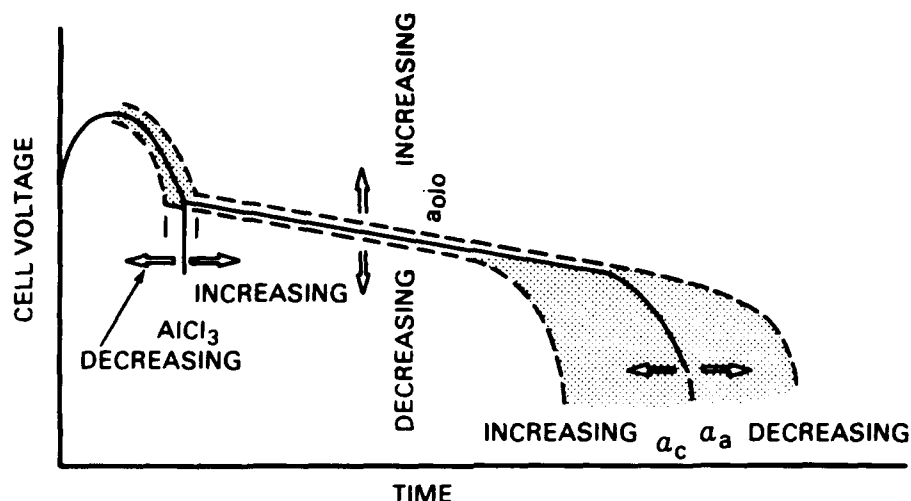
Figure 20. Schematic representation of a galvanostatic discharge curve; effect of change in kinetic parameters (Driscoll et al., 1985).

etc., which becomes more pronounced and penetrates deeper into the structure with further passage of time.

Reaction rate distribution in porous electrodes cannot be measured directly. Thus, one can only verify the calculated profiles indirectly, e.g., by examining the distribution of precipitated $LiCl$ within the cathode structure. Electron dispersive x-ray analysis (EDAX) of electrodes from partially discharged cells employing acid electrolyte was performed elsewhere (Szpak & Driscoll, 1983; Driscoll et al., 1985). These results did show that the charge transfer reaction occurs initially in the electrode segment close to the electrode/separator interface, as suggested by the model. Experimental profiles at later times, show the development of a weak minimum which, however, does not penetrate as deep as calculated. The likely reason for this discrepancy is the assumed relation between active surface area and the porosity.

3.3.1.2. Optimum Electrolyte Composition. Transport properties in the electrolyte phase are the most important input data in calculating the electrolyte concentration needed to optimize the cell lifetime. Excellent agreement between the model and experimental data is obtained for the relationship between the initial electrolyte concentration and the cell lifetime. As shown in figure 22, the optimum cell lifetime for neutral solutions is predicted to be at a concentration of 1.5 M $LiAlCl_4$ while lab-
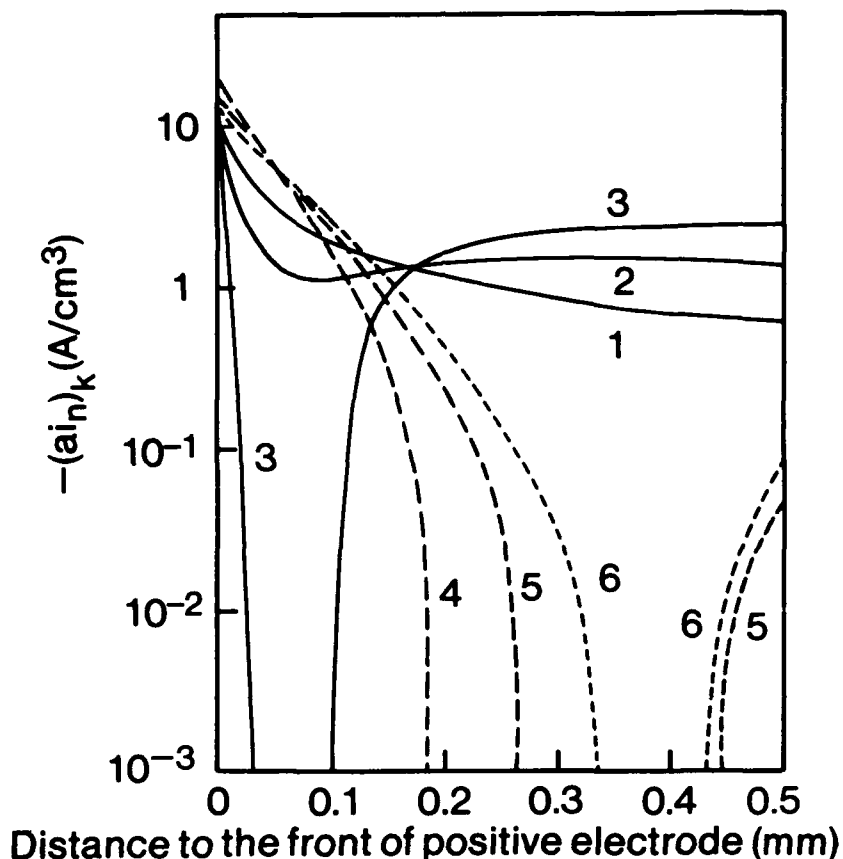
Figure 21. Reaction distribution in the positive electrode at different utilizations: (1) 0.6%, (2) 1.49%, (3) 1.79%, (6) 11.36% (Tsaur & Pollard, 1984b).

oratory data show that 1.6 M is the optimum concentration. This excellent agreement has been realized only after the relevant data were obtained (Szpak & Venkatasetty, 1983).

3.3.1.3. Cathode Thickness.

On the basis of a large number of experiments, Driscoll (1984) established that the optimum power densities are obtained with cathode thickness between 2.6×10^{-4} and 4.0×10^{-4} m . The calculated effect of the electrode thickness on the cell lifetime for discharge rates comparable to the experimental conditions, shown in figure 23, is in excellent agreement. Evidently, increasing
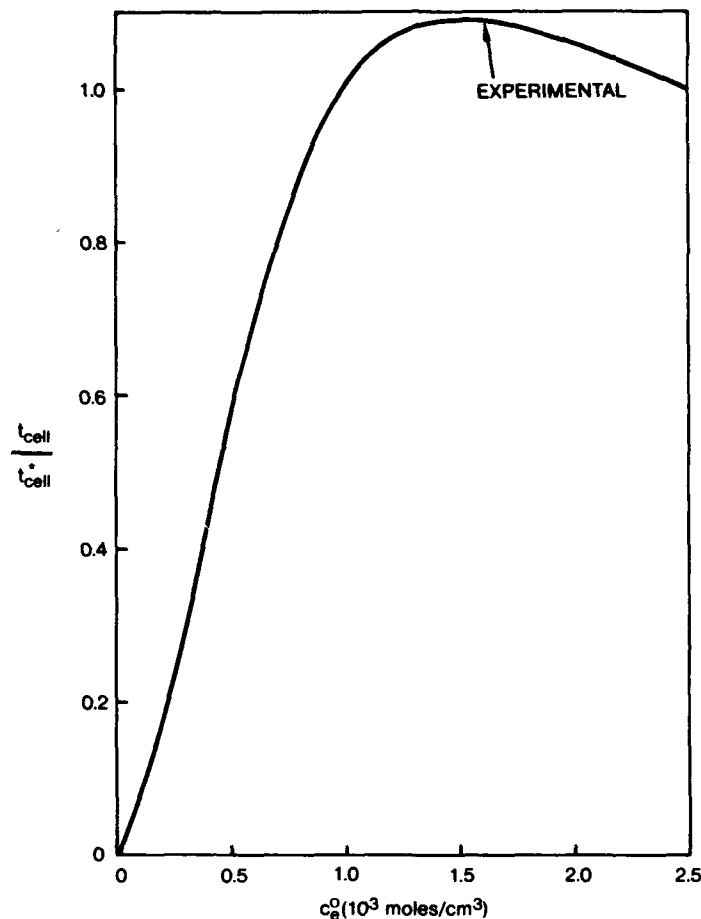
Figure 22. Calculated dependence of cell lifetime on electrolyte composition (Tsaur &
Pollard, 1984a).

the thickness beyond the value of $L_{p2} = 4.0 \times 10^{-4}$ m does not improve cell life-time (or power output) significantly because the reaction does not penetrate the added electrode volume. Such increases would only reduce the volumetric energy and power density of the cell. On the other hand, reducing the thickness below $L_{p1} = 2.6 \times 10^{-4}$ m lowers the cell lifetime dramatically and imposes stringent quality control requirements because, in this region, the lifetime is sensitive to small changes in electrode thickness.

3.3.1.4. Electrode Swelling. Expansion of the positive electrode during cell discharge was first reported by Marincic in a series of papers (Marincic, Epstein, & Goebel, 1975; Marincic, 1976a, 1976b; Marincic & Koffmann, 1976). Somewhat later, Szpak and Driscoll (1983) re-examined this problem. They emphasized the impor-

41
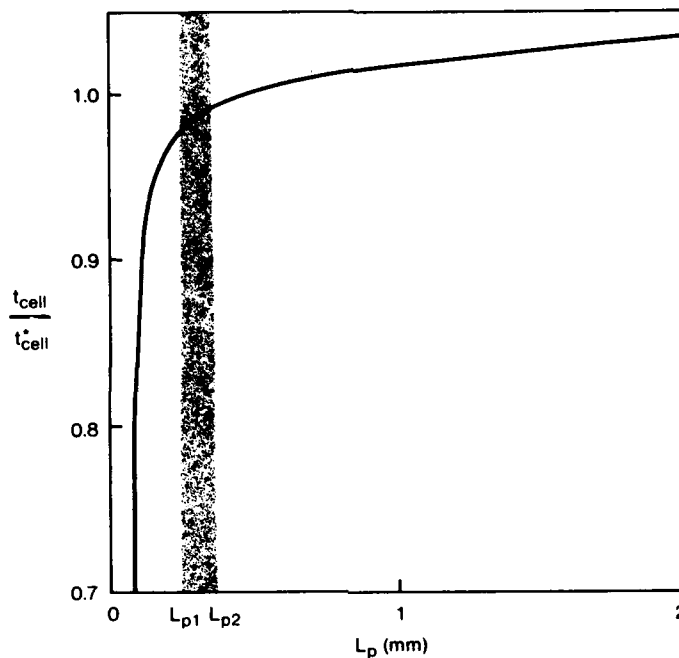
Figure 23. Calculated dependence of cell lifetime as a function of electrode thickness (Driscoll et al., 1985).

tance of porosity and, in particular, pore size distribution and concluded that a 30-percent increase in cell lifetime is possible if space for electrode expansion during discharge is provided. The calculated increase in cell lifetime is much higher, viz., 75 percent, provided that all free space generated in the course of cell discharge can be utilized.

3.4. THERMAL MANAGEMENT

In its simplest form, thermal management requires maintaining the battery temperature within prescribed limits during the course of discharge. Although these limits may vary, the upper limit for a Li battery should not exceed the melting point of lithium if the initiation of highly exothermic reactions is to be avoided. However, the temperature range has not been firmly established as yet. Reportedly, experience with high-rate batteries indicates that 410 K is the highest safe-operating temperature, however, claims have been made that the $Li/SOCl_2$ interface is stable above the melting point of lithium (Babai, Bababigi, & Bineth, 1984).

42

The rate of heat generation in a discharging battery, derived from the first and second laws of thermodynamics, is

$$q = j[U(0) - U(j)] + \sigma \tag{16}$$

where σ is a function representing the rate of heat generation arising from other than purely kinetic processes. Thus,

$$\sigma = \frac{jT}{F} \sum_m \left(\frac{\partial U_m(0)}{z_m \partial T} \right)_p + \sum_n \left(\frac{\partial H}{\partial \xi_n} \right)_{p,T} \frac{d\xi_n}{dt} \tag{17}$$

where the first term is q_{ent} for the m charge transfer processes and the second term is the change in enthalpy arising from the n chemical reactions. This function can be evaluated experimentally and the nature and the magnitude of some of the heat sources assessed (Godshall & Driscoll, 1984). For example, it has been shown that localized heat source due to corrosion of Li in $SOCl_2$ increases with an increase in the discharge current (Szpak & Driscoll, 1987).

Since the total heat generation of a discharging battery is a function of local current density and temperature, eqs. (16) and (17), it follows that, to obtain the temperature profiles within the interior of an operating battery, eqs. (18) and (19) must be solved simultaneously

$$\lambda \nabla U + j = 0 \tag{18}$$

$$c_v \frac{\partial T}{\partial t} = \mathbf{div}(\kappa \nabla T) + \sigma. \tag{19}$$

Equations (18) and (19) are coupled by the dependence of λ on temperature and of σ on both temperature and solution conductivity. In practice, it is convenient to express the heat generation in terms of discrete sources, i.e.,

$$\sigma = \sum_n \sigma_n$$

with the main source being attributed to the joule heating in the cell functional elements, i.e., polarization of individual electrodes and internal cell resistance. On occasion, additional heat sources may be identified, e.g., due to intercell currents always present in the reserve type design and chemical reactions between the cell components and reaction products.

The boundary and initial conditions must reflect the mode of battery discharge and be consistent with battery design. Parnell and Szpak (1985) reported on the temperature distribution within a module consisting of a large number of identical, disc-shaped cells of bipolar construction. In such a design, heat transport in the axial direction is minimal, except at the terminal cells. In practice, this leaves only one spatial dimension to consider.

3.4.1. Model Predictions vs. Experiment

In contrast to batteries containing aqueous electrolytes where solutions of eqs. (18) and (19) with constant coefficients yield satisfactory results, realistic analysis of the $Li/SOCl_2$ battery requires that these coefficients reflect changes that have occurred in the electrolyte phase, in particular, changes in solution composition and temperature. The use of average values for thermal and electrical properties results in higher cell temperatures and larger temperature gradients. The practical implications are obvious: uniform temperature profile indicates uniform cd distribution and, consequently, uniform consumption of reactants and uniform reduction in the porosity of the positive electrode. In addition, because of lower cell temperature, either higher cell currents or, alternatively, longer discharge times can be realized before the cell interior temperature exceeds an a priori set limit. Parnell and Szpak (1985) suggested that to obtain agreement with experiment, the model must consider changes in the individual elementary processes that take place during the cell discharge, i.e., changes in the coefficients and sources in eqs. (18) and (19). This inclusion renders the differential equations nonlinear and forces a numerical solution of the relevant equations. Using this procedure, good agreement between the computed and observed temperature has been obtained, figure 24. They also found that in the cathode limited cells the prime heat source resides in the cathode structure when the cathode porosity becomes less than ca 20 percent.

3.4.1.1. Activation Under Load. As a rule, a high-rate, reserve battery is activated at open circuit. There are, however, operational situations requiring activation under load. To simulate this requirement, the rate of electrolyte penetration into the cell must be specified. Parnell and Szpak (1985) expressed the penetration rate in the form of the time-dependent increase in the electrode active area by an arbitrarily selected expression,

$$a(t) = a_{max}(1 - e^{-\beta t}) \tag{20}$$

44
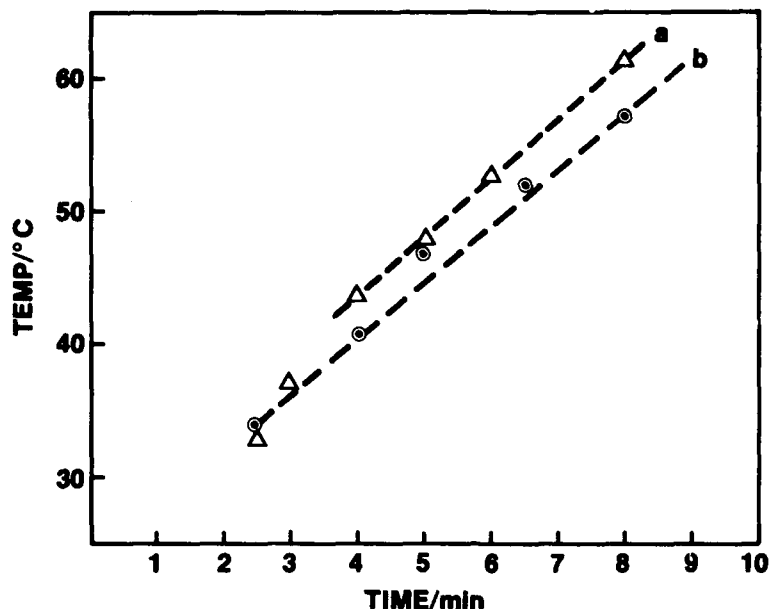
Figure 24. Computed and measured temperatures at the inner cell diameter:
(a) experimental, (b) computed for variable coefficients (Parnell & Szpak, 1985).

where the β parameter determines the rate at which the active segment of a cell grows or, alternatively, the rate at which local cd decreases with time.

A plot of temperature versus time at the point of the electrolyte entry is shown in figure 25. Evidently, the slower the fill rate, the higher the initial temperature. When the cell is completely filled, the effect is less and is indistinguishable after about 6 minutes. The major conclusion concerning safety is that activation under load should be discouraged unless precautions are taken to assure a fast and reliable fill.

3.5. CELL/BATTERY MODELING – CATASTROPHIC THERMAL RUNAWAY

In this system, designed for high rates of discharge, violent reactions have occurred during the development process. A number of explanations have been offered, but with very little substantiating data except for clear cases of thermal runaway. Szpak, Gabriel, and Driscoll (1987) examined the initiation and progress of the catastrophic thermal excursion by considering a heat source extrinsic to the normal mode of cell operation, i.e., heat source $q_1(r)$ representing joule heating arising from an internal

45
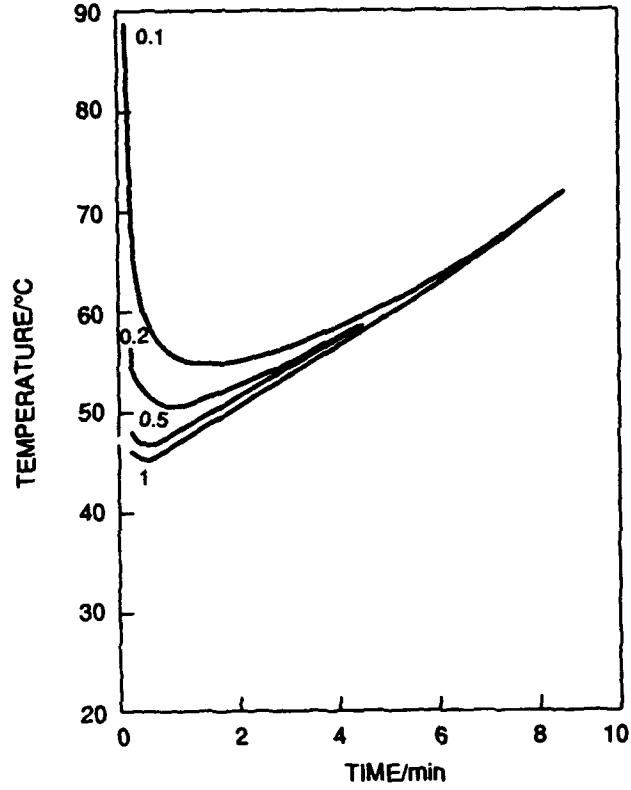
Figure 25. Temperature/time relationship as a function of filling rate under load (Parnell & Szpak, 1985).

short circuit. As the temperature rises locally above the critical temperature T_{cr}, this source activates the intrinsic , $q_2(r,t)$ associated with the exothermic reaction involving lithium and other cell components e.g. , $SOCl_2$

$$q_2 = -\Delta H_r k_0 c \exp(-E/RT)\Phi(T - T_{cr}). \tag{21}$$

Equation (21) expresses the strength of the intrinsic heat source as a product of the heat of reaction, $-\Delta H_r$, and the reaction rate. The Heaviside unit step function is employed to account for the protective action of the $LiCl$ film, always present whenever metallic Li is in contact with $SOCl_2$, i.e.,

$$\Phi(T - T_{cr}) = 0; \text{ for } T < T_{cr}$$

$$\Phi(T - T_{cr}) = 1; \text{ for } T > T_{cr}.$$

46

The concentration term in eq. (21) must satisfy the diffusion equation

$$\frac{\partial c}{\partial t} = \mathbf{div}(D\nabla c) - k_\mathrm{o} c \exp(-E/RT) \tag{22}$$

where the sink term is the reaction rate. To complete the mathematical description, the initial and boundary conditions must be specified. They assume as initial conditions uniform temperature and solution concentration and the boundary condition at $r = a$ are the fluxes given by eqs. (23) and (24)

$$-\lambda\frac{\partial T}{\partial r} = h_1(T - T_0), \tag{23}$$

$$\frac{\partial c}{\partial r} = 0. \tag{24}$$

These conditions allow heat transport in the radial direction but disallow mass transport across this boundary.

Evolution of temperature profiles with time following the activation of the extrinsic heat source are shown in figure 26. At first, the temperature profiles are those associated with centrally localized heat sources, curves 1 and 2. As soon as the critical temperature is exceeded, the temperature profile changes to that arising from two sources: $q_1(r)$ and the time-dependent intrinsic source $q_2(r,t)$ causing the distortion in temperature profiles, curves 3 and 4. With a further passage of time, the temperature profiles take on a skewed, spike-like appearance, indicating the narrowing of the reaction zone and a rapid increase in the heat intensity, curves 5 and 6, followed by a period of stabilization, curves 7 and 8.

The catastrophic event is characterized by a period of induction, followed by ignition and propagation of a narrow, very hot zone of burning Li with temperatures well above the melting points of aluminum and stainless steel. An example of thermal runaway caused intentionally in a 2000-Ah cell is shown in six photographs in figure 27. An analysis of numerous videotapes of battery ventings was consistent with these features: the existence of an induction period, followed by ignition, propagation of a reaction zone and flame extinction which, as a rule, follows the venting of a cell. Furthermore, the evolution of temperature profiles using liquid crystals deposited on an external cell surface follows such a sequence (Driscoll & Szpak, 1985).
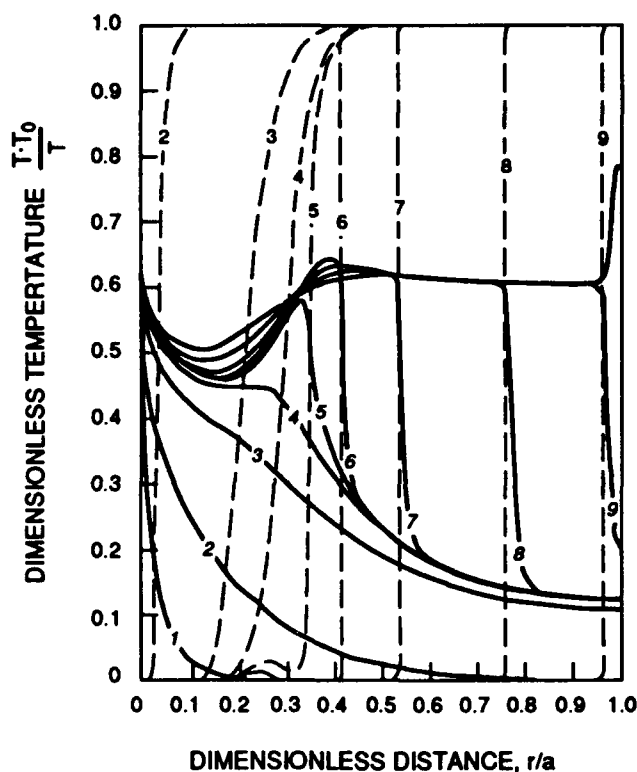
Figure 26. Evolution of temperature (solid lines) and concentration (dashed lines) following the activation of an extrinsic heat source (Szpak et al., 1987).

3.6. MODULE/BATTERY MODELING – INTERCELL CURRENTS

By definition, an intercell current is an ionic current that originates in one cell and terminates in another (Szpak, Gabriel, & Driscoll, 1984). This current does not perform any useful work; on the contrary, it is a parasitic current resulting not only in a loss of power but also in a loss of capacity, and may contribute to the premature failure of individual cells by the formation of passive films, dendritic growths, or by the corrosion of structural parts.

In a discharging cell, two processes occur at the negative electrode: charge transfer and transport of Li^+ ions through the protective $LiCl$ film. The thickness of this film depends on the electrolyte composition and the rate of battery discharge. While the situation at the positive electrode is far more complex, we assume that each elementary process obeys a generalized Ohm's law, i.e., it can be described by an

48
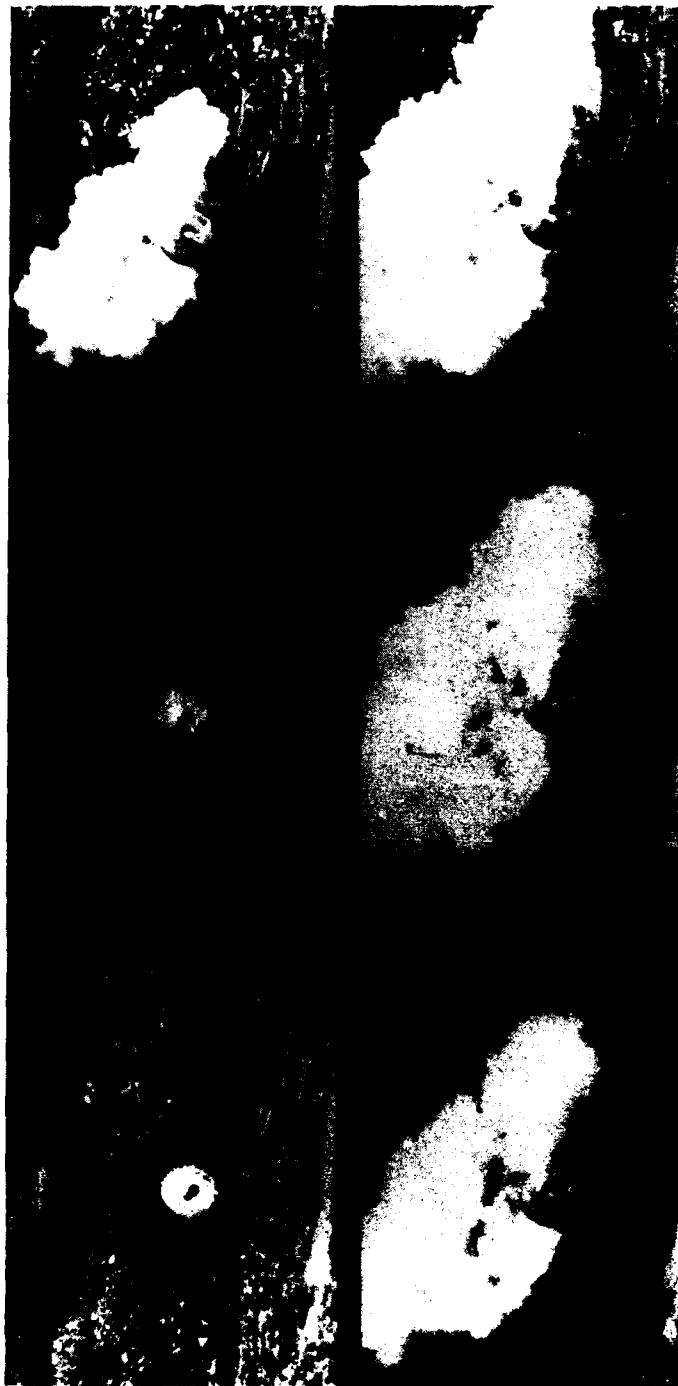
Figure 27. Illustration of the progress of catastrophic thermal runaway in a 2000-Ah $Li/SOCl_2$ cell (Szpak et al., 1987).

equation of the type, $j = k\chi$, relating the flux j to the driving force, χ, through a phenomenological rate constant, k. Such a description permits the construction of an electric circuit analog, shown in figure 28, to represent the overall process occurring in the cell interior. It is noteworthy that this type of representation has served as the starting point in practically all cases reported in the literature (Ksenzhek & Koshel, 1970, 1971; Nesterov, Razevig, & Korovin, 1974; Onishchuk, 1972; Thiele, Scheiff, & Matschiner, 1983; Kaminski & Savinell, 1983). This approach provides a simple means of treating intercell currents that yields results in agreement with observation.
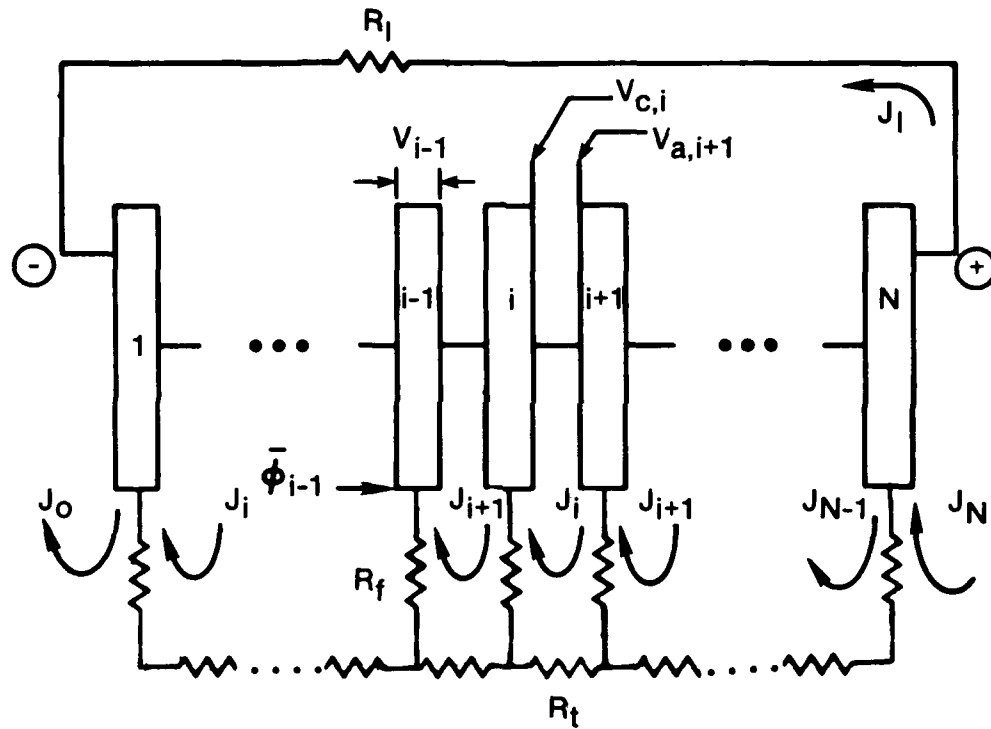
Figure 28. Battery representation by equivalent electric circuit analog. V_{i-1}': cell voltage; Φ_{i-1}: potential at manifold inlet to $j - 1$-th cell; J_i: circulating current; J_l: loop current in an external resistor R_l; R_f: manifold feedline resistor; R_t: equivalent feed-tube resistor. Control volume indicated by dashed line (Szpak et al., 1984).

Assuming the constancy of phenomenological coefficients associated with the ionic current and replacing them with equivalent resistances, $R_{t,i}$ and $R_{f,i}$, the loop equations for the current, J_l and an external load, R_l, are given by

$$J_l R_l = \sum V_i \ ; \ i = 1, 2, 3, ..., N. \tag{25}$$

50

The circulating currents in the fill path, J_i, obey

$$-J_{i-1}R_{f,i} + J_i(R_{f,i} + R_{f,i+1} + R_{t,i}) - J_{i+1}R_{f,i+1} = \Phi_{i+1} - \Phi_i \; ; \; i = 1, 1, ..., N-1. \quad (26)$$

Additional statements needed to complete the circuit description are: circulating currents in the zero-th and N-th segments, $J_0 = J_N = 0$; the bipolar plate is equipotential, i.e., $V_{a,i+1} = V_{c,i}$; the total anodic current, e.g., in the i-th cell is a sum of the load current J_l and the circulating current J_{i+1}; and the intercell current I_i is the difference in the circulating currents in the i-th and i-1 th segments, $I_i = J_i - J_{i-1}$.

Equations (25) and (26) were formulated for a discrete model. They can be reformulated for a continuous model that has the advantage of admitting solutions in a closed form (Ksenzhek & Koshel, 1970, 1971). The selection between these approaches depends upon the desired accuracy and the specifics of the electrochemical system. For example, the continuous model may not be relevant for calculating intercell currents in batteries where operation terminates due to blocked electrode surface (Szpak et al., 1984). For the simple case, that with constant coefficients, solutions to eqs. (25) and (26) can be obtained in a closed form, viz.,

$$J_l = \frac{N(1 - \xi)U}{R_l + N(1 - \xi)R_z} \quad (27)$$

$$J_i = J_p \left(1 - \frac{\lambda^{N-i} + \lambda^i}{\lambda^N + 1} \right) ; i = 0, 1, 2, ..., N \quad (28)$$

$$I_i = J_p \left(\frac{\lambda - 1}{\lambda^N + 1} \right) \left(\lambda^{N-i} - \lambda^{i-1} \right) \; i = 1, 2, ..., N \quad (29)$$

where

$$J_p = \frac{R_l U}{R_1 + N(1 - \xi)R_z}$$

$$\lambda = 1 + Y + \sqrt{Y(2 + Y)} \; ; \; Y = \frac{R_t + R_z}{2R_f^*}$$

$$\xi = \frac{R_z}{R_t + R_z} \left[1 - \frac{(\lambda^N - 1)(\lambda + 1)}{N(\lambda^N + 1)(\lambda - 1)} \right]$$

51

and

$$R_j^* = R_f + R_p - R_z \left(\frac{\sigma^2}{\sigma_a \sigma_c}\right).$$

For a given number of cells, the relative distribution of both the circulati d intercell currents depends on the value of the parameter λ. This parameter is a function of the ratio $(R_l + R_z)/R_j^*$, i.e., it depends on the battery design as well as on the properties of the electrolyte and the kinetics of the charge transfer reaction. In particular, for large values of R_t, λ will be large while for large values of R_j, λ will be near unity. In the latter case, the tails of the intercell current distributions extend into the battery with a shape depending on the number of cells. In contrast, for large λ , the terminal cells carry most of the intercell currents independently of the number of cells in a module. In practice, it is desirable to have large R_t because it minimizes the circulating currents, J_i, which means the intercell currents in the terminal cells are also small and the current reversal does not occur, i.e., the dendritic growth and the corrosion of bipolar plates is avoided.

Often, to meet performance requirements, a multimodule battery is assembled. An example of a multimodule assembly is shown in figure 29. In general, an assembly can contain either an odd or an even number of modules which, when connected in parallel, share positive/positive, $(+/+)$, and negative/negative, $(-/-)$, interfaces. In an assembly of an odd number of modules, only one configuration is possible, viz., one positive and one negative assembly terminal. For an even number of modules, two configurations are possible — both assembly terminals are either positive or negative.

The formulation of governing equations is the same as for the single module except for the matching conditions at the $(+/+)$ and the $(-/-)$ interfaces between the neighboring modules. To avoid ambiguity, quantities associated with a module are identified here by a preceding index in parenthesis, e.g., $^{(m)}J_l$ denotes the load current generated by the $m-$ th module. For an $M-$ module battery, the potential across the load is,

$$V = R_l \sum_{m=1}^{M} {}^{(m)}J. \tag{30}$$

As before, the circulating currents in terminal cells of a battery are zero. However, in terminal cells of a module, i.e., at coupling interfaces between modules, the circulating
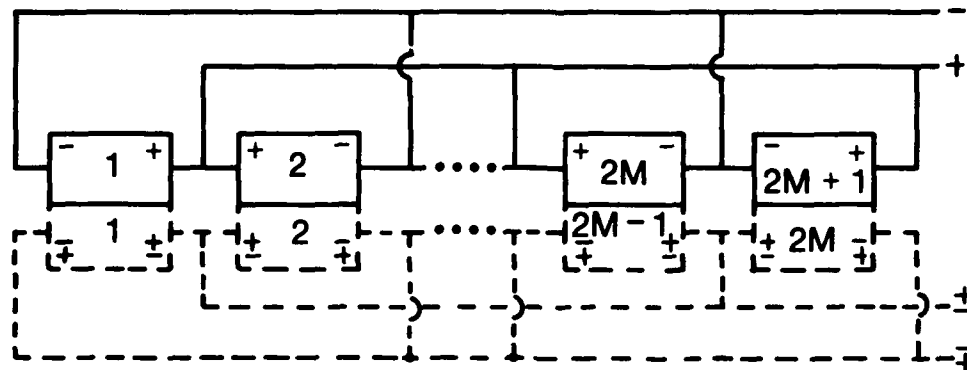
Figure 29. Schematic representation of a multimodule battery. (a) solid lines for an odd number of modules, (b) dashed lines for an even number of modules (Szpak et al., 1990).

currents are not necessarily zero; in particular they are

$$^{m-1}J_N = -^{(m)}J_N = J_{(m-1),(m)}$$

$$^{m}J_0 = -^{(m+1)}J_0 = J_{(m),(m+1)}$$

where $J_{(m-1),(m)}$ and $J_{(m),(m+1)}$ are the coupling currents between modules. The mathematics is straightforward but somewhat lengthy. The reader is referred to original work (Nesterov et. al., 1974).

3.6.1.   Model Predictions vs. Experimental Observation

A number of specific situations can be examined. Here, we limit the discussion to the distribution of circulating and intercell currents, conditions leading to current reversal, and reduction of power output. We complete the discussion by examining the behavior of a multimodule battery.

3.6.1.1. Distribution of Intercell and Circulating Currents. The distribution of intercell and circulating currents in a $Li/SOCl_2$ multicell module is shown in figure 30. It is seen that, independent of the number of cells in the module, maximum circulating currents are at the central cells, whereas the intercell currents are largest at the ends. Also, the intercell currents change their signs from positive to negative, i.e., from entering the cell at the negative end of a module to exiting the cell at

53

the positive ends. Evidently, in a module having a small number of cells, all cells generate intercell currents. However, as the number of cells increases, the centrally located cells contribute less and, in the case of an 80-cell module, the majority of cells contribute nothing at all to the intercell current. The practical implication is that, as the number of cells increases, losses in the extractable energy approach a limiting value and that most of the module suffers little, if any, from reactant underutilization. The shape of the distribution curve of the intercell current implies that a battery may be viewed as consisting of segments, viz., a central segment where cells operate with equal anodic and cathodic currents and segments involving terminal cells where the underutilization of electroactive materials occurs.
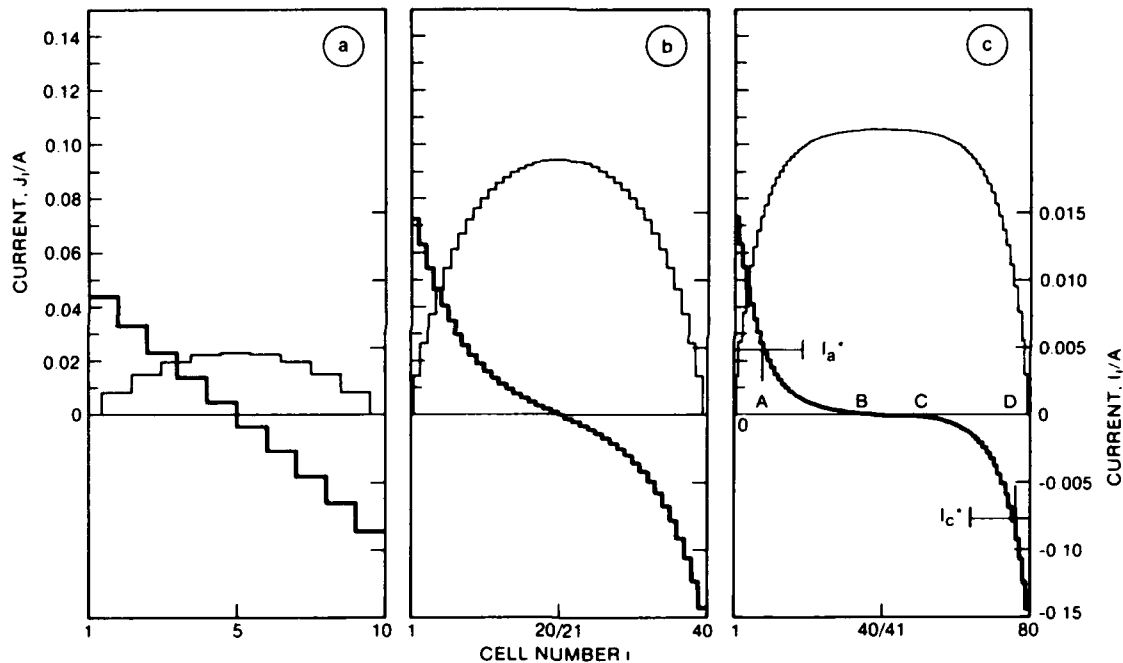
Figure 30. Distribution of circulating (thin line) and intercell currents (heavy line) as a function of the number of cells: (a) small number of cells ($N = 10$), (b) moderate number of cells ($N = 40$), (c) large number of cells ($N = 80$). Current reversal indicated (Szpak et al., 1984).

3.6.1.2. Cell Current Reversal. Szpak et al. (1984) have shown that, if the intercell current exceeds a critical value, I_{cr}, which, for a given set of design parameters, depends on the module load, the cell current can be reversed over a part of an electrode in one or more cells, as shown in figure 30c. In particular, for the current into the cell, the cell current reversal occurs on the anode, while for the exiting intercell current, it takes place on the cathode. Thus, at the negative end of a module, in a

number of cells, dendritic growth of metallic Li is possible and is frequently observed, while the positive electrode, in a corresponding, but not necessarily equal number of cells, suffers either corrosion or passivation. The effect of cell current reversal is shown in figure 31 where photographs taken in the vicinity of the feedline region show distinct evidence of electrochemical activities at the positive and negative ends of a module with no measurable changes in the central part.
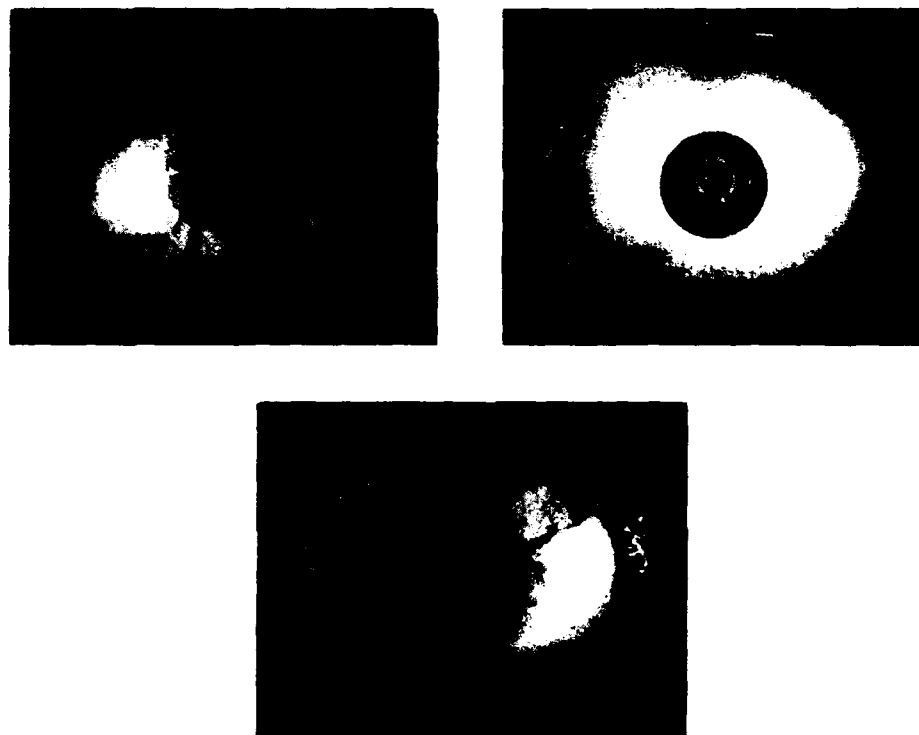
Figure 31. Detrimental effect of intercell current at the cell entrance and within the annular feedline: (top left) cell located at the negative end – dendritic growth of metallic lithium indicated by arrow, (top right) cell located in the central region of an 80-cell module – no visible changes, (bottom) cell located at the positive end – corrosive attack indicated by an arrow (Szpak et al., 1984).

3.6.1.3. Power Losses. The presence of a common electrolytic path also adversely affects the module power output. Gabriel and Szpak (1989) examined power losses in a simple case of a module containing N identical cells represented by an electric circuit analog with constant coefficients. A plot of dimensionless power, Π_a, as a function of dimensionless resistance, ρ, shown in figure 32, indicates that the power into the load exhibits a maximum at $\rho = 1 - \zeta$, while battery own power (Godshall & Driscoll, 1984) decreases monotonically with increasing ρ. It is noted that for a given ζ, the power consumption, $\Pi_b - \Pi_l$ increases from ζ to unity with decreasing

p. This simple model accounts for dissipative losses occurring during the discharge and gives their distribution for small intercell currents. The initial distribution of dissipative processes is symmetrical with a shift in the distribution occurring in the course of module discharge. The magnitude of this shift depends on the charge transfer reactions and the manifold design. Defective cells may create highly localized heat sources which, in turn, may initiate a catastrophic event.
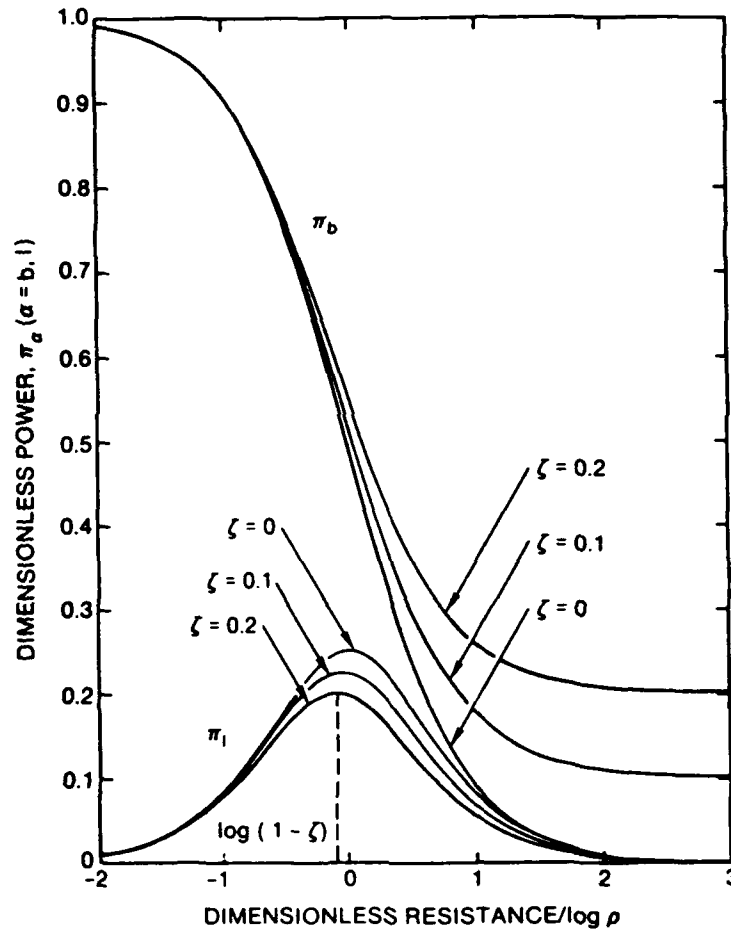
Figure 32. Plot of dimensionless power, Π_α with $\alpha = l, b$ as a function of dimensionless resistance, ρ, for $\zeta = 0.0, 0.1$, and 0.2, as indicated (Gabriel & Szpak, 1989).

A technologically important aspect of battery scale-up is its effect on the distribution of load currents from individual modules. The addition of modules reduces the individual load currents while maintaining a smooth current delivery to the main line,

56

except toward the end of battery discharge when crossovers among module currents occur, indicating current sharing that does not interfere with the power output. As illustrated in figure 33, the measured delivery of total current is smooth, but the current supplied by individual modules varies. The experimentally measured currents in a three-module battery, shown in figure 34, exhibit features that are in agreement with calculated individual and nodal currents. The addition of modules to a well-designed and constructed multimodule battery does not appear to increase safety concerns, i.e., does not inherently cause an increase in the imbalance of intercell currents. By well-designed and constructed batteries, we mean the following restrictive conditions apply: all modules contain the same number of cells and the construction of the cells and their performances are statistically reproducible.
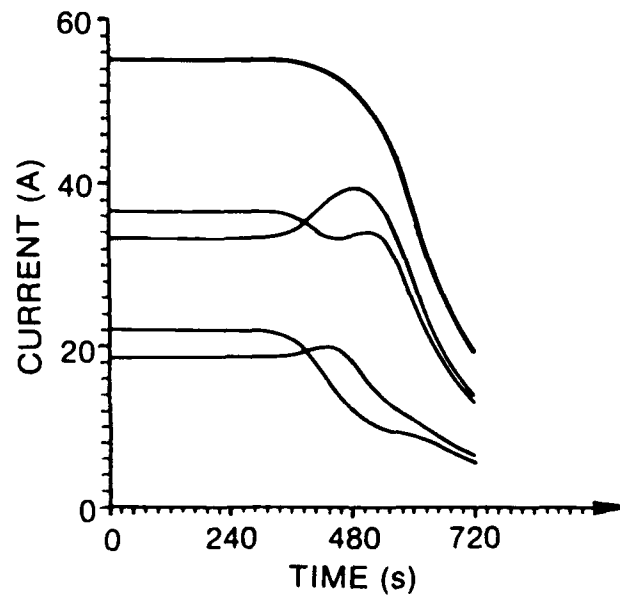
Figure 33. Calculated load current variation for three-module battery assembly (for input parameters refer to Gabriel, et al., 1990).
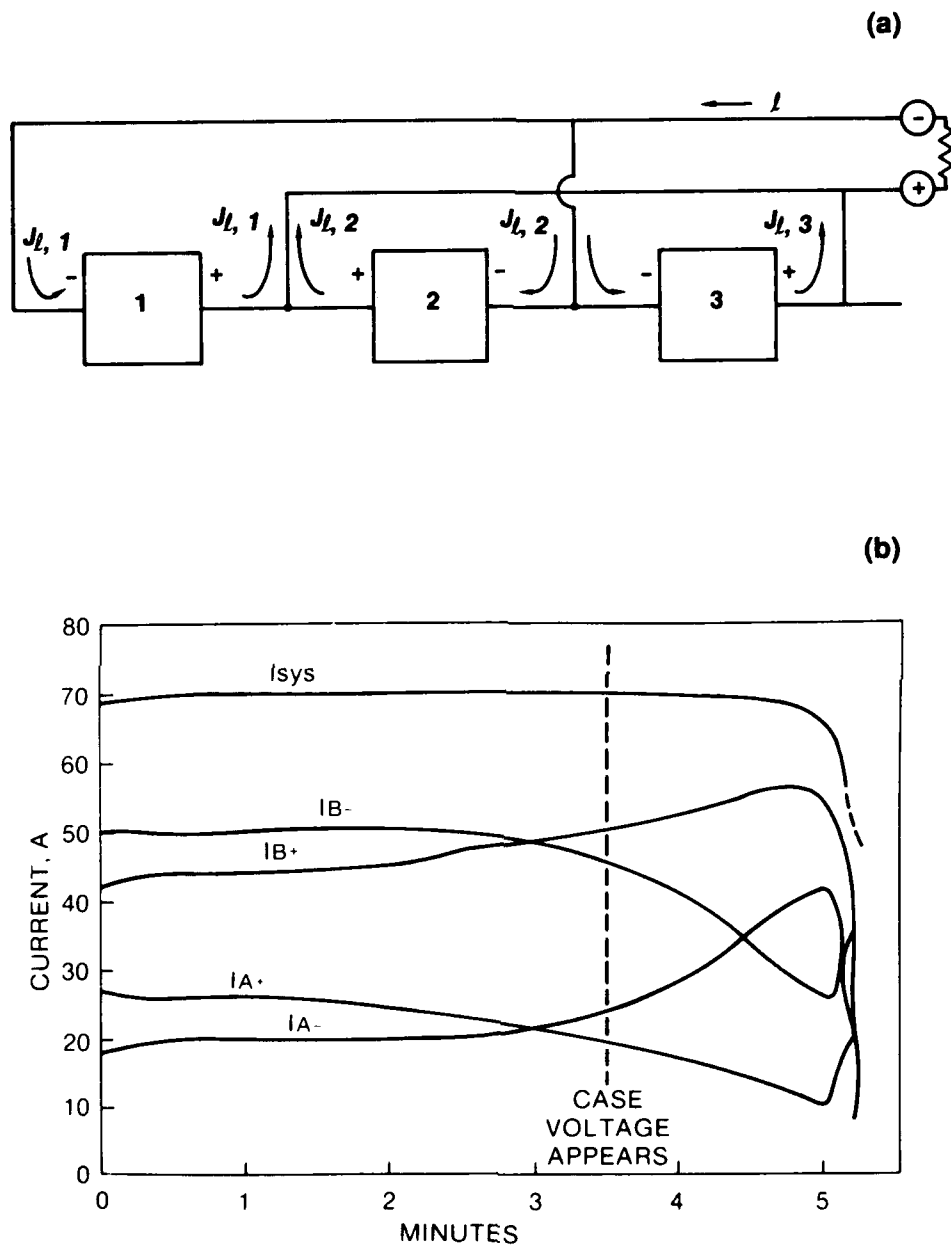
Figure 34. Nodal load current variation in an experimental three-module assembly: (a) electric circuit analog of a three-module battery, (b) measured current variation during battery discharge (Szpak et al., 1990).

58

4. FABRICATION AND QUALITY CONTROL

4.1. INTRODUCTORY COMMENTS

The problems encountered in fabrication and quality control become more difficult to resolve as the expected performance level is increased. To meet the design criteria, i.e., to maximize the extractable energy content for a given power required, a set of optimizing procedures is performed. These optimization procedures favored a thin cell design. In practice, this means separating all cell components with minimum ohmic losses. The efficient operation of reactors designed for electrochemical processing, including energy-conversion devices, often requires the installation of a common electrolytic path. There are numerous advantages associated with this approach, viz., bipolar cell construction, controlled supply of reactants and removal of products, as well as, a reliable means of thermal management. These advantages, however, are partially offset by the parasitic shunting action of the intercell currents (Szpak et al., 1984). Briefly, these currents not only reduce the power output but often affect the structural integrity of battery functional elements. Modeling and practical experience have shown, that in the case of well-designed modules connected electrically in parallel and hydraulically in series, an increase in the number of modules does not create serious problems (Szpak et al., 1990). However, in an assembly of modules with one or more defective cells, or with a sufficiently large variation among the cell functional elements, a situation arises that substantially reduces the battery lifetime and, on occasion, may lead to catastrophic events.

4.2. MODULE ASSEMBLY/QC POINTS

From the point of view of battery fabrication and operation, two interrelated areas require special attention. The first area involves problems connected with the activation time for which an internal distribution system for the flow of electrolyte must be devised. Usually, more than one fill tube running through the length of the module are needed. Short activation times of a large battery present special difficulties because, to realize uniform and fast loading, two sets of mutually contradicting requirements must be simultaneously satisfied. First, the separator must be porous

enough to permit a rapid flow of electrolyte. Yet, the pore size must be small enough to prevent the penetration of carbon particles and eliminate the development of internal shorts. In addition, the separator must be mechanically strong to prevent tearing and shape distortion by the forced flow of electrolyte during activation. To illustrate the inherent difficulties caused by a rapid flow of electrolyte, note that a tenfold decrease in the separator porosity necessitates a hundredfold increase in pressure to maintain the same flow rate.

The second area requiring attention is thermal management. Often, the heat capacity of the battery is insufficient to maintain the operating temperature within safe limits during extended periods of high discharge. Since a considerable amount of heat must be rejected to the surroundings, either a highly conductive path must be provided between the cell interior and the module external heat transfer surface, while concurrently maintaining electrical isolation of the energy section from the heat rejection surface, or a flowing electrolyte must be used.

4.3.   FABRICATION OF CELL FUNCTIONAL COMPONENTS

A typical fabrication sequence of a module and the pertinent quality control (QC) points, are summarized in a block diagram in figure 35. The cell functional elements, e.g., positive and negative electrode structures, are first fabricated. Then, other components such as separators, bipolar plates, current collectors, etc., are cut to size, followed by the process of stacking the cells and compressing the stack to the required thickness. Finally, a means for battery activation or electrolyte circulation are provided to complete the process of module assembly. The compliance with specification demands counting the number of cells in a module, measuring the cell/module thickness, and inspecting the quality of seals. Quality control measures are closely connected with the fabrication steps and the dynamics of the cell/module operation (Gabriel et al., 1990). In the course of component fabrication, both the amount of stored electroactive material and the geometrical constraints of the porous structure are controlled. The control of the purity and amount of the electroactive material presents no special problems. On the other hand, the control of the geometrical constraints of a porous electrode matrix is a serious and, in many instances, unresolved problem.
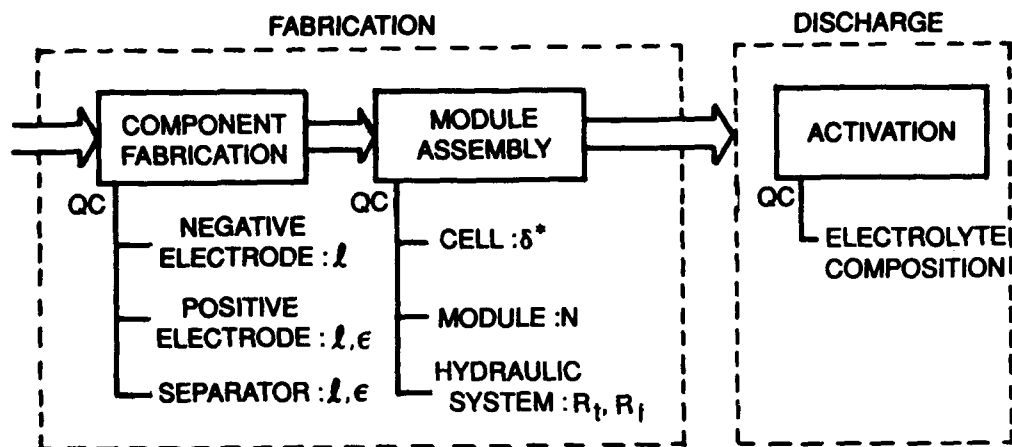
Figure 35. A block diagram showing the fabrication sequence for module/battery assembly and QC requirements: l – thickness, N – number of cells, R_f and R_t – feedline and fill-tube resistances respectively, δ^* – electrode separation, ϵ – porosity (Gabriel et al., 1990).

4.3.1. Positive Electrode

While fabricating the positive electrode, the following factors need to be considered: large specific surface area, uniform loading, and sufficient mechanical strength. Fabrication methods, and the resulting properties of the positive electrode, play a crucial role in achieving the required performance level. The fabrication of these electrodes is, as a rule, protected by patent rights and guarded as proprietary information. The most common matrix for the high-discharge rate $Li/SOCl_2$ battery is Teflon-bonded Shawinigan black containing various additives such as dispersed copper (Giattino & Catanzarite, 1979), platinum (Klinedinst, 1981), and iron and cobalt phthalocyanines (Venkatasetty, 1981). The role of binders is to assure the mechanical strength while the intended role of additives is to modify the current distribution, by changing either the reaction path or the growth habits of the precipitated reaction product(s), or both.

Quality control is limited to a strict adherence to the prescribed fabrication procedures and the quality of raw materials used. Uniform porosity and intimate contact between the electrode matrix and the bipolar plate is necessary to prevent film formation by elemental sulfur (Nowak et al., 1988).

61

4.3.2.   Bipolar Plate

The bipolar plate serves two functions: it provides electronic conductivity between adjacent cells and it forms a thermal path for rejecting heat from the cell interior. The construction material must be chemically inert with respect to the electrolyte. Nickel and stainless steel foils satisfy these requirements. However, for operating at high-discharge rates, $Ni-$ clad Cu foils are used to facilitate heat transfer. Quality control procedures include visual inspection and checks for specified dimensions.

4.3.3.   Lithium Foil

Battery grade metallic lithium foil of various thicknesses is available and shipped in steel containers under an argon atmosphere. Once the container is open, the material must be handled in a dry room with less than two percent relative humidity.

4.3.4.   Thionyl Chloride Electrolyte

Thionyl chloride is a common material available in either technical or purified grades. As a rule, thionyl chloride is further purified by distillation over Li chips, dipentene, or triphenyl phosphite. It is noteworthy that impurities have a negligible effect on the performance of high-discharge rate, reserve batteries. However, for active cells, impurities can and do have a deleterious effect, primarily during storage (Driscoll et al., 1976). The electrolyte is prepared by dissolving $LiCl$ and Al_2Cl_6, which are purchased as anhydrous, reagent grade salts and are normally used without further purification.

4.3.5.   Separator

Separator materials include glass, ceramic, and organic porous sheets. The function of a separator in a battery is twofold: to assure and maintain a positive separation between the negative and positive electrodes and to provide an ionically conductive path. In a specialty battery an additional requirement is imposed: sufficient porosity to meet activation time requirements and mechanical strength to prevent damage during activation.

4.4. MODULE ASSEMBLY

The module is the basic building block in the design of a multikilowatt $Li/SOCl_2$ battery employing a static electrolyte. In addition to cells needed to produce electric power and a means to deliver it to an external circuit, the module also contains the hull section. The basic module assembly procedure involves: stacking the individual elements, compressing the stack to the final dimension, sealing the outer and inner cell edges, installing the hull section and forming the thermal joint. The fabrication sequence is summarized in figure 36. An endplate, insulator plate, and collector plate are placed in sequence on the lower platen of the press. This is followed by assembly of the cell components, viz., the cathode, separator, and an anode/bipolar subassembly. This sequence is repeated until the required number of cells is assembled. The last anode (Li foil) is attached to the collector plate. Installing an insulator plate and an endplate complete the module stacking. The component stack is then compressed to within a fraction of a millimeter of the final height. Bolts and spacers are inserted and the stack is compressed to the final height. After the module is compressed and bolted, it is ready for sealing.
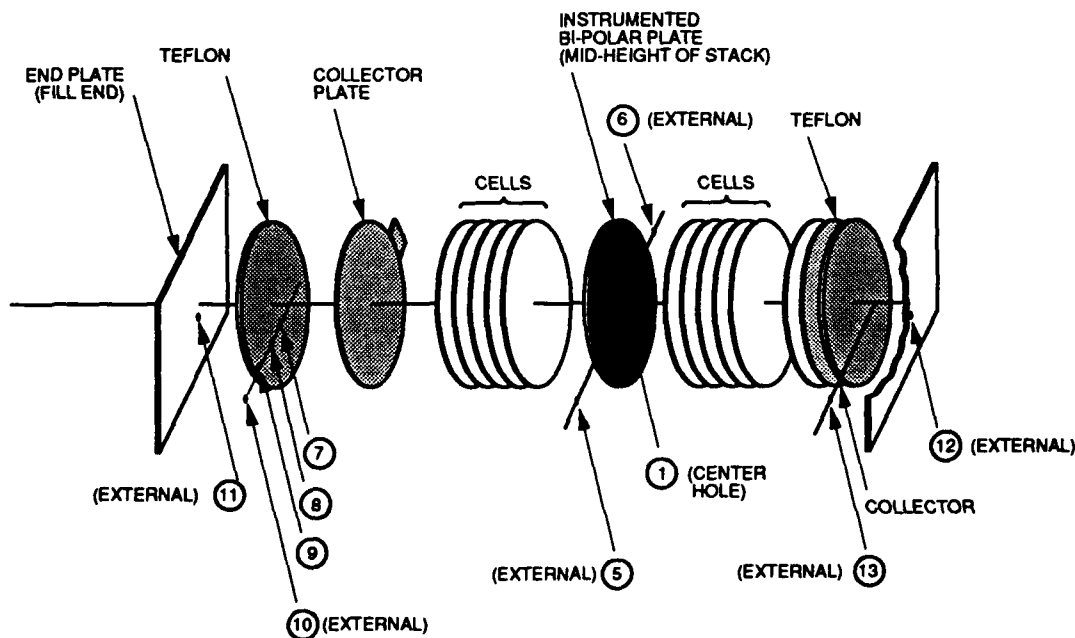
Figure 36. Exploded view of a module section illustrating the installation sequence of cell components. Numerals indicate the location of thermocouples.

The last and final step in module fabrication is completion of the thermal joint. This is done by a metal that fills the gap between the epoxy seal on the outside diameter of the stack and the hull. The module is preheated and the molten alloy is poured through a small hole in the hull section, figure 37.
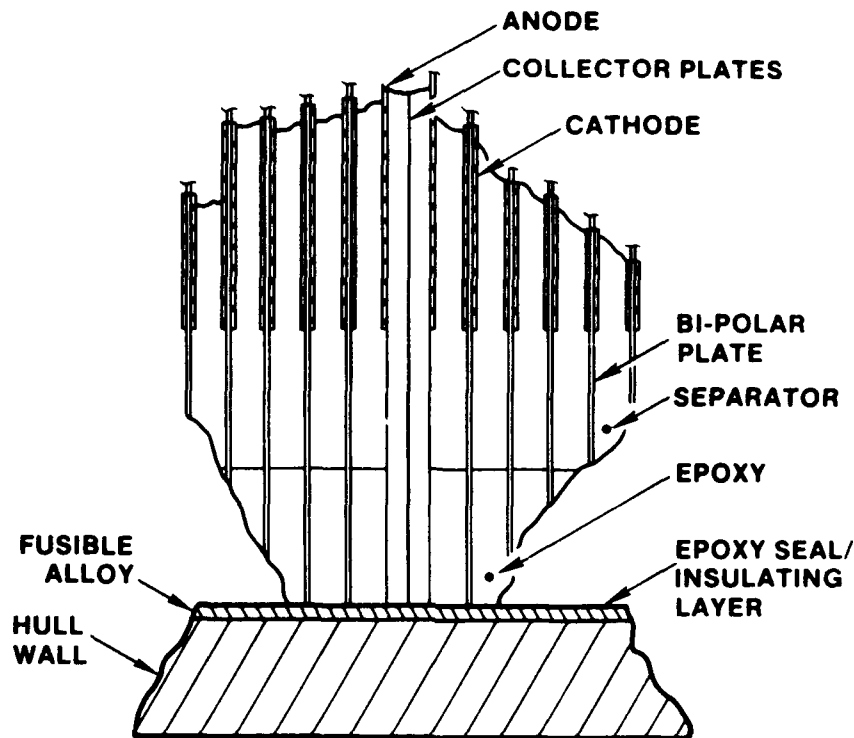
Figure 37. Details of thermal joint design.

Methods for reducing the intercell currents in electrochemical reactors have been discussed, among others, by Grimes, Bellows and Zahn (1983). These methods are not suitable in the present design. In general, specific designs for reducing or eliminating intercell currents are considered proprietary information. However, all methods for reducing the intercell currents rely on increasing the values of R_t and R_f in the module as indicated by the λ parameter, section 3.6. There are many ways to do this. One method is to coat the bipolar plate next to the fill hole with a suitable plastic material that swells when in contact with the electrolyte. Another technique is illustrated in figure 38. Here, the action of the intercell current is redirected to prevent the formation of an internal short. This is done by installing teflon disks of unequal diameter.

64
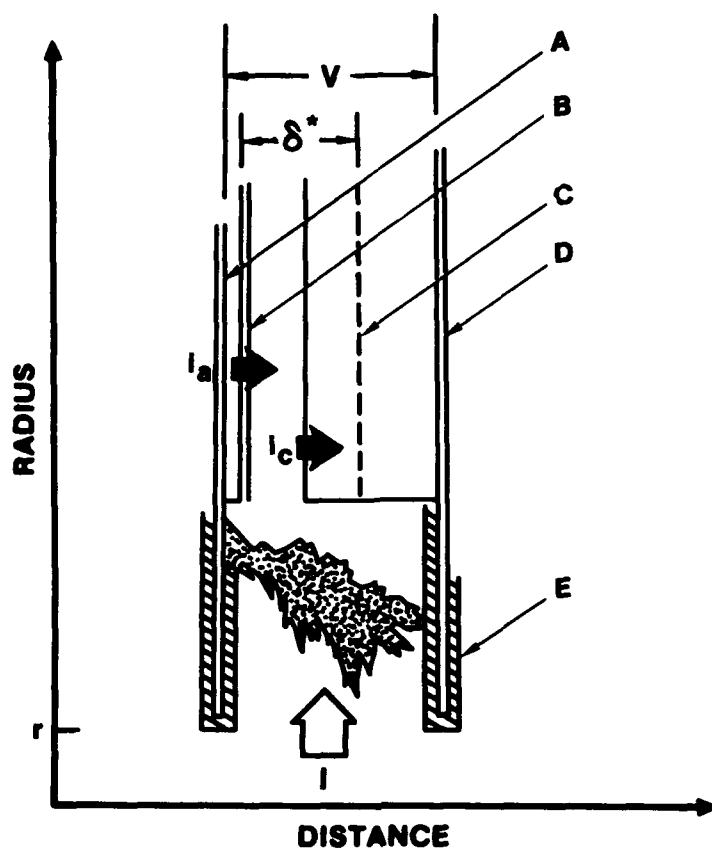
Figure 38. Method preventing internal short generated by intercell current. (A) Li foil, (B) protective $LiCl$ film, (C) porous carbon cathode, (D) bipolar plate, (E) teflon disks, (I) intercell current, i_a, i_c – anodic and cathodic cell currents; δ^* – effective cell thickness.

4.5. MULTIMODULE ASSEMBLY

The two- and three-module batteries are assembled by using the same technique as for a single module, i.e., endplate, insulator, and collector plates are positioned and the cell stack is built up in sequence: anode, separator, cathode and bipolar plate – until the required number of cells are in place. The first module is completed by placing a collector plate on the last cathode. The second module is built with the order of active cell components reversed, i.e., following the sequence: cathode, separator, anode and bipolar plate. The inverted stacking order places the high-voltage end of one module adjacent to the high voltage end of the next module and the ground end of one module to the ground end of the next module. This arrangement avoids a voltage gradient of the magnitude of several hundreds of volts

across the collector plate when the battery is activated. Of course, such high voltages would cause extremely high intermodule current flow which, in all probability, would lead to catastrophic failure.

Quality control is normally achieved by measuring the impedance and phase angle of the cell as a function of frequency. Well-made cells show capacitances that fall within a standard deviation of 5 percent of the mean. Deviations greater than this are associated with a problem within the cell. The method does not permit a determination of the exact nature of the problem. However, the two most common causes are nonuniform cell spacing and the presence of internal shorts.

5. CONCLUDING REMARKS

In organizing this presentation, we attempted to illustrate advantages arising from a rational transition process when developing an electrochemical power source designed to operate at its limits by summarizing our approach and results based on such a transition philosophy. Although we selected the $Li/SOCl_2$ couple for this purpose, such an approach is, undoubtedly, applicable to other systems as well and is an example of current trends in the development of electrochemical cells. In fact, the discussion of the concept of transition from research to design and construction of electrochemical devices was the subject of a recent Palladium Medal Address (Newman, 1991).

The thionyl chloride electrolyte system, both neutral and acidic, has a complex composition that determines the elementary reactions that occur on discharge. Electroreduction rarely involves free thionyl chloride, rather, adducts with $AlCl_3$ and Li^+ undergo electroreduction preferentially. The various species involved in the electroreduction, both reactants and products are now known. However, the exact way in which the final reactants fall apart to form products, is not yet clear.

The $Li/SOCl_2$ system has been modeled, quite successfuly on several levels, including cell, module, and assembly of modules. Modeling has contributed significantly to an understanding of battery operation by providing the basis for both the design and understanding of electrode thickness and porosity, catalytic effects, thermal management, and intercell currents. In addition, modeling guided the development of

quality control (QC) procedures and considerations.

QC is primarily a matter of careful selection of materials, fabrication of components, and assembly of these components to the final cell, module, or battery configuration. Most unusual battery occurrences can be traced to failure of one or more QC procedures rather than, as believed early in the development cycle, to unknown chemical p. cesses. As stated, modeling provides a reasonable description of the characteristics and behavior of modules and batteries. Specific designs are proprietary data or are patent-protected and thus cannot be presented.

$Li/SOCl_2$ technology has come a long way since the initial recognition of its value as a battery chemistry. We believe that much of this progress has resulted from a focused effort to pursue a logical progression of transitions through the R&D cycle. These efforts, as summarized above, have elucidated the chemistry of the system, the optimal design features of cells and modules, the assembly of these cells or modules to batteries, and the resultant characteristics of these assemblies. Again, $Li/SOCl_2$ is used here only as an example. Other battery technology developments could benefit from such an approach.

6. LIST OF SYMBOLS

Multiple use of the same symbol for different quantities and vice versa was employed to conform with their usage in quoted references.

a	area, m^{-2}
c	concentration, mole dm^{-3}
c_p	specific heat, J g^{-1} K^{-1}
e^-	electron, charge
D	diffusion coefficient, m s^{-2}
E	energy (activation energy in eq. (21))
F	Faraday constant, 96487 C/equiv
ΔG	Gibbs free energy, J

ΔH	enthalpy, J
h	heat transfer coefficient, W cm^{-3} K^{-1}
I	current, A
i	current, A
i	running index
J	cell current, A
j	current density, A m^{-2}
j_0	exchange current density, A m-2
K_s	solubility product, mol^2 kg^{-2}
k	rate constant (dimension consistent with reaction order), eqs. 12, 13, 14
l	length (coordinate), m
m, n	running indices
m	morphology parameter, eq. 13
$p(l, t)$	morphology parameter, eqs. 11, 15
p	pressure, atm
q, Q	quantity of heat, J
R	gas constant, 8.3143 J mol^{-1} deg^{-1}
R	resistance, Ohm, eqs. 25, 26
r	rate, s^{-1}
r	radius, m
ΔS	entropy, J deg^{-1}
T	temperature, K
s	specific surface, m^{-1}, eqs. 11, 15
t	time, s
U	potential, V
V	volume, m^3
V	potential, V, eqs. 25, 30
v	volume fraction, eq. 11
v	scan rate, mV s-1

W	work, J
x	coordinate
z	valence
α	transfer coefficient, eq. 10
β	parameter, eq. 20
ϵ	efficiency, eqs. 11, 15; sec. 1.3
ζ	independent variable defined in text
λ	independent variable defined in text, sec. 2.6
λ	volume conductivity, $Ohm^{-1}m^{-1}$, eq. 18
λ	thermal conductance, $W\ m^{-1}K^{-1}$, eq. 23
λ	parameter, sec. 2.6; design parameter, sec. 3.5
η	overpotential, V, eq. 10
θ	surface coverage
ξ	degree of advancement, eq. 27
ξ	parameter, sec. 2.6; design parameter, sec. 3.5
σ	source term (heat), J, eq. 17
κ	thermal conductivity, $J\ cm^{-1}\ s^{-1}\ deg^{-1}$, eq. 19
Φ	potential, V, eq. 26
Π	dimensionless power, sec. 3.5
ρ	dimensionless resistance, sec. 3.5

7. REFERENCES

Ashley, K. and S. Pons. 1988. "Infrared Spectroelectrochemistry," *Chem. Rev.*, 88, 673.

Auborn, J.J., K.W. French, S.I. Lieberman, V.K. Shaw, and A. Heller. 1973. "Lithium Anode Cells Operating at Room Temperature in Inorganic Electrolytic Solutions," *J. Electrochem. Soc.*, 120, 1613.

Babai, M., S. Bababigi, and J. Bineth. 1984. "The Stability of the Lithium/Thionyl Chloride System at Elevated Temperatures," *Proc. Symp. Li-batteries*, vol. 84-1, The Electrochemical Society, Inc., Pennington, NJ.

Bagotzky, V.S. and A.M. Skundin. 1980. *Chemical Power Sources*, Acad. Press Inc., London.

Bard, A.J. and L.R. Faulknner. 1980. *Electrochemical Methods: Fundamentals and Applications*, John Wiley and Sons, Inc., New York, NY.

Blomgren, G.E., V.Z. Leger, T. Kalnooki-Kis, M.L. Kronenberg, and R.J. Brodd. 1979. "Projected Mechanism for Thionyl Chloride and Sulfuryl Chloride Cathode Reactions," *Power Sources 7*, J. Thompson, Editor, Academic Press, New York, NY.

Bockris, J. O'M. and S. Srinivasan. 1969. *Fuel Cells: Their Electrochemistry*, McGraw-Hill Book Company, New York, NY.

Bockris, J. O'M. and A.K.N. Reddy. 1972. *Modern Electrochemistry*, vol. II, Plenum Press, Inc., New York, NY.

Bowden, W.L. and A.N. Dey. 1980. "Primary $Li/SOCl_2$ Cells XI. $SOCl_2$ Reduction Mechanism in a Supporting Electrolyte," *J. Electrochem. Soc.*, 127, 1419.

Bronsted, J.N. 1955. *Principles and Problems in Energetics*, Interscience Publishers, Inc., New York, NY.

Carter, B.J., H.A. Frank, and S. Szpak. 1984. "Reaction Production Current or Potential Reversal in $Li/SOCl_2$ Cells," *J. Power Sources*, 13, 287.

Carter, B.J., R.M. Williams, F.D. Tsay, A. Rodriguez, S. Kim, M.M. Evans, and H.A. Frank. 1985, "Mechanistic Studies Related to the Safety of $Li/SOCl_2$ Cells," *J. Electrochem. Soc.*, 132, 525.

Conway. B.E. and M. Dzieciuch. 1963. "New Approaches to the Study of Electrochemical Decarboxylation and the Kolbe reaction," *Can. J. Chem.*, 41, 21.

Dey, A.N. 1976. "Scanning Electron Microscopic Studies of the Lithium-Film Growth and the Voltage-Delay Phenomenon Associated with the Lithium-Thionyl Chloride Inorganic System," *Electrochim. Acta*, 21, 377.

Dey, A.N. 1987. *Lithium Batteries*, vol. 87-1, The Electrochemical Society, Inc., Pennington, NJ.

Driscoll, J.R., G.C. Holleck, and D.E. Toland. 1976. "Reactions in Lithium-Thionyl Chloride Cells," *Proceedings of the 27th Power Sources Symposium*, Atlantic City, NJ.

Driscoll, J.R. 1984. Unpublished data.

Driscoll, J.R., R. Pollard, J.J. Smith, and S. Szpak. 1985. "Development of a High-Rate $Li/SOCl_2$ System: Theory vs. Practice," *Power Sources 10*, L.J. Pearce, Editor, The Paul Press.

Driscoll, J.R. and S. Szpak. 1985. "Thermal Behavior of Electrochemical Cells by Liquid Crystal Display," *J. Power Sources*, 14, 321.

Gabano, J.P. 1983. *Lithium Batteries* , Academic Press, Inc., London.

Gabriel, C.J. and S. Szpak. 1989. "Power Losses in Batteries with a Common Electrolytic Path," *J. Power Sources*, 25, 215.

Gabriel, C.J., P.A. Mosier-Boss, S. Szpak, and J.J. Smith. 1990. "Intercell Currents in Assembly of Modules: Quality Control Considerations," *J. Power Sources*, 32, 353.

Giattino, L.R. and V.O. Catanzrite. 1979. "High Power Battery," *US Patent*, no. 4,167,608.

Godshall, N.A. and J.R. Driscoll. 1984. "Determination of the Thermoneutral Potential of $Li/SOCl_2$ Cells," *J. Electrochem. Soc.*, 131, 2221.

Grimes, P.G., R.J. Bellows, and M. Zahn. 1983. *Electrochemical Cell Design*, R.E. White, Editor, Plenum Press, London.

F rris, W.S. 1958. "Electrochemical Studies in Cyclic Esters," *Dissertation*, U.C. Berkeley.

Hecht, H. 1947. "Dehydration of Metal Chloride Hydrates with Thionyl Chloride or Carbonyl Chloride," *Z. Anorg. Chem.*, 254, 44.

Istone, W.K. and R.J. Brodd. 1984. "The Mechanisms of Thionyl Chloride Reduction at Solid Electrodes," *J. Electrochem. Soc.*, 131, 2467.

Kaminski, E.A. and R.F. Savinell. 1983. "A Technique for Calculating Shunt Leakage and Cell Currents in Bipolar Stacks Having Divided and Undivided Cells," *J. Electrochem. Soc.*, 130, 1103.

Klinedinst, K.A.. 1981. "Cathode-Limited $Li/SOCl_2$ Cells," *J. Electrochem. Soc.*, 128, 2507.

Ksenzhek, O.S. and N.D. Koshel. 1970. "Current Leakages in High-Voltage Batteries with a Total Collector. I," *Elektrokhimija*, 6, 1587.

Ksenzhek, O.S. and N.D. Koshel .1971a. "Current Leakage in High-Voltage Batteries with a Common Manifold. II," *Elektrokhimija*, 7, 353.

Ksenzhek, O.S and N.D. Koshel .1971b. "Current Leakage in High-Voltage Batteries with a Common Collector. III," *Elektrokhimija*, 7, 850.

Lanson, D. and J.P. Descroix. 1984. *Electrolytes for $Li/SOCl_2$ Batteries: The Ternary System $LiAlCl_4 - SO_2 - SOCl_2$*, SAFT, Romainville, France.

Long, D.A. and R.T. Bailey. 1963. "Spectroscopic Studies of Solvent Systems Part I. Solutions of $AlCl_3$ in $SOCl_2$," *Trans. Faraday Soc.*, 59, 594.

Madou, M.J. and S. Szpak. 1984. "Investigation of $SOCl_2$ Reduction by Cyclic Voltammetry and AC Impedance Measurements," *J. Electrochem. Soc.*, 131, 2471.

Madou, M.J., J.J. Smith, and S. Szpak. 1987. "Comments on Electroreduction of $SOCl_2$," *J. Electrochem. Soc.*, 134, 2794.

Marincic, N, J. Epstein, and F. Goebel. 1975. "Performance of Lithium Batteries with Organic and Inorganic Solvents," *J. Appl. Electrochem.*, 5, 313.

Marincic, N. 1976a. "Materials Balance in Primary Batteries I. Lithium Inorganic Cells at Low Discharge Rates," *J. Appl. Electrochem.*, 6, 51.

Marincic, N. 1976b. "Materials Balance in Primary Batteries II. Lithium Inorganic Cells at High Discharge Rates," *J. Appl. Electrochem.*, 6, 263.

Marincic, N. and D.B. Koffmann 1976. "Materials Balance in Primary Batteries. III. Computer Aided Design for Standard Size Lithium-Thionyl Chloride High Power Cells," *J. Appl. Electrochem.*, 6, 463.

Mosier-Boss, P.A., R.D. Boss, C.J. Gabriel, S. Szpak, J.J. Smith, and R.J. Nowak. 1989a. "Raman and Infrared Spectroscopy of the $AlCl_3 - SOCl_2$ System," *Trans Faraday Soc. 1*, 85, 11.

Mosier-Boss, P.A., S. Szpak, J.J. Smith, and R.J. Nowak. 1989b. "$LiCl - AlCl_3 - SOCl_2$ System: Structures, Species and Equilibria," *J. Electrochem. Soc.*, 136, 1282.

Mosier-Boss, P.A., S. Szpak, J.J. Smith, and R.J. Nowak. 1989c. "Electroreduction of $SOCl_2$ I. $AlCl_3 - SOCl_2$ System on Pt Electrode," *J. Electrochem. Soc.*, 136, 2455.

Mosier-Boss, P.A., S. Szpak, J.J. Smith, and R.J. Nowak. 1990. "Effect of Electrode Material on $SOCl_2$ Electroreduction," *Electrochim. Acta*, 35, 1787.

Mosier-Boss, P.A., S. Szpak, J.J. Smith, and R.J. Nowak. 1991. "Mechanistic Aspects of Oxyhalide Electroreduction: The $SOCl_2 - AlCl_3 - LiCl$ and $SO_2Cl_2 - AlCl_3 - LiCl$ Systems," *Primary and Secondary Lithium Batteries*, vol. 91-3, The Electrochemical Soc., Inc., Pennington, NJ.

Murray, R.W. 1986. "Chronoamperometry, Chronocoulometry, and Chronopotentiometry," in *Physical Methods of Chemistry Volume II: Electrochemical Methods*, John Wiley and Sons, Inc., New York, NY.

Nesterov, B.P., T.A. Razevig, and N.V. Korovin. 1974. "Distribution of Stray Currents in Batteries with Common Collectors – A Discrete Problem," *Elektrokhimija*, 10, 1088.

Newman, J. 1991. "From First Principles to Cell Design," *Palladium Medal Address*, The Electrochemical Society Meeting, Phoenix, AZ.

Nicholson, R.S. and I. Shain. 1964. "Theory of Stationary Electrode Polarography: Single Scan and Cyclic Methods Applied to Reversible, Irreversible, and Kinetic Systems," *Anal. Chem.*, 36, 706.

Nowak, R.J., D.R. Rolison, J.J. Smith, and S. Szpak. 1988. "Role of $Fe - Pc$ in a Discharging $Li/SOCl_2$ Cell," *Electrochim. Acta,* 33, 1313.

Onishchuk, V.A. 1972. "Optimization of the Electrical Parameters of Multivolt Batteries of Electrochemical Power Sources in Relation to the Method of Electrolyte Supply," *Elektrokhimija,* 8, 698.

Parnell, L.A. and S. Szpak. 1985. "Thermal Behaviour of $Li/SOCl_2$ Batteries of Thin Cell Design," *Electrochim. Acta,* 30, 913.

Salkind, A.J. 1987. *History of Battery Technology,* vol. 87-14, The Electrochemical Society, Inc., Pennington, NJ.

Salmon, D.J., M.E. Peterson, L.L. Henricks, L.L. Abels, and J.C. Hall. 1982. "Spectroscopic Studies of the Hazards of $Li/SOCl_2$ Batteries During Anode-Limited Cell Reversal," *J. Electrochem. Soc.,* 129, 2496.

Schlaikjer, C.R., F. Goebel, and N. Marincic. 1979. "Dischar$_t$ Reaction Mechanisms in Li/SO $_2$ Cells," *J. Electrochem. Soc.,* 126, 513.

Spandau, H. and E. Brunneck. 1952. "Ionic Reactions in Thionyl Chloride as Solvent," *Z. Anorg. Chem.,* 270, 201.

Szpak, S. and J.R. Driscoll. 1983. "Investigation of Positive Electrode Characteristics in High Rate $Li/SOCl_2$ Cells," *J. Power Sources,* 10. 343.

Szpak, S. and H.V. Venkatasetty. 1983. "Properties of $SOCl_2$-Based Electrolytes. 1. Conductivity, Viscosity and Density," *J. Chem. Eng. Data,* 28, 47.

Szpak, S., C.J. Gabriel, and J.R. Driscoll. 1984. "$Li/SOCl_2$ Battery Intercell Currents," *J. Electrochem. Soc.,* 131, 1996.

Szpak, S. and H.V. Venkatasetty. 1984. "Transport Properties of Aluminum Chloride-Thionyl Chloride-Based Electrolytes," *J. Electrochem. Soc.,* 131, 961.

Szpak, S. and J.R. Driscoll. 1987. "Assessment of $Li/SOCl_2$ Battery Technology: Reserve, Thin-Cell Design," NOSC TR 1154, vol I (April). San Diego. CA.

Szpak, S., C.J. Gabriel, and J.R. Driscoll. 1987. "Catastrophic Thermal Runaway in Lithium Batteries," *Electrochim. Acta,* 32. 239

Szpak, S., C.J. Gabriel, J.J. Smith, and J.R. Driscoll. 1990. "Intercell Currents in Assembly of Modules," *J. Electrochem. Soc.,* 137, 849.

Szpak, S. and J.J. Smith. 1990. "Transition Issues Associated with the Development of the $Li/SOCl_2$ Battery Technology," *Naval Research Reviews*, vol. XLII, 12.

Szpak, S. 1991. "Experimental Simulation of Porous Electrodes," in *Techniques for Characterization of Electrodes and Electrochemical Processes*, R. Varma and J.R. Selman, Editors, John Wiley and Sons, Inc., New York, NY.

Thiele, W., M. Scheiff, and M. Matschiner. 1983. "Contribution to Calculation and Minimiztion of Bipolar Electrolyzer Current Loss at Bipolar Electrolytic Cell," *Electrochim. Acta.*, 26, 1005.

Tsaur, K.C. and R. Pollard. 1984a. "Mathematical Modeling of the Lithium, Thionyl Chloride Static Cell. I. Neutral Electrolyte," *J. Electrochem. Soc.*, 131, 975.

Tsaur, K.C. and R. Pollard. 1984b. "Mathematical Modeling of the Lithium, Thionyl Chloride Static Cell. II. Acid Electrolyte," *J. Electrochem. Soc.*, 131, 984.

Tsaur, K.C. and R. Pollard. 1986. "Precipitation of Solids in ELectrochemical Cells," *J. Electrochem. Soc.*, 133, 2296.

van Rysselberghe, P. 1966. "Some Aspects of the Thermodynamic Structure of Electrochemistry," in *Modern Aspects of Electrochemistry*, J. O'M. Bockris, Editor, Plenum Press, Inc., New York NY.

Venkatasetty, H.V. and D.J. Saathoff. 1981. "Properties of $LiAlCl_4 - SOCl_2$ Solutions for $Li/SOCl_2$ Battery," *J. Electrochem. Soc.*, 128, 773.

Venkatasetty, H.V. 1981. "Electrocatalysts for Cathodes to Enhance Their Activity to Reduce Thionyl Chloride in Lithium/Thionyl Chloride Batteries," *US Patent*, No. 4,167,600.

Venkatasetty, H.V. 1984. *Lithium Battery Technology*, John Wiley and Sons, Inc., New York, NY.

APPENDIX A – EXPERIMENTAL

METHODS OF ANALYSIS OF THE BULK ELECTROLYTE

Introduction

Vibrational spectroscopy (Raman and infrared) has be n shown to be a sensitive technique for probing solvation and association phenomena (Popovych & Tomkins, 1981). Information on the intermolecular forces, the structure of solvents, and the nature of solvation can be derived using vibrational spectroscopy. Solute-solvent interactions not only affect the vibrational spectra of the solvents, but also lead to the appearance of new vibrational bands due to solute-solvent complexation. Information on bond properties as well as inter and intramolecular interactions can be assessed from the vibrational frequencies and their shifts, band intensities, depolarization ratios, and excitation profiles.

Instrumentation

Infrared spectra were obtained on a Nicolet 5DXB FT-IR spectrometer with a resolution of 4 cm^{-1}. Barnes demountable cells with $AgCl$ windows and a 15-μm teflon spacer were used.

The Raman spectra were recorded on a system composed of a Lexel model 85 Ar-ion laser emitting at 488 nm, which was chopped at 20 Hz, a sample chamber with coupling and collecting optics, a Spex model 1400-11 scanning double monochromator with photon-counting preamplifier and line driver, a photon-counting integrator (Miller, 1968), and a digital synchronous detector. The samples were contained in a Helma model 162 F stoppered quartz cell. The cell chamber was flushed with dry nitrogen to prevent condensation on the cell windows when operating below room temperature. Temperatures were controlled to within ±0.01°C. Most of the spectra were recorded at a laser power of 50 mW.

Resolution of Spectral Bands

Raman and infrared vibrational bands have both a Lorentzian and a Gaussian contribution. While the width of the Lorentzian line is an intrinsic property of the

molecule, depending on the ratio of the decay time to the lifetime of the initial state, the Gaussian distribution is related to the interaction with the environment, particularly with the nearest neighbors of the excited molecule (Gabriel, Mosier-Boss, & Szpak, 1987). The observed excitation profiles arise from the convolution of the Lorentzian and Gaussian contributions and assume the form of the Voigt profile

$$f(\nu, \nu_0, \Delta\nu_L, \Delta\nu_G) = \frac{2\ln 2}{\pi^{\frac{3}{2}}} \frac{\Delta\nu_L}{\Delta\nu_G^2} \int_{-\infty}^{\infty} \frac{\exp(-y^2)}{a^2+(y-\omega)^2} dy \qquad (A1)$$

where $a = \Delta\nu_L\sqrt{(\ln 2)/\Delta\nu_g}$, $\omega = 2(\nu - \nu_0)\sqrt{(\ln 2)/\Delta\nu_g}$ and ν_0, $\Delta\nu_L$ and $\Delta\nu_G$ are, respectively, the center frequency and the full widths at half maximum of the Lorentzian and Gaussian distributions that characterize the line (diBartolo, 1968).

In a dynamic system composed of N number of species, the experimentally observed spectral band, $S(\nu)$, is a superposition of N lines that are approximated by the following expression

$$I(\nu) = C_o(\nu - \alpha) + \sum_{i=1}^{N} C_i f(\nu, \nu_0, \Delta\nu_{Li}, \Delta\nu_{Gi}) \qquad (A2)$$

where the function $f(...)$ is defined in eq. (A1). Because $f(...)$ is normalized, C_i is the area of the fundamental Lorentzian line of the i-th species. The linear term $C_o(\nu - \alpha)$ accounts for a sloping baseline.

The least square fit of eq. (A2) to the experimental data is constructed by minimizing the test function, F, given by

$$F = \sum_{j=1}^{M} [S(\nu_j) - I(\nu_j)]^2 / (M - P) \qquad (A3)$$

where M is the number of data points in the measured spectrum, $S(\nu)$, and P is the number of variable parameters characterizing the spectral intensity calculated by eq. (A2). The minimization of F, eq. (A3), was carried out using the Nelder-Mead algorithm (Nash, 1979). The number of lines N is selected from consideration of the vibrational mode under investigation, the chemical nature of the components, as well as from the minimization procedure. Constraining the line widths to be greater than the data point separation and including the factor $(M - P)$ in eq. (A3), places an upper limit on the value of N that will minimize F. The integral appearing in eq. (A1) was evaluated by the method of Romberg quadrature (Barakat, 1980) where

A-2

the $+\infty$ and $-\infty$ limits were replaced by $+3$ and -3. Computational round off errors, truncation errors in evaluation of eq. (A1), and scatter in the intensity data broaden the minimum in F, occasionally making it difficult to select the global minimum from several local minima. Except for the truncation error, this difficulty is not specific to the Voigt profile, nor to the Nelder-Mead algorithm, but is characteristic of nonlinear optimization.

Molecular Orbital Calculations

The MO calculations were performed using either AMPAC or MOPAC. AMPAC was developed at the University of Texas, Austin, Texas. MOPAC is an upgraded version of AMPAC developed by Dr. Jimmy Stewart at the U.S. Air Force Academy, Colorado Springs, Colorado. Both AMPAC and MOPAC are general purpose, semiempirical molecular orbital packages. These calculations yield information on the size, shape, and charge distribution within molecules and complexes.

METHODS EMPLOYED TO EXAMINE $SOCl_2$ ELECTROREDUCTION

In Situ Infrared Spectroscopy

Electrochemical Cell. The spectroelectrochemical cell is shown in figure A1. The body of the cell was made of a machinable ceramic material chemically resistant to $SOCl_2$ (Macor, Dow Chemical). A demountable $AgCl$ window was sealed against the cell body by an O-ring (Kalrez, DuPont Chemical). The working electrode was a polished metal foil sealed to a glass tube using a chemically resistant epoxy (Epoxy Patch C, Hysol Corp.). Ohmic contact to the metal foil was achieved using a conductive epoxy. The working electrode was held in place in the cell body by an O-ring (Kalrez, DuPont Chemical) and a teflon bushing. The counter and reference electrodes were a Pt wire ring and a $Ag/AgCl$ wire in a teflon sleeve, respectively. These two electrodes were sealed to the cell body (Epoxy Patch C, Hysol Corp.). A variable distance between the window and working electrode surface was provided; however, each set of measurements was carried out at a fixed distance. The pathlengths were calibrated with neat CCl_4.
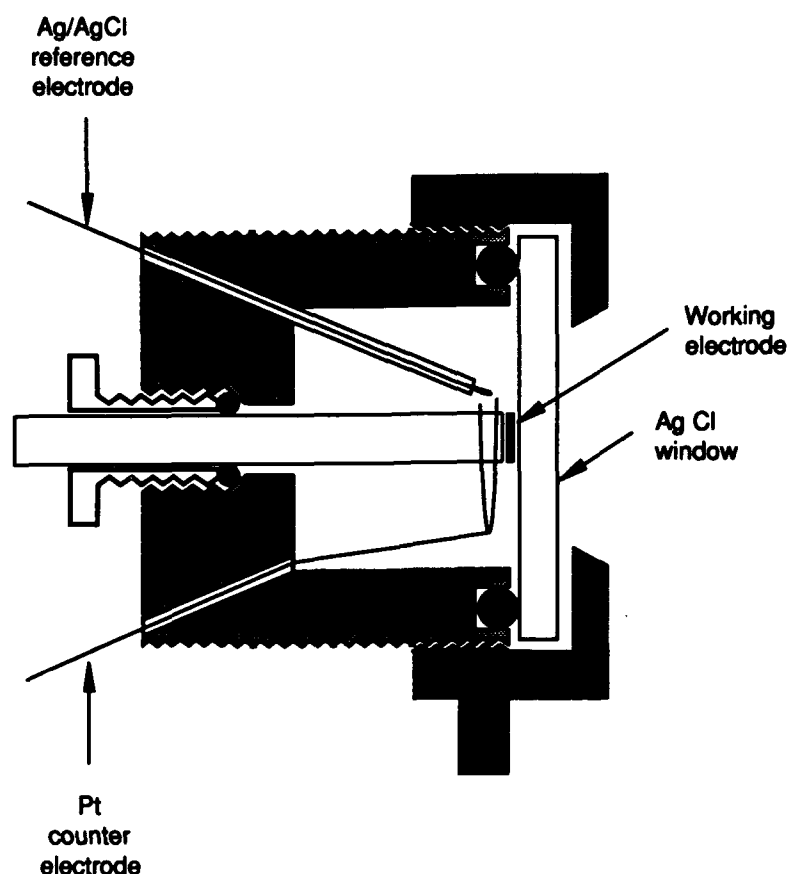
Figure A1. Design of spectroelectrochemical cell used in in situ IR reflectance spectroscopy.

Instrumentation. All in situ infrared spectra were obtained using the Nicolet 5DXB FT-IR spectrometer described earlier. The spectroelectrochemical cell was placed at a 45° angle inside the spectrometer using a specular reflectance apparatus (Spectra-Tech, Model 500). Overpotentials were applied using a PAR model 173 potentiostat.

Relaxation Techniques

Electrochemical Cell. Figure A2 shows the two-chamber electrochemical cell used in the relaxation experiments. The body of the cell is constructed of glass and has three glass-threaded joints (Ace Glass). The two chambers are separated by a coarse glass frit. One chamber contains the working and reference electrodes while the other has the counter electrode. The working electrode was a metal foil permanently mounted on a glass tube using chemically resistant epoxy (Epoxy Patch C, Hysol corp.). Ohmic contact was provided using conductive epoxy. The reference electrode

was a *Ag/AgCl* wire in a teflon sleeve. Prior to the experiment, the reference electrode was immersed in a fritted eyedropper containing the electrolyte. This prevented the corrosion of the reference electrode during the course of the experiment. A coiled *Pt* wire served as the counter electrode. The electrodes were positioned in the cell body using O-rings (Kalrez, DuPont Chemical) and teflon bushings.
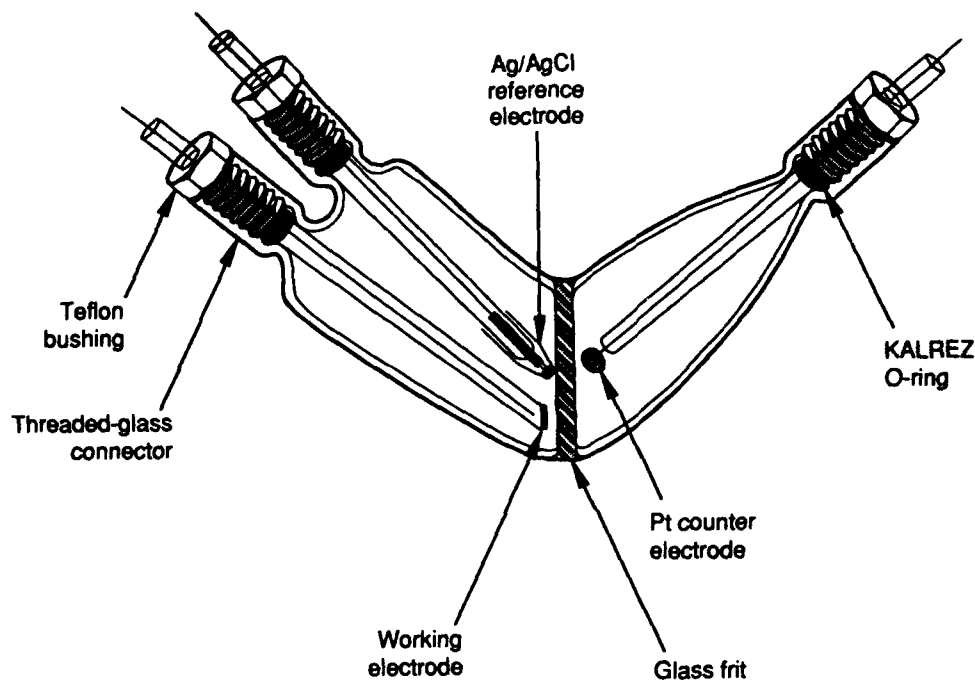
Figure A2. Design of electrochemical cell used in cyclic voltammetry and galvanostatic and potentiostatic pulsing experiments.

Instrumentation. The cyclic voltammograms and charging and relaxation curves for the galvanostatic and potentiostatic pulsing experiments were obtained with the aid of the computer-driven potentiostat, PAR model 173 with a 276 IEEE computer interface.

MODELING OF INTERCELL CURRENTS

Figure A3 shows the flowchart of the solution program used to calculate the intercell currents within an assembly of modules. In this approach, the geometry and

physical properties of the module(s) are first defined. The system parameters include the number of modules (maximum of 5), the number of cells per module (maximum of 90), porosity fineness of the cathodes, cathode use factor, anode reversed current factor and load resistance. The cell and feed tube porosities are assigned as described in section 3.6., using a random number generator. The porosities were chosen from the range 0.3 to 0.9 corresponding to limitations imposed by heat evolution (Parnell & Szpak, 1985) and practical considerations of cell construction. In the case of deficient modules, the number, location, and deficiency factor of the affected cells are defined. In these calculations, the effective electrode spacing is assumed to be the same for each cell within the module.

Once the system parameters have been established, the starting cell and feed tube conductivities are calculated and the time-step loop calculations are started. Within the time loop, the port input resistances are calculated (Szpak, Gabriel, & Driscoll, 1984) and the banded matrix for each module's loop currents are set-up. The module coupling equations for the coupling currents are computed from tridiagonal sets of linear equations – one set for each module. The reversed current for each cell is then computed as is the charge transferred by the reversed current (Szpak et al., 1984). The loop currents are used to calculate the charge transferred to each cathode. Using the charges transferred during the time increment, the new cell and feed tube conductivities are calculated (Szpak et al., 1990). The time is advanced by the incremental amount and the time-loop calculations are done from the new time.
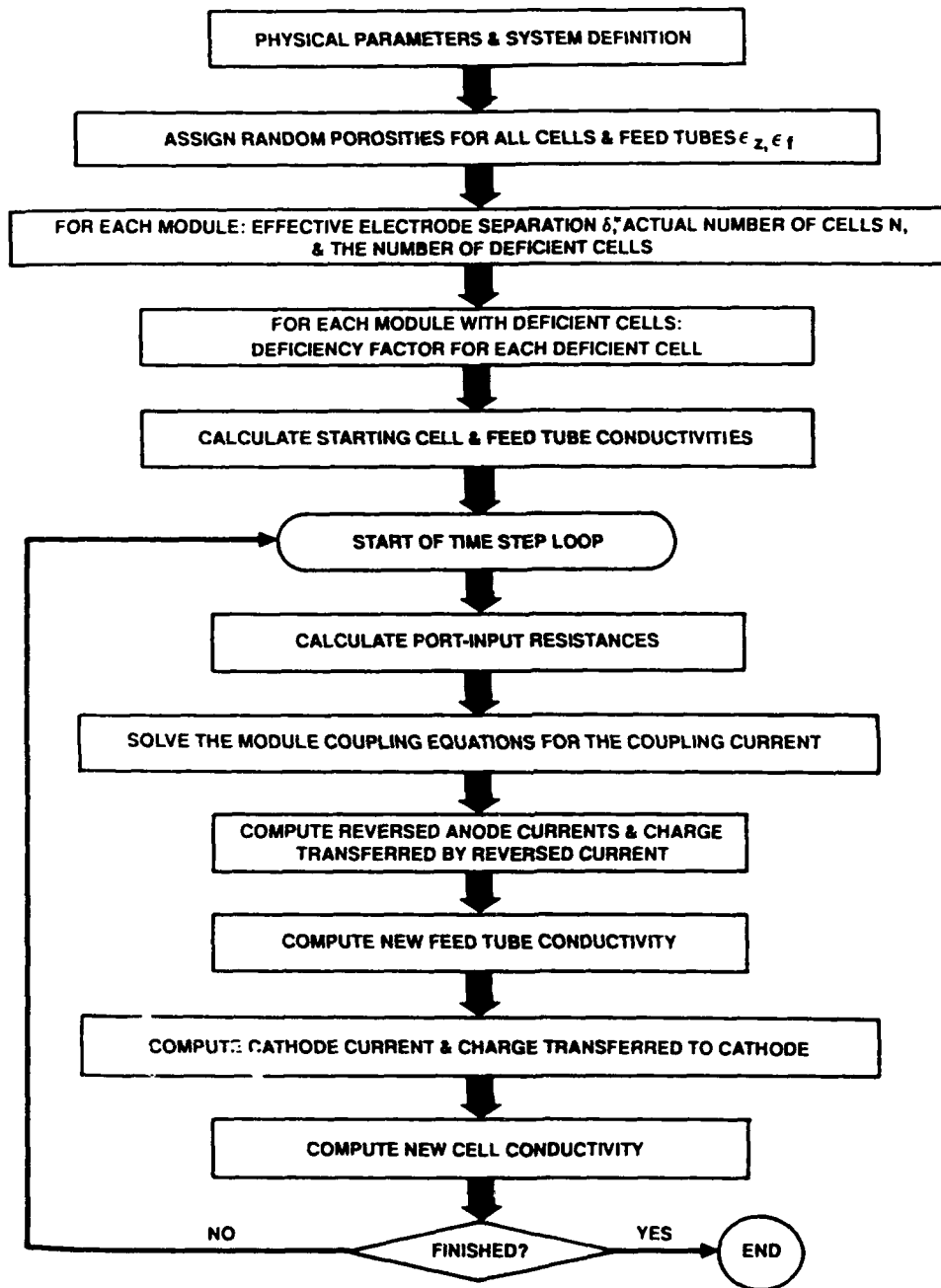
Figure A3. A flowchart calculating the characteristics of the multimodule battery assembly. (Gabriel et al., 1990).

REFERENCES

Barakat, R. 1980. *The Computer in Optical Research: Methods and Applications*, Springer Press, Berlin, Germany.

diBartolo, B. 1968. *Optical Interactions in Solids*, John Wiley and Sons, Inc., New York, NY.

Gabriel, C.J., P.A. Mosier-Boss, and S. Szpak. 1987. "Resolution of Vibrational Bands into Voigt Profiles," *Spectrochim. Acta*, 43A, 293.

Miller, S.A. 1968. "Inexpensive Photon Counting System for Raman Spectroscopy," *Rev. Sci. Instr,*, 39, 1923.

Nash, J.C. 1979. *Compact Numerical Methods for Computers: Linear Algebra and Function Minimization*, John Wiley and Sons, Inc., New York, NY.

Parnell, L.A. and S. Szpak. 1985. "Thermal Behaviour of $Li/SOCl_2$ Batteries of Thin Cell Design," *Electrochim. Acta*, 30, 913.

Popovych, O. and R.P.T. Tomkins. 1981. *Nonaqueous Solution Chemistry*, John Wiley and Sons, Inc., New York, NY.

Szpak, S., C.J. Gabriel, and J.R. Driscoll. 1984. "$Li/SOCl_2$ Battery Intercell Currents," *J. Electrochem. Soc.*, 131, 1996.

Szpak, S., C.J. Gabriel, J.J. Smith, and J.R. Driscoll. 1990. "Intercell Currents in Assembly of Modules," *J. Electrochem. Soc.*, 137, 849.

REPORT DOCUMENTATION PAGE

Public reporting burden for this collection of information is estimated to average 1 hour per response, including the time for reviewing instructions, searching existing data sources, gathering and maintaining the data needed, and completing and reviewing the collection of information. Send comments regarding this burden estimate or any other aspect of this collection of information, including suggestions for reducing this burden, to Washington Headquarters Services, Directorate for Information Operations and Reports, 1215 Jefferson Davis Highway, Suite 1204, Arlington, VA 22202-4302, and to the Office of Management and Budget, Paperwork Reduction Project (0704-0188), Washington, DC 20503.

1. AGENCY USE ONLY (Leave blank)	2. REPORT DATE March 1992	3. REPORT TYPE AND DATES COVERED Final: Oct 1990—September 1991

4. TITLE AND SUBTITLE
Li/SOCl$_2$ BATTERY TECHNOLOGY:
PROBLEMS AND SOLUTIONS

5. FUNDING NUMBERS
PE: 060236N
Proj: RV36I21
SUBPROJ: 57-ZE87-01
ACC: DN309109

6. AUTHOR(S)
P. A. Mosier-Boss and S. J. Szpak

7. PERFORMING ORGANIZATION NAME(S) AND ADDRESS(ES)
Naval Command, Control and Ocean Surveillance Center (NCCOSC)
RDT&E Division (NRaD)
San Diego, CA 92152-5000

8. PERFORMING ORGANIZATION REPORT NUMBER
NRaD TR 1484

9. SPONSORING/MONITORING AGENCY NAME(S) AND ADDRESS(ES)
Office of the Chief of Naval Research (OCNR-20T)
Independent Exploratory and Development Programs (IED)
Arlington, VA 22217

10. SPONSORING/MONITORING AGENCY REPORT NUMBER

11. SUPPLEMENTARY NOTES

12a. DISTRIBUTION/AVAILABILITY STATEMENT
Approved for public release; distribution is unlimited.

12b. DISTRIBUTION CODE

13. ABSTRACT (Maximum 200 words)

This report illustrates the advantages of using a rational transition process when developing an electrochemical power source designed to operate at its limits by summarizing the approach and results based on such a transition philosophy.

The thionyl chloride electrolyte system has a complex composition that determines the elementary reactions that occur on discharge. Electroreduction rarely involves free thionyl chloride; rather, adducts with AlCl$_3$ and Li undergo electroreduction, preferentially.

Modeling the Li/SOCl$_2$ system has contributed significantly to an understanding of battery operation by providing the basis for both the design and understanding of electrode thickness and porosity, catalytic effects, thermal management, and intercell currents. Modeling also guided the development of quality control (QC) procedures and considerations.

Li/SOCl$_2$ technology has come a long way since the initial recognition of its value as a battery chemistry. Much of this progress has resulted from efforts to pursue a logical progression of transitions through the R&D cycle. These efforts have elucidated the chemistry of the system, the best design features of cells and modules, the assembly of these cells or modules, and the resultant characteristics of these assemblies. The Li/SOCl$_2$ is used only as an example. Other battery technology developments could benefit from such an approach.

14. SUBJECT TERMS		15. NUMBER OF PAGES 96
Lithium battery thionyl chloride system cell battery modeling	electrochemical process thermal management intercell currents	16. PRICE CODE

17. SECURITY CLASSIFICATION OF REPORT UNCLASSIFIED	18. SECURITY CLASSIFICATION OF THIS PAGE UNCLASSIFIED	19. SECURITY CLASSIFICATION OF ABSTRACT UNCLASSIFIED	20. LIMITATION OF ABSTRACT SAME AS REPORT

21a. NAME OF RESPONSIBLE INDIVIDUAL	21b. TELEPHONE *(Include Area Code)*	21c. OFFICE SYMBOL
Dr. Pamela A. Mosier-Boss	(619) 553-1603	NRaD Code 574

INITIAL DISTRIBUTION

Code 0012	Patent Counsel	(1)
Code 0142	K. Campbell	(1)
Code 144	V. Ware	(1)
Code 574	P. Boss	(19)
Code 961	Archive/Stock	(6)
Code 964B	Library	(2)

Defense Technical Information Center
Alexandria, VA 22304-6145   (4)

Center for Naval Analyses
Alexandria, VA 22302-0268

Office of Naval Research
Arlington, VA 22217-5000

Naval Air Warfare Center
Weapons Division
China Lake, CA 93555-6001

Naval Surface Warfare Center
Dahlgren Division Detachment
Silver Spring, MD 20903-5000   (3)

Central Intelligence Agency
Washington, DC 20505

Jet Propulsion Laboratory
Pasadena, CA 91109

Brigham Young University
Provo, UT 84602

Texas A&M University
College Station, TX 77843

University of South Carolina
Columbia, SC 29208

Advanced Battery Systems
Cockeysville, MD 21030

Eveready Battery Company, Inc.
West Lake, OH 44145

Honeywell, Inc.
Bloomington, MN 55420

Lockheed Corporation
Sunnyvale, CA 94088-3504

Westinghouse Electric Corporation
Pittsburgh, PA 15236-0249

NCCOSC Washington Liaison Office
Washington, DC 20363-5100

Navy Acquisition, Research & Development Information Center (NARDIC)
Washington, DC 20360-5000

Naval Research Laboratory
Washington, DC 20375-5000

Naval Undersea Warfare Center Division
Newport, RI 02841

U. S. Department of Energy
Washington, DC 20585   (3)

U. S. Army Electronics Technology & Devices Laboratory
Fort Monmouth, NJ 07703-5000   (2)

Sandia National Laboratories
Albuquerque, NM 87185   (3)

Brookhaven National Laboratory
Upton, NY 11973

University of Houston
Houston, TX 77004

Rutgers University
Piscataway, NJ 08855

EIC Laboratories
Norwood, MA 02062

Galen Technology
San Jose, CA 95119

Lawrence Berkeley Laboratory
Berkeley, CA 94720   (2)

SRI
Menlo Park, CA 94025

END